INVESTIGATING MOLECULAR MECHANISMS UNDERLYING MORPHOGENETIC CELL SHAPE CHANGE

Christopher Daniel Higgins

A dissertation submitted to the faculty of the University of North Carolina at Chapel Hill in partial fulfillment of the requirements for the degree of Doctor of Philosophy in the Department of Biology in the College of Arts and Sciences.

Chapel Hill
2016

Approved by:

Bob Goldstein

Richard Cheney

Amy Maddox

Stephen Rogers

Kevin Slep

ABSTRACT

Christopher Daniel Higgins: INVESTIGATING MOLECULAR MECHANISMS UNDERLYING MORPHOGENETIC CELL SHAPE CHANGE
(Under the direction of Bob Goldstein)

Changes in cell shape are a fundamental feature of animal development driving the formation of ordered tissues from disordered groups of cells. One common type of animal cell shape change is apical constriction, where a cell or group of cells shrinks down one side more than others. Here, we seek to understand the molecular underpinnings that drive apical constriction using a simplified model system, the roundworm *Caenorhabditis elegans*. Early in *C. elegans* development, the endoderm precursor (E) cells undergo apical constriction. This cell shape change drives the internalization of the E cells. Previous work showed that the molecular motor non-muscle myosin II (NMY-2 in *C. elegans*) is required for E cell internalization, and is enriched and activated at the apical side of E cells where it is thought to generate force by pulling on a meshwork of filamentous actin in the cell cortex. We use particle image velocimetry to show that NMY-2 tagged with green fluorescent protein (GFP) localizes into distinct punctae which undergo centripetally-directed flow in the apical cortex of the E cells. We show that this flow occurs, surprisingly, before the initiation of cell shape change. We use laser nanosurgery to show that tension is established in the E cells' apical cortices prior to cell shape change, that this tension does not change as cells change shape, and that this tension exceeds that of a neighboring, non-apically constricting cell. This work suggests that apical

constriction may be governed not by the activation of myosin dynamics, but by a molecular clutch mechanically linking apical myosin dynamics to cell-cell junctions. We, therefore, sought to characterize the molecular nature of cell-cell junctions in the E cells to identify components that may contribute to this molecular clutch. We started by tagging with GFP all three essential members of the *C. elegans* cadherin-catenin complex (CCC), a complex known to contribute (albeit, redundantly) to apical constriction in the E cells. Spinning disk confocal fluorescence microscopy revealed that HMP-1/α-catenin-GFP, GFP-HMP-2/β-catenin, and HMR-1/cadherin-GFP all enriched at apical junctions as the E cells were undergoing apical constriction. We next showed that some CCC components require others to enrich apically. For example, HMR-1/cadherin requires HMP-1/α-catenin to enrich apically, suggesting that linking to the contractile actomyosin cytoskeleton might be required for apical enrichment. To test this we disrupted myosin dynamics using a temperature sensitive allele of *nmy-2* or by using RNA interference to disrupt *mrck-1*, a kinase required for myosin activation. Both treatments disrupted the apical localization of cadherin, indicating that myosin activity is required to establish an apicobasally polarized cell-cell junction in apically constricting cells.

To my wife Jessica and my children Josephine and Elliott whose support has sustained me through the desert

ACKNOWLEDGEMENTS

First, I would like to thank my wife, Jessica, for her continued support throughout the arduous journey of graduate school. I am truly fortunate to have such a bright and caring partner in life. I would also like to thank my children Josie and Elliott who constantly brighten my day.

I would like to thank my advisor, Bob Goldstein. Bob has been truly generous with his time and treasure throughout my time in his lab. He has allowed me great latitude to pursue my career ambitions outside of academia, and for that I am very grateful. He has also been an excellent source of scientific mentorship.

I would like to thank the members of my thesis committee: Dave Reiner, Amy Maddox, Richard Cheney, Kevin Slep, and Steve Rogers. You have been a truly inspired group that has provided invaluable advice to propel my project.

I thank my parents, who have provided me with all the opportunities I could ever ask for, and whose constant love and support sustains me every day.

I'd like to thank my lab mates past and present. You have made coming into work every day a true pleasure.

I'd like to thank the many friends I've made in graduate school. Your companionship and commiseration have made the journey much easier.

PREFACE

My fascination with biology really took off during high school. Susan Quigley, my senior year AP Biology teacher at Cardinal Newman High School in West Palm Beach, FL was a truly inspiring person whose enthusiasm about biology inspired me to learn more. So, as a freshman at Notre Dame, I started out as a biology major.

Initially, I wasn't sure whether I wanted to pursue a career in research or go to medical school like my dad did. He's a general surgeon, but he faced a similar decision once upon a time and wound up going into medicine, partly because of "fear of poverty."

I enjoyed my intro Biology course work, especially the stuff about cell biology. I decided during my sophomore year to take an intensive student-driven lab course called Advanced Cell Biology Research Lab. This course was run by Michelle Whaley, a truly wonderful person who poured immense time and passion into making this course excellent. As students, we worked closely with Notre Dame Biology Department faculty to design novel research projects. We designed experiments, ordered reagents, carried out the experiments, and analyzed and interpreted the data. There was no preset "answer" like in a typical teaching lab setting. These were new projects addressing genuinely open questions in cell biology.

My group worked on how a protein called NuMA organizes the spindles of cells with too many centrosomes. We used siRNA to knock down NuMA

in cultured mammalian cells, and we measured the percentage of spindles with monopolar, bipolar, and multipolar geometries. Our work suggested that NuMA was required for cells with extra centrosomes to condense those centrosomes into a bipolar spindle upon mitosis. This was interesting because cancer cells often contain too many centrosomes, and clustering of this kind would allow them to proliferate more effectively while also compromising mitotic fidelity, contributing to genomic instability.

I thought this work was really exciting. I also got really fascinated with the cytoskeleton, particularly microtubules. This fascination was what pushed me over the edge to go to graduate school.

I then joined the lab of the same professor I worked with during the Cell Biology Research Lab, Dr. Ted Hinchcliffe, to start an undergrad research project. Ted paired me up with his graduate student Liz Halpin (Collins), who got me started working on my own project in the lab. We wanted to understand how a family of proteins called tektins contributed to cytokinesis in mammalian cells. My project used biochemistry to identify the native size and shape of tektin complexes in cells, as well as tektin interactors. I was really excited by this work, and I wanted to pursue something similar in graduate school.

I wound up applying to a ton of places for grad school, and I interviewed at 4 or 5 of them. I really liked everywhere I visited. I wound up at UNC because my then girlfriend, now wife, Jessica was also applying to grad programs, and UNC was a place that we both got into. Also, UNC had an awesome group of researchers that were interested in the cytoskeleton, which I thought was really cool.

I did rotations in four labs in my first year, settling on Bob Goldstein's lab as my choice of a thesis lab. Bob's lab had a really nice group of people working in it at the time (and it still does). People seemed really engaged with what they were doing, but they were also really outgoing and friendly. It was a great environment to start out in.

I picked up on a project that was both very promising and very challenging. The project was initiated by a previous grad student in the lab, Minna Roh-Johnson. Minna noticed that the dynamics of the actin cytoskeleton during early morphogenetic movements of cells in the *C. elegans* embryo were really weird. Namely, the cytoskeletal dynamics driving cell shape change in the early embryo were deployed well in advance of the actual shape change. This meant that there might be a developmentally-regulated clutch that engages the cytoskeleton to the cell membrane.

I thought this sounded really cool. Plus, it offered me a chance to hit the ground running, and perhaps get my name on a nice paper in the early days of graduate school. We submitted the paper to *Nature* and it went out for review, but it bounced. We looked really closely at the reviewer comments and decided to try to address them as best we could. This meant booting up a new collaboration with Dan Kiehart's group at Duke doing really challenging laser cuts in early embryonic cells. With a lot of persistence, Serdar Tulu, then a postdoc in the Kiehart lab, and I managed to get it to work.

I also collaborated with Russ Taylor, a computer scientist at UNC, to adapt his program called ImageTracker to map out the cytoskeletal dynamics in an

unbiased way. This program gave us really nice maps with vectors that corresponded to the direction of cytoskeletal flow over time in our movies. I also did a bunch of new analysis for the paper, doing tedious manual tracking and quantifying apical areas at earlier timepoints than Minna had measured.

After a lot of work, we submitted the paper to *Science*. Initially, it got decent reviews, but the editor declined to publish. But after some persistence on Bob's end, we managed to get the editor to reconsider it, pending some additional experiments. This meant me going back to Duke and doing more challenging laser cut experiments with Serdar. Again, we managed to get these cuts to work: Serdar drove the scope, I mounted the embryos and analyzed the data afterwards.

During this time, we also booted up a collaboration with (now Nobel laureate) Eric Betzig to use his new contraption called a Bessel beam plane illumination microscope. In Eric's lab I worked with a postdoc, Liang Gao, to generate really nice 3D images of our embryos over time. The Bessel beam scope could go so much faster than what we had back in Chapel Hill, and illuminating from the side with a thin sheet of light meant that we could image for much longer without photobleaching or damaging the embryo. Eric was working on a new *Cell* manuscript at the time to describe the latest improvements in his Bessel beam instrument. Our data looked promising enough that Eric decided to include them in the manuscript, and I made it onto the author list.

At the end of the day, the Bessel beam confirmed what we already knew: actin cytoskeletal dynamics get going before cell shape change. But, it was

nice to see this in 3D, and in embryos that weren't compressed (which we had to do on the spinning disk to get all the features that we wanted to see in one plane).

We went back to *Science* and the paper got accepted. This was a huge relief. This process had dragged on longer than any of us thought it would, and it was great to finally have it behind us. Later that year, Eric's paper got into *Cell*, which was exciting.

The summer after the science paper got in (2012), I got to participate in the Physiology Course at the Marine Biological Laboratory in Woods Hole, MA. This was a truly wonderful experience. I got to meet a lot of very brilliant people, and work on fascinating problems in cell biology. I saw talks from leaders in the cell biology world and got to interact with them in the lab and, of course, in the bar. This was a truly inspiring summer, and I left feeling really excited about science and pursuing a career in academia.

When I made it back to Chapel Hill, real life set back in pretty quick. In the lab, I slammed my head against the wall (figuratively) trying to get biolistic bombardment to work to tag members of the cadherin catenin complex with fluorescent proteins. I wasted a ton of time trying to get this obscure and painful technique to work. In the end, I made some very dim strains, none of which were useful for the type of experiments I wanted to do.

Luckily, my labmate Dan Dickinson, came up with a new way to tag genes in *C. elegans* using the CRISPR/Cas9 nuclease to create custom cuts in the genome and repairing those cuts by homologous recombination. The constructs to do CRISPR could be injected into worms, so bombardment was history. This

technique totally bailed out my project. Without it, I'm not sure what I would have done.

I wound up getting beautiful endogenously-tagged fluorescent strains for all of my major proteins of interest using CRISPR, and this allowed me to finally do the experiments I had been planning on for years. The results from this work are included here in Chapter 3.

In September of 2012, my wife and I welcomed our first child, Josie, into the world. Becoming a parent was a harrowing and wonderful experience, and it changed my outlook on things quite a bit. I realized that I really liked being a parent and spending time with my kids. I also realized that the hyper-competitive academic path would make this quite difficult, and offered very little financial support and even less job security along the way.

I started to look at other options. Initially, I thought I might enjoy research in an industry setting such as a biotech or a pharmaceutical company. I tried to do some networking and I met with a few people who have these types of jobs. Most of these people had done postdocs and then transitioned into industry. I wasn't sure I actually wanted to do a postdoc, so I wound up bailing on this path.

Also around this time, my good friend from early in graduate school, Jacob Sawyer, jumped ship on academia and took a job with Nikon Instruments, a microscope company. Jacob seemed to really enjoy his new job, and it was enlightening to see how much happier he seemed in this role compared to his time in academia.

I figured that a job in the imaging industry would fit my interests and skills quite well. I would still get to work with microscopes, which I loved. I would get to see a lot of cool, new science. But I wouldn't have to deal with the boring, tedious parts like writing or tracking on hazy dots in images. Also, I wouldn't have to write grants or papers, and I would be paid a lot better than I would in academia.

It sounded like a really good deal, so I started to look into available jobs. I applied to Leica in October 2014 for a super travel-heavy confocal/SuperRes support job. The technology was really cool, but it would have taken me away from my family quite a bit.

In the end, I decided to turn it down, although the interview process was a really positive experience.

Early in 2015, a job opened up with Nikon in Durham and Chapel Hill. The job was perfect for what I wanted. It would be a local rep job covering just Duke and UNC, with almost no overnight travel. We wouldn't have to move, I wouldn't have to travel, and I would get to work with my old buddy Jacob. It was super-ideal. I applied, interviewed up in New York at Nikon HQ, and I got the job. The only catch was that I would have to start in April 2015, and my grad school work wasn't quite done yet.

I scrambled like crazy to get everything together before I left the lab, and while I did get a lot of things done, there was still a lot more to do. Much of this thesis has been written on the road during my mentor training period, in the early days of my job at Nikon. It has been a truly stressful time, for me somewhat, but especially for my wife and kids. I can't wait for this to be done.

TABLE OF CONTENTS

LIST OF FIGURES……..……....xvi

LIST OF ABBREVIATIONS…….……..……xvii

CHAPTER 1: BACKGROUND AND SIGNIFICANCE……..……1

References…….……6

CHAPTER 2: ASYMMETRIC CELL DIVISION: A NEW WAY TO DIVIDE UNEQUALLY……...7

Abstract…..……..7

Main Text…….……7

Figures…….……..12

References…….……..……14

CHAPTER 3: TRIGGERING A CELL SHAPE CHANGE BY EXPLOITING PRE-EXISTING ACTOMYOSIN CONTRACTIONS……16

Abstract……..……16

Results and Discussion……..……17

Materials and Methods……..……..23

Strains and worm maintenance……..……23

RNA interference (RNAi)……..……...23

DIC and fluorescence microscopy……..……..…24

Bessel beam plane illumination microscopy and structured illumination.....24

Analysis of F-actin, myosin and membrane dynamics by spinning disk confocal microscopy…….25

Imaging and analysis of *Drosophila* ventral furrow……25

Analysis of Ea/p apical constriction speeds……26

Computer simulation……27

Analysis of myosin dynamics during spontaneous network failures and after laser-cutting……28

Analysis of myosin and membrane movements……29

FRAP……29

Labeling cell surfaces with Quantum Dots……30

Figures……30

References……58

CHAPTER 4: MYOSIN ACTIVITY POLARIZES THE CADHERIN-CATENIN COMPLEX IN APICALLY CONSTRICTING CELLS……62

Introduction……63

Materials and methods……66

C. elegans culture……66

Mounting for imaging……66

Spinning disk confocal imaging……66

Image analysis……67

CRISPR/Cas9 triggered homologous recombination……67

RNA interference……68

nmy-2-ts experiment……68

Results……69

A novel system in which to study *in vivo* roles for the CCC……69

Endogenous fluorescent tagging reveals spatiotemporally non-uniform localization of cadherin-GFP to sites of cell-cell contact……..……..70

The CCC accumulates to varying degrees at different apical junctions…..……...71

Early centripetal myosin contractions do not deplete CCC from the apical junctions……..……..72

Cadherin requires α and β catenin for apical junction enrichment……..……..74

Actomyosin contractility regulates CCC distribution in apically-constricting cells…….……...76

Discussion…….……77

Figures…….……..82

References……..……..96

CHAPTER 5: FUTURE DIRECTIONS……..……..99

References……..……105

LIST OF FIGURES

Figure 2.1 Asymmetric cortical myosin in mitotic cells can position the cytokinetic furrow asymmetrically……12

Figure 2.2 A proposed mechanism for asymmetric furrow positioning……..13

Figure 3.1 Actomyosin contraction precedes the rapid shrinking of the apical surface……31

Figure 3.2 Periodic actomyosin coalescence occurs before apical cell profiles shrink in Drosophila gastrulation……..33

Figure 3.3 Cortical tension associated with apical constricton is established early and changes little as apical shrinking accelerates in *C. elegans*……35

Figure 3.4 Targeting classical cadherin and Rac signaling prevents coupled movements but not actomyosin contraction……..37

Figure 3.5 Images of myosin and plasma membrane at four timepoints in gastrulation, collected by Bessel beam structured plane illumination (Planchon et al., 2011)……39

Figure 3.6 Movements of myosin and F-actin……41

Figure 3.7 The actomyosin network is contractile and dynamic……..43

Figure 3.8 Diagram of early and late stage movements……45

Figure 3.9 Estimating the efficiency of actomyosin network-contact zone connection by comparing data from a simulation to data from cells……...46

Figure 3.10 Overlying cell surfaces appear to move centripetally, as the myosin particles do, during the early stage……..47

Figure 3.11 Embryos deficient in cadherin-catenin complex proteins and Rac signaling have gastrulation defects……..….50

Figure 3.12 *hmr-1(RNAi); ced-5(n1812)* embryos appear to have normal endomesodermal cell fates and normal F-actin and myosin localization……52

Figure 3.13 *hmr-1(RNAi); ced-5(n1812)* embryos failed to establish coupled movements during late stages……..……54

Figure 3.14 Centripetal myosin movements occurred in multiple cells…….55

Figure 3.15 PIV of Ea and MSap cells at early and late stages…….57

Figure 4.1 HMR-1/cadherin-GFP enriches non-uniformly at cell-cell contacts in early *C. elegans* embryos……82

Figure 4.2 Cadherin-Catenin Complex (CCC) enriches apically in apically constricting cells……..…84

Figure 4.3 HMR-1/Cadherin-GFP enriches differentially over time at different cell borders associated with apically constricting cells…….86

Figure 4.4 Cadherin Catenin Complex (CCC) components enrich at apical cell-cell junctions and do not display centripetal co-transport with actomyosin……87

Figure 4.5 Some Cadherin Catenin Complex (CCC) components are interdependent for apical enrichment……89

Figure 4.6 Myosin activity is required for apical enrichment of the Cadherin Catenin Complex (CCC) in apically constricting cells……..…91

Figure 4.7 Cas9/CRISPR triggered homologous recombination permits insertion of fluorescent protein genes at endogenous cadherin catenin complex (CCC) genes in the *C. elegans* genome……..…93

Figure 4.8 Quantification of embryonic fluorescence in knock-in/knockdown embryos permits stage-specific verification of knockdown effectiveness……94

LIST OF ABBREVIATIONS

AB	Anterior blastomere
ATP	Adenosine triphosphate
ATPase	Adenosine triphosphatase
C	Carboxy
CCC	Cadherin-catenin complex
cDNA	Complementary deoxyribonucleic acid
CI	Confidence interval
CRISPR	Clustered regularly interspaced short palindromic repeats
DNA	Deoxyribonucleic acid
dsRNA	Double stranded ribonucleic acid
E	Endodermal precursor
EMS	Endomesodermal precursor cell
F-actin	Filamentous actin
GFP	Green fluorescent protein
min	Minute
MRCK	Myotonic dystrophy kinase related cdc42 binding kinase
MS	Mesodermal precursor cell
PCR	Polymerase chain reaction
RNA	Ribonucleic acid
ts	Temperature sensitive

CHAPTER 1: BACKGROUND AND SIGNIFICANCE

Morphogenesis is characterized by the establishment of ordered tissues from less ordered collections of cells; that is, decrease in entropy. The second law of thermodynamics requires the input of energy to achieve such a decrease. In biology, such energy is stored largely in the nucleotide adenosine triphosphate (ATP), and it is harnessed by a wide variety of enzymes which produce energy by hydrolyzing ATP into inorganic phosphate and adenosine diphosphate (ADP). Two major hydrolyzers of ATP in eukaryotic cells are the filament building block protein actin and its motor protein myosin. Both of these proteins are essential for the generation of cell-and-tissue scale order during morphogenesis, and both will be central to this dissertation.

Actin is a highly abundant protein in most eukaryotic cells and its polymerization into actin filaments (F-actin) is a major means by which eukaryotic cells achieve micron-scale organization using nanometer-sized protein building blocks. F-actin is a polar filament (i.e. its ends are non-identical) composed of tens to thousands of G-actin (globular) subunits arranged head to tail in a helix. In cells, F-actin is highly dynamic with new subunits being added constantly to the dynamic "barbed" end and lost from the less dynamic "pointed end."

The assembly of G-actin subunits into F-actin filaments is tightly regulated in eukaryotic cells by a host of proteins. These proteins function by catalyzing nucleation of new filaments, speeding polymerization of existing filaments, capping

filament ends, preventing capping of filament ends, severing filaments, cross-linking filaments, nucleating branched filament arrays, and disassembling filament branches. Actin nucleators are largely confined to the plasma membrane and so actin filaments typically associate tightly with the plasma membrane.

Actin filaments also act as protein tracks upon which myosin motor proteins hydrolyze ATP to produce mechanical work. Myosins are a diverse set of proteins which have the ability to bind a wide variety of cargoes largely through their divergent tail domains. However, all myosins are united by the presence of a motor head domain (Mooseker and Cheney, 1995). Myosin II is the motor responsible for the skeletal muscle contractions with which I am typing this document. Myosin II also has non-muscle orthologues which are present in virtually all eukaryotic cell types. Non-muscle myosin II is known to enrich in the cleavage furrow during cytokinesis where it is thought to be important for driving inward furrow progression, although the precise mechanism by which myosin II promotes cytokinesis remains an area of intense study.

Non-muscle myosin II also is required for several types of morphogenetic movements (Munjal and Lecuit, 2014). Cells deploy a variety of movements in order to establish ordered tissues in a developing embryo. These include convergent extension (cells in a monolayer shrink down along one axis preferentially to drive the elongation of a tissue), epiboly (cells thin and spread over a larger surface area), delamination (cells exit a tissue monolayer), and apical constriction (cells shrink down their contact-free surface to drive tissue bending). The molecular players and

mechanisms driving these morphogenetic movements are often conserved across phyla. This work will focus on apical constriction.

Apical constriction is a cell shape change required for development of diverse metazoans (Sawyer et al., 2010). Despite the taxonomically diverse array of animals deploying apical constriction, its molecular underpinnings are surprisingly well-conserved. That is, apically constricting cells rely on a core set of cytoskeletal machinery to drive movements (Martin and Goldstein, 2014). Namely, cells assemble a meshwork array of actomyosin preferentially on their contact-free surface (Martin et al., 2009; Roh-Johnson et al., 2012). The meshwork contracts due to the force-producing activity of non-muscle myosin II which is transmitted across cell-cell boundaries through structures known as adherens junctions (AJs). Further, the edges of the cells' apical contacts bind to the contractile apical actomyosin meshwork driving the shrinkage of the apical surface and drawing the cells neighboring the apically-constricting cells closer together. When deployed in isolation, apical constriction can result in the internalization of cells from the embryonic surface or the exit of cells from an epithelium (also known as epithelial to mesenchymal transition). When deployed by multiple cells at once, apical constriction can drive tissue-scale furrow formation or tissue bending (Martin and Goldstein, 2014).

During vertebrate development, apical constriction is deployed in concert with convergent extension to drive formation and closure of the neural tube (i.e. the nascent brain and spinal cord) (Wallingford et al., 2013). Here, cells positioned along the dorsal side of the embryo in a region known as the neural plate undergo apical

constriction and convergent extension, driving the formation of neural folds and tissue lengthening. The neural folds then undergo tissue-scale fusion, developing nascent cell-cell adhesions with cells from the adjacent fold. This fusion results in the formation of a closed tube which will then go on to form the brain and spinal cord of the animal (Copp and Greene, 2010).

Significantly, neural tube closure is one of the most error-prone aspects of human development (Copp and Greene, 2010; Wallingford et al., 2013). Defects in neural tube closure give rise to debilitating birth defects such as spina bifida and anencephaly as well as miscarriage. In the work that follows, I use a highly tractable invertebrate model to dissect the molecular mechanisms of apical constriction with the hope that understanding fundamental mechanisms will contribute a clearer picture of human disease.

The *C. elegans* gastrula provides a tractable system in which to study the cell biological mechanisms of apical constriction (Lee and Goldstein, 2003). Tractability derives from the following key features: 1) powerful genetic methods of *C. elegans* including the ability to disrupt gene function with RNAi and mutants and the ability to edit the genome with CRISPR/Cas9 triggered homologous recombination 2) an optically clear embryo with minimal autofluorescence that is amenable to live fluorescence imaging, 3) a limited number of cells present (26-28, depending on the stage) allowing for the precise determination of cell and non-cell autonomous contributions to morphogenesis. *C. elegans* also offers advantages that make it a generally attractive laboratory model such as low cost of maintenance and storage, short generation time, and large brood size.

Here, we investigate the molecular mechanisms contributing to apical constriction using the *C. elegans* gastrula as a model system. In this system, the cells fated to become the endoderm (i.e. gut) are born onto the outside of the embryo and must undergo apical constriction to internalize (Lee and Goldstein, 2003). These cells, also called E cells or Ea and Ep enrich NMY-2, the predominant *C. elegans* non-muscle myosin expressed in early embryos, at their apical surfaces (Nance et al., 2003). NMY-2 assembles into punctae at the apical surfaces of the E cells which contract centripetally over time. Initially NMY-2-GFP punctae move centripetally without corresponding movement in the apical cell-cell junctions (Roh-Johnson et al., 2012). We call these uncoupled movements. Later, cell-cell contacts move in concert with centripetally moving NMY-2-GFP.

Here, I seek to examine the interplay between cell-cell adhesion components and the underlying actin-myosin cytoskeleton. I do this by generating fluorescently tagged versions of cell-cell junction components at endogenous genetic loci and testing which ones colocalize with actin and myosin and which ones colocalize with cell-cell junctions. I then ask whether myosin activity is required for the localization of these components. This study reveals new insights about the molecular nature of cell-cell junctions during apical constriction. It will be interesting to see the extent to which these insights represent general properties of the highly-conserved cadherin-catenin complex and actomyosin cytoskeletal machinery and whether they will be broadly applicable across metazoa.

REFERENCES

Copp, A.J. and Greene, N.D.E. (2010). Genetics and development of neural tube defects. J. Pathol. *220*, 217–230.

Lee, J.-Y. and Goldstein, B. (2003). Mechanisms of cell positioning during C. elegans gastrulation. Development *130*, 307–320.

Martin, A.C. and Goldstein, B. (2014). Apical constriction: themes and variations on a cellular mechanism driving morphogenesis. Development *141*, 1987–1998.

Martin, A.C., Kaschube, M., and Wieschaus, E.F. (2009). Pulsed contractions of an actin–myosin network drive apical constriction. Nature *457*, 495–499.

Mooseker, M.S. and Cheney, R.E. (1995). Unconventional Myosins. Annu. Rev. Cell Dev. Biol. *11*, 633–675.

Munjal, A. and Lecuit, T. (2014). Actomyosin networks and tissue morphogenesis. Dev. Camb. Engl. *141*, 1789–1793.

Nance, J., Munro, E.M., and Priess, J.R. (2003). C. elegans PAR-3 and PAR-6 are required for apicobasal asymmetries associated with cell adhesion and gastrulation. Development *130*, 5339–5350.

Roh-Johnson, M., Shemer, G., Higgins, C.D., McClellan, J.H., Werts, A.D., Tulu, U.S., Gao, L., Betzig, E., Kiehart, D.P., and Goldstein, B. (2012). Triggering a Cell Shape Change by Exploiting Pre-Existing Actomyosin Contractions. Science *335*, 1232–1235.

Sawyer, J.M., Harrell, J.R., Shemer, G., Sullivan-Brown, J., Roh-Johnson, M., and Goldstein, B. (2010). Apical constriction: A cell shape change that can drive morphogenesis. Dev. Biol. *341*, 5–19.

Wallingford, J.B., Niswander, L.A., Shaw, G.M., and Finnell, R.H. (2013). The continuing challenge of understanding, preventing, and treating neural tube defects. Science *339*, 1222002.

CHAPTER 2: ASYMMETRIC CELL DIVISION: A NEW WAY TO DIVIDE UNEQUALLY

The following was published as a Current Biology *Dispatch (Higgins and Goldstein, 2010). I wrote the text in collaboration with my advisor Dr. Bob Goldstein.*

Summary

It has long been known that cells can divide unequally by shifting the mitotic spindle to one side. Two recent reports identify an alternative way to generate daughter cells of different sizes.

Main text

All good cell biologists know that the mitotic spindle determines the plane of cytokinesis. Ray Rappaport, the godfather of cytokinesis (Canman and Wells, 2004), showed that experimentally moving a spindle could change the site of cytokinesis (Rappaport, 1985), and cytokinesis can be prevented by removing the spindle from a cell at least a few minutes before the cytokinetic furrow normally forms (Hiramoto, 1956; Rappaport, 1981). Recent work has begun to outline a mechanism for the furrow-inducing activity of the mitotic spindle. Astral microtubules and midzone microtubules affect myosin distribution and actin architecture through local RhoA activation and Rac inactivation at the equatorial cortex, where the actin and myosin will form a contractile 'purse string' (Glotzer, 2005; Canman, 2009; Bement, et al., 2006). In nearly all cells, the spatial relationship between the spindle

and the actomyosin-rich furrow is consistent with the above causal relationships: the spindle's position predicts accurately where furrowing will occur.

However, exceptions exist. In 2000, Kaltschmidt and colleagues (2000) reported live imaging of microtubules in *Drosophila* neuroblasts and showed a cell division plane that did not lie midway between the two spindle poles, but instead lay closer to one of the poles, resulting in daughter cells of two different sizes. Now a new report from Cabernard and colleagues (2010) provides evidence that the furrow can be positioned independently of the spindle in these neuroblasts, by a mechanism that involves an asymmetric enrichment of cortical myosin in mitotic cells. A second report from Ou and colleagues (2010) reports a similar mechanism in another system, a *Caenorhabditis elegans* neuroblast, and tests directly the role of asymmetric myosin enrichment in controlling daughter cell size. The new results challenge the universality of the mitotic spindle as the primary determinant of furrow positioning, establishing an asymmetric cortical enrichment of myosin during mitosis as an alternative means to divide unequally in some cells.

Drosophila neuroblasts divide asymmetrically, producing a larger daughter that retains stem-cell characteristics and a smaller daughter that differentiates. Cabernard and colleagues (Cabernard, et al., 2010) showed by live imaging of neuroblasts that myosin localized in an unexpected pattern during mitosis, becoming enriched asymmetrically in the cell cortex on the side where the smaller daughter cell will form (Fig. 2.1). Interestingly, this enrichment was established even before any mitotic spindle asymmetries were apparent, suggesting that the myosin asymmetry was not caused by any observed spindle asymmetries. Indeed, cells with

spindles rotated out of their normal axis still had normal myosin enrichment on the basal side of the cell. The rotated spindle and the basal myosin each appeared to induce a furrow — a double furrow! What does it mean? In *Drosophila* neuroblasts, the myosin crescent appears to provide an independent, parallel mechanism for cleavage furrow positioning, along with canonical spindle-derived cues.

Ou and colleagues (2010) investigated the asymmetric division of another cell, a *C. elegans* neuroblast. Division of a particular neuroblast, called QR.a, produces daughter cells of different sizes and fates, with the larger daughter becoming a neuron, and the smaller daughter undergoing apoptosis. Despite this asymmetry of size and fate, the mitotic spindle of this cell is aligned in the center at metaphase, just as in *Drosophila* neuroblasts (Cabernard, et al., 2010; Ou et al., 2010). And just as in *Drosophila* neuroblasts, the authors show that myosin becomes enriched asymmetrically in the cortex of one side of the cell during anaphase, on the side that will form the smaller daughter cell.

Ou *et al.* (2010) propose a mechanism for how asymmetric myosin might drive unequal cell division: cortical contractility driven by the myosin crescent could shrink one hemisphere of the dividing cell, driving cytoplasmic flow through the ingressing cleavage furrow and resulting in two differently-sized daughter cells (Fig. 2.2). To test myosin's role in specific regions of the cell, they used chromophore-assisted laser inactivation (CALI), a technique that uses reactive products emitted upon fluorophore excitation to locally inactivate proteins (Diefenbach, et al., 2002; Jacobson, et al., 2008; Wang, et al., 1996). They found that CALI of GFP–myosin in the region where it is enriched could prevent that side of

the dividing cell from shrinking normally, leading in some cases to equal cell division (Fig. 2.1), whereas CALI of a control GFP-tagged molecule could not. Interestingly, in some cases in which daughter cell size was affected, cell fate was also affected. The results show that asymmetric enrichment of myosin in mitosis can locally affect the size and the fate of a nascent daughter cell.

With mitotic cells constricted at one end by cortical actomyosin-derived forces, the resulting cell shape resembles one of the classic Rappaport experiments. After his retirement as a professor, Ray Rappaport and his wife Barbara, both in their 70s at the time, published a paper in which they reported the effect of squeezing mitotic cells into conical shapes (Rappaport and Rappaport, 1994). Why squeeze cells into conical shapes? A computer model developed by Albert Harris and Sally Gewalt (1989) had predicted that cells of this shape could be used to distinguish between existing models for spindle positioning. Interestingly, the result of changing cell shape was similar to that shown in worm and fly neuroblasts: the furrow formed closer to the narrow end of the cell, instead of midway between the two spindle poles (Fig. 2.1). The authors interpreted this as resulting from a more effective interaction between the spindle and the cortex at the narrow end of the cell, as the cortex in this end of the cell lies closer to the spindle.

The Rappaports' result shows that tapering one end of a cell can result in the furrow forming closer to the spindle pole at that end of the cell. Might the asymmetric myosin observed in worm and fly neuroblasts affect furrow position in this way? Myosin is itself a key furrow component, so an indirect effect of myosin on furrow positioning through cell shape — allowing the spindle and cortex to more effectively

interact at one end of the cell — might seem circuitous. Indeed, in fly neuroblasts, Cabernard *et al.* (2010) were able to eliminate the spindle altogether by colcemid treatment and then genetically bypass the spindle checkpoint, and they found that the basal myosin enrichment and asymmetric cytokinesis still occurred. This result establishes the new mechanism as a truly independent mechanism, not requiring the mitotic spindle. It will be interesting to learn the extent to which this will stand as an independent mechanism in other systems.

How does myosin localize asymmetrically in mitotic cells? Temporal and spatial mechanisms must be involved. Metaphase-arrested *Drosophila* neuroblasts failed to localize myosin asymmetrically, suggesting that myosin localization must be temporally linked to mitotic progression, like asymmetric spindle positioning in certain cells (Cabernard, et al., 2010; McCarthy Campbell, et al., 2009). The authors show that spatial regulation of myosin depends on familiar players, a PAR-1-like kinase called PIG-1 in *C. elegans* neuroblasts, and the asymmetric Pins protein in *Drosophila*, which has well-established roles in spindle positioning (Cabernard, et al., 2010; Ou et al., 2010; McCarthy Campbell, et al., 2009; Siller and Doe, 2009). These molecular links are likely to serve as key steps toward dissecting the mechanisms of asymmetric myosin distribution in mitotic cells.

Figures

Figure 2.1: Asymmetric cortical myosin in mitotic cells can position the cytokinetic furrow asymmetrically

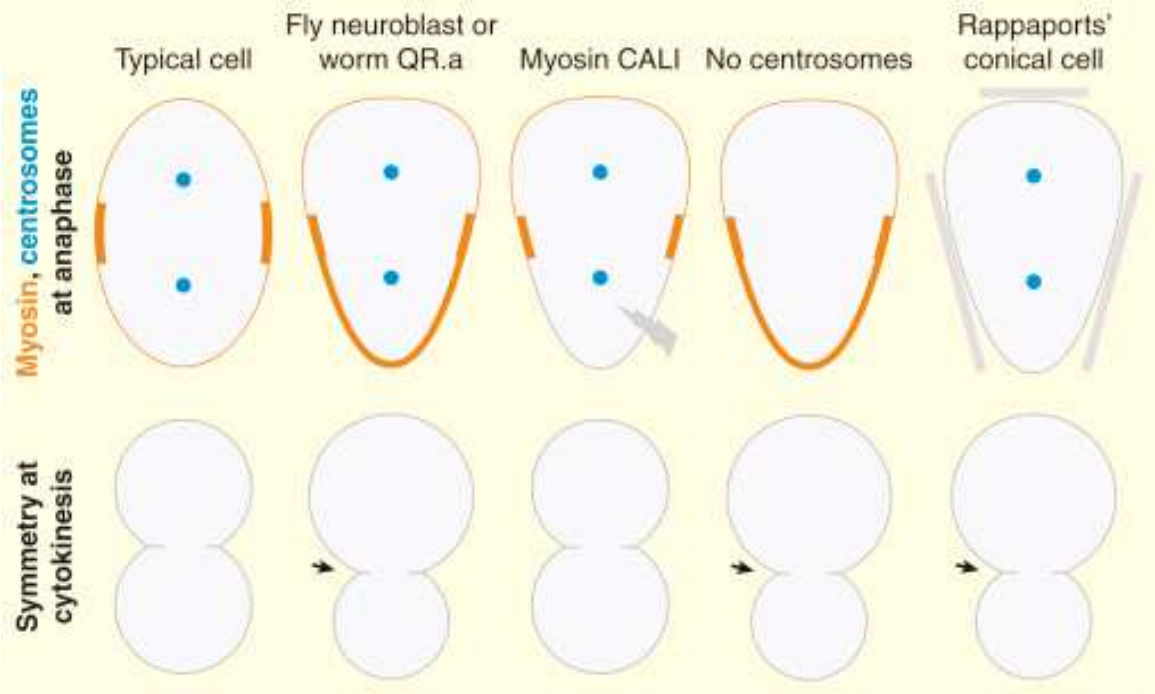

Diagram of myosin and spindle pole (centrosome) positions at anaphase (top), and the resulting cytokinetic furrow position (bottom). Thicker regions of myosin represent cortical regions with myosin enrichment.

Figure 2.2: A proposed mechanism for asymmetric furrow positioning

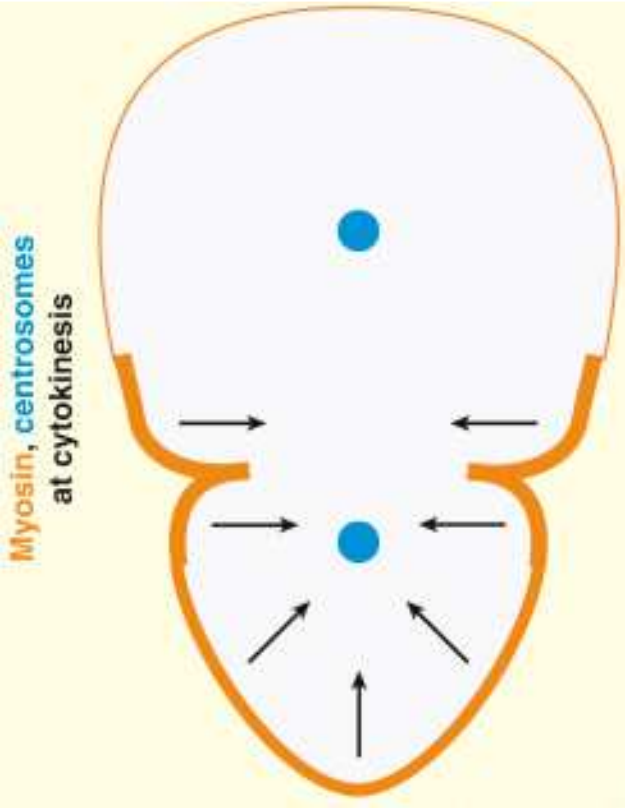

Model proposing how an asymmetric myosin crescent can affect daughter cell size (after Ou et al., 2010). Arrows represent actomyosin-driven contractions shrinking one end of the cell during cytokinesis.

REFERENCES

Canman, J.C. and Wells, W.A. (2004). Rappaport furrows on our minds: the ASCB Cytokinesis Meeting Burlington, VT July 22-25, 2004. J. Cell Biol *166*, 943–948.

Rappaport, R. (1985). Repeated furrow formation from a single mitotic apparatus in cylindrical sand dollar eggs. J. Exp. Zool. *234*, 167–171.

Hiramoto, Y. (1956). Cell division without mitotic apparatus in sea urchin eggs. Exp. Cell Res. *11*, 630–636.

Rappaport, R. (1981). Cytokinesis - cleavage furrow establishment in cylindrical sand dollar eggs. J. Exp. Zool. *217*, 365–375.

Glotzer, M. (2005). The molecular requirements for cytokinesis. Science *307*, 1735–1739.

Canman, J.C. (2009). Cytokinetic astrology. J. Cell Biol. *187*, 757–759.

Bement, W.M., Miller, A.L., and von Dassow, G. (2006). Rho GTPase activity zones and transient contractile arrays. Bioessays *28*, 983–993.

Kaltschmidt, J.A., Davidson, C.M., Brown, N.H., and Brand, A.H. (2000). Rotation and asymmetry of the mitotic spindle direct asymmetric cell division in the developing central nervous system. Nat. Cell Biol. *2*: 7–12.

Cabernard, C., Prehoda, K.E., and Doe, C.Q. (2010). A spindle-independent cleavage furrow positioning pathway. Nature *467*, 91–94.

Ou, G., Stuurman, N., D'Ambrosio, M., and Vale, R.D. (2010). Polarized myosin produces unequal-size daughters during asymmetric cell division. Science *330*, 677–680.

Diefenbach, T.J., Latham, V.M., Yimlamai, D., Liu, C.A., Herman, I.M., and Jay, D.G. (2002). Myosin 1c and myosin IIB serve opposing roles in lamellipodial dynamics of the neuronal growth cone. J. Cell Biol. *158*, 1207–1217.

Jacobson, K., Rajfur, Z., Vitriol, E., and Hahn, K. (2008). Chromophore-assisted laser inactivation in cell biology. Trends Cell Biol. *18*, 443–450.

Wang, F.S., Wolenski, J.S., Cheney, R.E., Mooseker, M.S., and Jay, D.G. (1996). Function of myosin-V in filopodial extension of neuronal growth cones. Science *273*, 660–663.

Rappaport, R. and Rappaport, B.N. (1994). Cleavage in conical sand dollar eggs. Dev. Biol. *164*, 258–266.

Harris, A.K. and Gewalt, S.L. (1989). Simulation testing of mechanisms for inducing the formation of the contractile ring in cytokinesis. J. Cell Biol. *109*: 2215–2223.

McCarthy Campbell, E.K., Werts, A.D., and Goldstein, B. (2009). A cell cycle timer for asymmetric spindle positioning. PLoS Biol. *7*, e1000088.

Cordes, S., Frank, C.A., and Garriga, G. (2006). The C. elegans MELK ortholog PIG-1 regulates cell size asymmetry and daughter cell fate in asymmetric neuroblast divisions. Development *133*: 2747–2756.

Siller, K.H. and Doe, C.Q. (2009). Spindle orientation during asymmetric cell division. Nat. Cell Biol. *11*, 365–374.

CHAPTER 3: TRIGGERING A CELL SHAPE CHANGE BY EXPLOITING PRE-EXISTING ACTOMYOSIN CONTRACTIONS

The following was published as a Science *report (Roh-Johnson, et al., 2012). I performed the experiments and analyzed the data in Figure 3.3 B-C examining cortical tension by laser cutting and measuring recoil rates. I also contributed significantly to Figure 3.1 by collecting and analyzing data to measure closure rate over time (D-F) and depicting plasma membranes closing over time (C). Finally, I adapted the particle image velocimetry program, ImageTracker, to analyze myosin and membrane dynamics by constructing vector maps. These maps can be found in Figures 3.1H, 3.3C, and 3.4B-C. I also contributed edits to the final draft of the manuscript.*

Introduction

Apical constriction changes cell shapes, driving critical morphogenetic events including gastrulation in diverse organisms and neural tube closure in vertebrates. Apical constriction is thought to be triggered by contraction of apical actomyosin networks. We found that apical actomyosin contractions began before cell shape changes in both *C. elegans* and *Drosophila*. In *C. elegans*, actomyosin networks were initially dynamic, contracting and generating cortical tension without significant shrinking of apical surfaces. Apical cell-cell contact zones and actomyosin only later moved increasingly in concert, with no detectable change in actomyosin dynamics or cortical tension. Thus, apical constriction appears to be triggered not by a change in

cortical tension but by dynamic linking of apical cell-cell contact zones to an already contractile apical cortex.

Results and Discussion

During development, dramatic rearrangements of cells and epithelia play key roles in shaping animals (Friedl and Gilmour, 2009; Odell et al., 1981; Sawyer et al., 2010; Weijer, 2009). Many rearrangements are driven by apical constriction, including neural tube closure (Sawyer et al., 2010), failure of which is a common human birth defect (Copp and Greene, 2010). Apical constriction is generally driven by contraction of apical actomyosin networks (Sawyer et al., 2010). However, it is not well understood how the stresses and tensions generated by actomyosin networks produce cell shape changes in developing organisms (Grill, 2011).

To address this issue, we examined cortical actomyosin dynamics during *C. elegans* gastrulation. In *C. elegans*, two endodermal precursor cells (Ea and Ep) internalize by apical constriction (Lee and Goldstein, 2003; Lee et al., 2006; Nance and Priess, 2002). Transgenic green fluorescent protein (GFP) myosin II-containing particles formed in each cell's apical cortex, enriched in Ea/p similarly to endogenous myosin (Nance and Priess, 2002). The ability to resolve large numbers of particles made it possible to track the detailed dynamics of actomyosin networks (Fig. 3.1A; Fig. 3.5). Neighboring myosin particles moved short distances toward each other into multiple coalescence points, with most particles moving centripetally (toward the center of the apical cell surface), and with new particles forming near apical cell boundaries (Fig. 3.1B; Fig. 3.6). These particles appear to be components of contracting actomyosin networks, because F-actin coalesced similarly (Fig. 3.6),

and myosin particles near the center of each coalescence moved at a slower speed than those further away (Fig. 3.7) as seen in other contracting actomyosin networks (Munro et al., 2004). Particle tracking and fluorescence recovery after photobleaching (FRAP) experiments suggested that the networks were continuously remodeled by exchange of myosin molecules on and off particles as expected (Fig. 3.7).

To investigate how apical actomyosin networks shrink apical cell surfaces, we tracked the outlines of these surfaces, the apical cell-cell contact zones, quantitatively (Fig. 3.1C–D). Apical areas shrunk gradually or not at all at first (Fig. 3.1D–F) and then accelerated. We predicted that actomyosin contraction would also begin gradually and accelerate in concert with the contact zones (Fig. 3.1E). Instead, myosin particles moved centripetally quite rapidly throughout this period (Fig. 3.1F; 3.19 ± 0.14 μm/min, mean ± 95%CI), at first with little or no accompanying contact zone movement. Myosin particles near contact zones at first streamed away from the contact zones, which were in many cases almost stationary, suggesting that the actomyosin network and contact zones were only weakly mechanically connected at this stage (Fig. 3.1G; we refer to actomyosin contractions without contact zone movement as uncoupled movements). Later, contact zones appeared to move almost in unison with many of the myosin particles (Fig. 3.1G; referred to as coupled movements), suggesting that the myosin and contact zones may have become mechanically connected. Contact zones were never seen to overtake myosin particles in the Ea/p cortex, suggesting that neighboring cells were not simply migrating over Ea/p cells.

Our observations were not entirely consistent with a simple pattern of uncoupled movements early and coupled movements later (Fig. 3.8); instead, some variation existed at each stage. Tracking movements by particle image velocimetry (PIV) demonstrated that in general, the myosin particles and contact zones moved increasingly in unison as time progressed (Fig. 3.1H). We confirmed this result by measuring the rates of individually tracked myosin particles and nearby contact zones, defining the difference between these two rates as a slipping rate (Fig. 3.1I). Actomyosin contractions appeared to drive contact zone movements with ~25% efficiency in early stages, increasing to ~81% efficiency near the end of Ea/p internalization, based on comparing measurements from cells with a computer simulation (Fig. 3.9). Labeling cell surfaces with Quantum Dots or a plasma membrane marker demonstrated that cell surfaces moved in concert with underlying actomyosin network contractions; i.e. there may be strong frictional force or drag force between the actomyosin network and the overlying plasma membrane (Fig. 3.10). Thus, slipping between actomyosin and membrane occurred specifically at apical cell contact zones, and the relationship between cytoskeletal dynamics and cell shape change during apical constriction is more dynamic than existing models (Odell et al., 1981; Sawyer et al., 2010) predict.

To determine if the phenomenon we found is conserved in other systems, we examined *Drosophila* ventral furrow cells (Materials and Methods), in which periodic actomyosin contractions cause apical cross-sectional profiles to shrink in pulses (Martin et al., 2009). We noticed myosin accumulations in some cells even before shrinking of apical profiles began (Fig. 3.2A). Myosin coalesced and moved either

toward or away from stationary membranes, and thus was not well connected to contact zone movements at first (Fig. 3.2B). One or more rounds of myosin enrichment and dissipation occurred in most cells (89%; n=55) before apical profiles began to shrink (Fig. 3.2C–E). These early actomyosin contractions occurred periodically, with a time interval of 75 ± 24s, similar to that previously measured just after this stage, during apical constriction (Martin et al., 2009). Some of the early contractions might contribute to cell surface flattening in *Drosophila*, because apical surfaces are not yet completely flattened at this stage (Dawes-Hoang et al., 2005), although many early contractions were not centripetally directed (Fig. 3.2B). Myosin moved at a faster rate than did nearby contact zones at first, and this difference was significantly reduced later, as also observed in *C. elegans* (Fig. 3.2F). Thus, the early activation of actomyosin contraction, before apical cell profiles begin to shrink, might be a conserved feature of apical constriction.

We hypothesized that a change in the apparent efficiency of actomyosin-contact zone connections suggested by our *C. elegans* results might be a secondary effect of changes in viscoelastic properties, for example stiffening or softening of actomyosin networks in contracting cells or their neighbors. We tested this in two ways. First, we analyzed a naturally occurring phenomenon. The apical networks in Ea/p cells occasionally failed spontaneously, with centripetally moving myosin particles suddenly springing away from one another (Fig. 3.3A). During recoil, myosin particle movements slowed exponentially, suggesting that the apical cortex behaves as a viscoelastic network (Fabry et al., 2001; Mayer et al., 2010; Wottawah et al., 2005), and initial recoil speeds and their exponential decays were similar

between early and late stages, suggesting little change in cortical tension or stiffness of the network over time (Mayer et al., 2010; Toyama et al., 2008) (Fig. 3.3B). Second, we cut the cortical actomyosin network using a focused UV laser beam and measured initial recoil speed as a quantitative estimate of tension in the network (Fernandez-Gonzalez et al., 2009; Hutson et al., 2003; Kiehart et al., 2000; Martin et al., 2010; Rauzi et al., 2008; Solon et al., 2009). The cortical network recoiled rapidly from cuts in Ea/p (Fig. 3.3B,C), again with little change in initial recoil speed between early and late stages (Fig. 3.3B). Cutting a neighboring cell's cortex produced a recoil that also did not change significantly over time, and that was slower than in Ea/p (Fig. 3.3B), suggesting that network tension is lower in this cell. Thus, the large difference in the degree of coupled movement between early and late stages is accompanied by little measurable difference in the viscoelastic properties of cortical networks. These results reveal that the cortical tension associated with apical constriction (Fig. 3.3D) is established well before apical constriction begins, and suggest that the differences between early and late stages might be explained by a change in efficiency of actomyosin-contact zone connections alone.

These results support a picture in which a continuously coalescing apical actomyosin network adds little cortical tension as it begins to move apical cell contact zones, i.e. the tension involved in coalescing the apical actomyosin network is great compared to the small additional tension required to pull contact zones. Although this model may appear counterintuitive, it is in fact consistent with estimates of forces in other biological systems on this size scale (Grill et al., 2001; Hutson et al., 2003).

Our results build a model of apical constriction in which the relevant cytoskeletal dynamics can run constitutively, transitioning to driving rapid cell shape change at a later time. We speculate that there may exist in this system a molecular clutch – a regulatable, molecular connection between actomyosin networks and contact zones, transmitting the forces generated by actomyosin contraction to the contact zones. Molecular clutches coordinate actin dynamics and adhesion formation in migrating growth cones and cultured cells (Mitchison and Kirschner, 1988). Our results raise the possibility that there might be developmentally regulated clutches functioning in epithelial morphogenesis. Indeed, targeting a cadherin-catenin complex and a Rac pathway prevented the transition to coupled movements, genetically separating coupled movements from contractions in this system (Fig. 3.4, Fig. 3.11, Fig 3.12, and Fig. 3.13). Thus, cadherin-catenin complex members, Rac pathway targets, or proteins that function alongside either might contribute to a clutch. Temporal regulation of actin nucleators at contact zones could also function as a clutch, if actin polymerized in a centripetal direction from contact zones primarily at early stages. In either model, gradual engagement of a clutch would stabilize connections between a contracting actomyosin network and cell-cell boundaries. Alternatively, resistance to a slipping clutch could change over time, for example because neighboring cells lose tension. This alternative appears unlikely because we detected no change in neighboring cell tension over time. Instead, we speculate that the degree of engagement of a molecular clutch might determine the rate of apical shrinking. As apical shrinking proceeds, this rate might be limited

additionally by the rate at which apical membrane can be removed (Lee and Harland, 2010).

Recent work has highlighted a number of actomyosin-based mechanisms that drive cell shape changes in morphogenesis (Kasza and Zallen, 2011; Lecuit et al., 2011; Martin et al., 2010). Periodic contractions of actomyosin networks, flows of actomyosin, and an actomyosin-based ratchet make contributions to changing cell shapes (He et al., 2010; Martin et al., 2009; Rauzi et al., 2010; Solon et al., 2009). Here we found that the actomyosin contractions and cortical tension associated with a cell shape change are established even before the cell shape change begins. Thus, the immediate trigger for apical constriction is not the activation of actomyosin contractions or a change in cortical tension, which highlights the dynamic nature of the connections between the actomyosin cytoskeleton and the sites of cell-cell adhesion as a key area of interest for understanding morphogenesis mechanisms.

Materials and Methods

Strains and worm maintenance

Nematodes were cultured and handled as described (Brenner, 1974). The following mutant and reporter strains were used: MT4417 ced-5(n1812) dpy-20(e1282) IV referred to here as ced-5; MS126 unc-119(ed4) III; irIs16 [tbx-35::NLS::GFP]; JJ1473 zuIs45 [nmy- 2::NMY-2::GFP; unc-119 (+)]; referred to here as NMY-2::GFP, JJ1317 zuIs3 [end- 1::GFP], OD70 ltIs44 [pie-1:: mCherry::PH domain of PLCdelta] (mCherry::PH) (Kachur et al., 2008), PF100 nnIs [unc-119(+) pie-1 promoter::GFP::Dm-moesin437–578 (amino acids 437–578 of D. melanogaster Moesin)] referred to here as GFP::MOE, and LP54 mCherry::PH;

NMY-2::GFP. LP54 was constructed by crossing OD70 mCherry::PH males with JJ1473 NMY-2::GFP hermaphrodites. The NMY-2::GFP; ced-5 and mCherry::PH; NMY-2::GFP; ced-5 strains were constructed by crossing ced-5 hermaphrodites with NMY-2::GFP or mCherry::PH; NMY-2::GFP males, respectively. Imaging was performed at 20°C–23°C for all strains.

RNA interference (RNAi)

RNAi by injection was performed according to a standard protocol (Dudley et al., 2002). Double stranded RNA was injected at a concentration of 100 ng/ul. Embryos were analyzed 22- 25 hours later.

DIC and fluorescence microscopy

Embryos were mounted and DIC images were acquired as described (McCarthy Campbell et al., 2009). Time-lapse images were acquired at 1 μm optical sections every 1 minute and analyzed with Metamorph software (Molecular Devices). Gastrulation was scored by examination of whether the Ea/p cells were completely surrounded by neighboring cells at the time that Ea/p divided. If Ea/p divided without being completely surrounded, we scored gastrulation as having failed. Spinning disk confocal images were acquired and processed as described (Lee et al., 2006). Epifluorescent images to analyze cell fate were acquired and processed as described (Lee et al., 2006). Embryos expressing end-1::GFP or tbx-35::GFP were mounted laterally and GFP images were acquired at gastrulation stages.

Bessel beam plane illumination microscopy and structured illumination

Embryos were mounted onto poly-L-lysine-coated coverslips at a specific angle such that the ventral surface was facing the detection objective and the long axis of the embryo was perpendicular to the path of the Bessel beam. The sample chamber was filled with egg buffer (Hepes pH 7.2 25mM, NaCl 110mM, KCl 4mM, Mg Acetate 5mM, CaCl2 5mM). For timelapse movies, approximately forty 200nm thick optical sections were captured every three seconds with both 488nm and 561 nm linear excitation. For whole embryo renderings, 5-phase structured illumination was combined with Bessel beam plane illumination. Point spread functions were calculated, and images were translated and deconvolved as previously described (Planchon et al., 2011). Three-dimensional renderings were created using Amira software (Visage Imaging). Resolution for whole embryo is 194 nm, 238 nm, 419 nm in x, y, z respectively for myosin and 217 nm, 264 nm, 472nm for membrane.

Analysis of F-actin, myosin and membrane dynamics by spinning disk confocal microscopy

Myosin and F-actin were filmed using a fluorescently-tagged non-muscle myosin II heavy chain and a fluorescently-tagged actin binding domain of moesin. Ventrally placed embryos were generally imaged beginning shortly before or just as MSa/p cells divided, as Ea/p apical flattening had completed or almost completed by this time in ventrally-mounted embryos, allowing collection of images of the entire apical surface of cells by 1- or 2-plane spinning disk confocal microscopy. Images were acquired of NMY-2::GFP (Nance et al., 2003) and mCherry::PH (Kachur et al., 2008), or GFP::MOE and mCherry::PH, every 3 or 5 seconds, either during a stage we define as the early stage (from Ea/p birth to 8 minutes after the MSa/p cells divided) or during the late stage (8 or more minutes after the MSa/p cells divided),

unless otherwise indicated, imaging in two planes as diagrammed in Fig. S2. Kymographs were made using Metamorph software. The MTrackJ ImageJ plugin was used to track myosin particles and calculate myosin velocities. To calculate slipping rates, ImageJ software was used to generate kymographs of individual myosin particles and nearby apical cell-cell contact zones. The velocities of myosin and membrane were each calculated. The difference in speed (along the axis of myosin movement) between myosin and membrane was determined. Quantum Dots (Molecular Probes) were applied to cell surfaces on devitellinized embryos, n=6 Quantum Dots in three embryos.

Imaging and analysis of *Drosophila* ventral furrow

mat-67; spider-GFP squash-mCherry/TM3 Drosophila embryos (a gift from Adam Martin and Eric Wieschaus) were collected over a 4 hour period. Embryos were devitellinized by 10% sodium hypochlorite treatment for 5 minutes, and mounted on their ventral sides in halocarbon oil. Three planes that were 1.5 μm apart for each of squash-mCherry and spider-GFP were taken every 5 seconds. The three merged planes of squash-mCherry and a single plane of spider-GFP were used for analysis. Movies that we generated, as well as movies kindly provided by Adam Martin that began earlier than analyzed before (Martin et al., 2009), were analyzed with Metamorph and ImageJ software. Membrane and myosin containing patches were tracked along the same axis, and the rates were determined. Myosin rates were subtracted from membrane rates and plotted before apical shrinking and during apical shrinking. To measure myosin fluorescence intensities and apical area over time, ImageJ was used to measure apical area in the most apical plane. Three

planes of myosin were merged, and maximum fluorescence intensity was measured. Apical area and myosin intensity were then plotted as a ratio over the initial measurement, over time before and during apical shrinking.

Analysis of Ea/p apical constriction speeds

Three 2-micron steps of ventrally placed wild-type or *cadherin/hmr-1* depleted embryos expressing mCherry::PH were taken every 5 seconds. The z-planes were merged, and the apical area was calculated every 25 seconds using ImageJ software. An average radius was calculated based on the area. To calculate closure speed, the radius at each time point was subtracted from the average of the prior three time points. Early timepoints tended to show little or no decrease in area, contrary to a linear trend. We tested whether the data fit, or failed to fit, a linear trend, by fitting the data from all 10 4 recordings (in Fig. 1D) to a linear and then a quadratic trend by standard methods, via regressions with dependent errors, with the error process represented as a second order autoregressive model. We found that the fit was indeed best (the Akaike information criterion was minimized) for the quadratic trends vs. the linear trends in nine out of ten of the curves, and the coefficient for the quadratic term was significant for each of these nine models. This result provides convincing evidence of a non-linear trend in the data, with early timepoints showing little or no decrease in apical area.

Computer simulation

A program was written with the goal of simulating apical network contractions with varying efficiency of connection to contact zones using minimal assumptions. The program is available upon request. In the program, a coalescence center point

is chosen at a distance from a contact zone, particles are drawn at randomized angles and distances from this center, and particles are moved toward the coalescence point at a speed proportional to their individual distances from the center, to simulate marks placed on a homogenously contracting two-dimensional sheet. A single contact zone is drawn and moved either not at all, or at a fraction of the speed that particles at the same distance would move equivalent to the percent efficiency of connection, or at the same speed as particles at that distance would move, to simulate 0 to 100% efficiency connection between the contact zone to the contracting network. The program reports the speed of movement of particles along one axis, just as we measured from cells. The speed of contact zone (membrane) movement in the same direction was subtracted from this, resulting in velocities near zero when particles and contact zones moved in concert, positive values when particles moved faster than a contact zone along the same direction, and the most negative values when they moved in opposite directions (for example, for particles on the opposite side of the coalescence point, the side further from the contact zone). Iterations were run with randomized distances between the coalescence center and the contact zone to generate the data graphed in Fig. S5. The y intercept for 0% coupling simulation data was assigned a value matching an average speed specifically for myosin particles near contact zones, which we measured in cells during the early stage, 4.70 μm/min.

Analysis of myosin dynamics during spontaneous network failures and after laser-cutting

For spontaneous failures, myosin images at t_i (initial timepoint) and t_f (final time point) were acquired and overlain. Using Metamorph software, the distance at

which myosin particles moved during the meshwork failures was measured, and a speed was calculated. These myosin speeds were then plotted against the distance of myosin particles from the center of the failure. To measure half-life, rates for myosin punctae that were within 1 μm of the meshwork failure were measured for 3 time points. An exponential curve was fitted along the graph, resulting in an R2 value of 0.91 for the early stage and 0.99 for the late stage, and $T_{1/2}$ was determined for each. Laser-cutting of the cell cortex was performed using a UV laser as in reference 14 using a single 3-ns pulse in each case. Sudden outward movement of myosin particles and failure of cells to lyse upon focusing the laser on the cell cortex of NMY-2::GFP expressing embryos were interpreted as disruptions to the cell cortex that did not 5 similarly disrupt the plasma membrane. Recoil speed was calculated using radial kymographs centered at each cut site, tracking recoiling myosin particles within 4.7 μm of each cut site.

Analysis of myosin and membrane movements

Images were taken every 3 secs or 5 secs, except in Fig. 1B, in which 150 ms intervals were used. The distance of a myosin particle at the end of a track from the center of an Ea/p cell was subtracted from the distance of a myosin particle at the beginning of a track from the center of an Ea/p cell. These values were plotted over time during Ea/p cell internalization. Negative values indicate centripetal myosin movements. Myosin particles were also tracked manually using the mTrackJ plugin for ImageJ software and traced over using Canvas software. For myosin velocity measurements, myosin particles were again manually tracked using the mTrackJ plugin. Approximately five particles were randomly selected per timepoint per

embryo and tracked at 3s intervals. Particles with lifetimes shorter than three intervals were discarded. Velocity was calculated by dividing the net displacement by the time elapsed. Directedness was calculated by dividing net displacement by the total path length of each particle. Myosin and membrane movements were also tracked by PIV using ImageTracker (http://www.cismm.org/downloads). Movements are represented by vectors, showing direction of movement, with the length of each vector proportional to the estimated speed. Vectors were summed over 2-minute periods to minimize the noise of apparently diffusional movements.

FRAP

Photobleaching of NMY-2::GFP was performed on a VT-HAWK (Visitech) microscope, equipped with an Orca R2 camera and a 100X VC Nikon objective. Images were taken every 5 seconds after photobleaching with the 491 nm and 561 nm 50 mW laser at 30% power. For photobleaching, the 488 nm laser was used at 100% transmission for 5 seconds on a region of interest. Nine cases with exponential recovery out of eleven total were used to calculate T1/2 and percent recovery using Prism GraphPad software.

Labeling cell surfaces with Quantum Dots

Gastrulation-stage embryos expressing end-1::GFP to mark the Ea/p cells were divitellinized using a standard protocol (Edgar, 1995; Lee and Goldstein, 2003), with the exception that the egg shells were manually removed in egg buffer instead of Edgar's Growth Medium (EGM) [37]. Quantum Dots (Invitrogen, Qdot 655 IVT carboxyl Quantum Dots) were diluted in egg buffer. Devitellinized embryos were moved to the Quantum Dot suspension, washed 1X with egg buffer and 2X in EGM.

The embryos were then mounted in EGM as described above. Images each for Quantum Dots and end-1::GFP were taken every 3 seconds. Movies were analyzed with Metamorph software.

Figures

Figure 3.1 Actomyosin contraction precedes the rapid shrinking of the apical surface

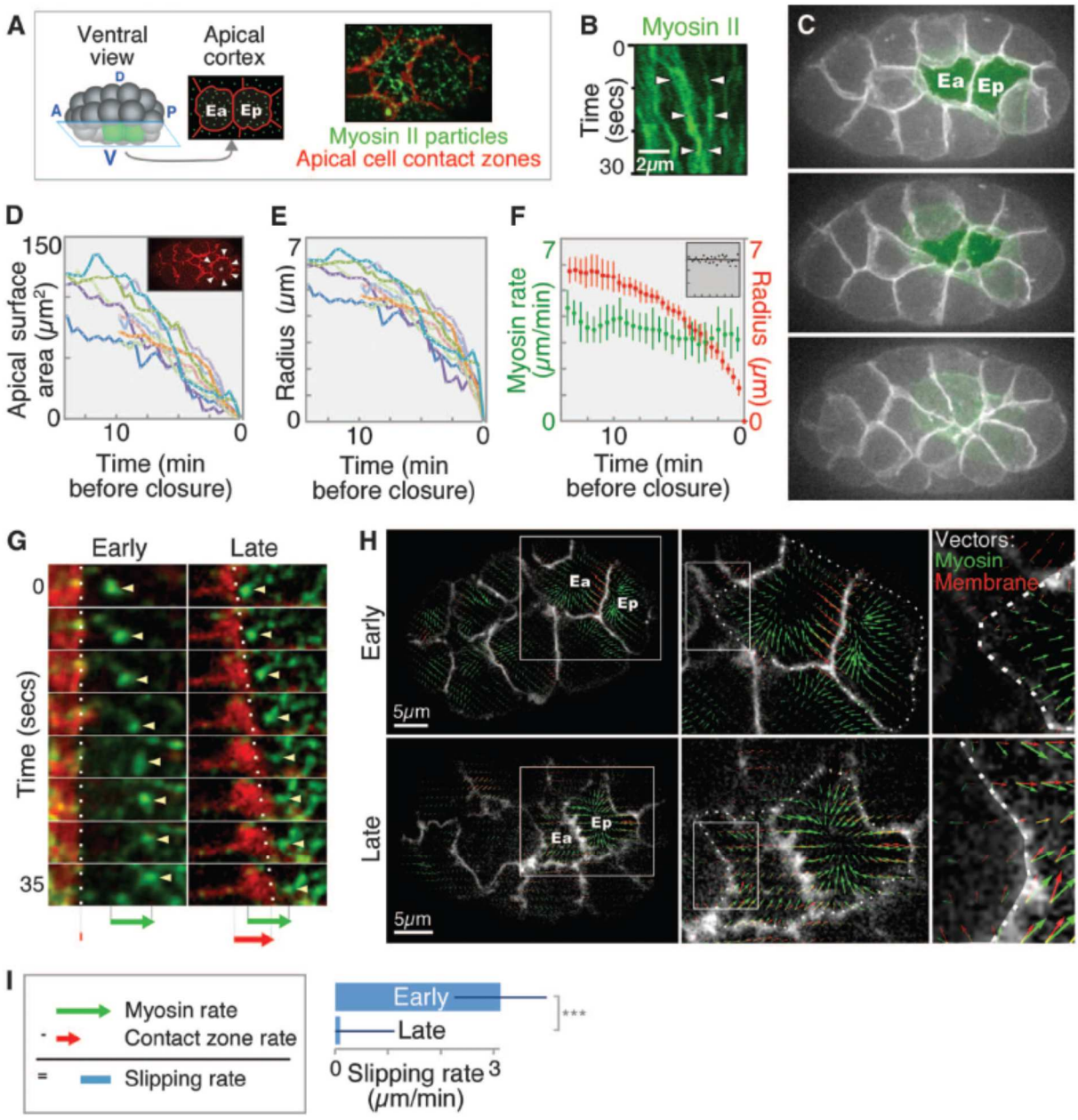

(A) Diagram of imaging method. (B) NMY-2::GFP coalescence (white arrowheads) in apical cortex of Ea/p cell. (C) Shrinking of apical surfaces during gastrulation (projections of 10 1-mm z planes, with Ea/p false-colored). (D) Ea/p cell apical

surface areas over 575 or 825 s (five embryos each) before closure of the apical surface. (Inset) Apical cell–cell contact zones (arrowheads) on Ep (asterisk). (E) Average radius of apical surfaces derived from area measurements. (F) Mean and 95% CI of radius and myosin particle rate over time. (Inset) Myosin directionality (net distance over total distance, vertical scale 0 to 1) over time (time scale: same as larger graph). (G) Movements of individual myosin particles (arrowheads) near contact zones (white dotted lines) in early or late stages of closure. Arrows at bottom indicate relative distances traveled by each. (H) PIV, three magnifications. Boxes indicate enlarged areas. Left to right are whole embryo at plane of Ea/p apical cortex, Ea/p cells (outlined by dotted line), and part of Ea at border with another cell. (I) Slipping rate calculated from individual particles and contact zones ($P < 0.001$, Student's t test).

Figure 3.2. Periodic actomyosin coalescence occurs before apical cell profiles shrink in Drosophila gastrulation

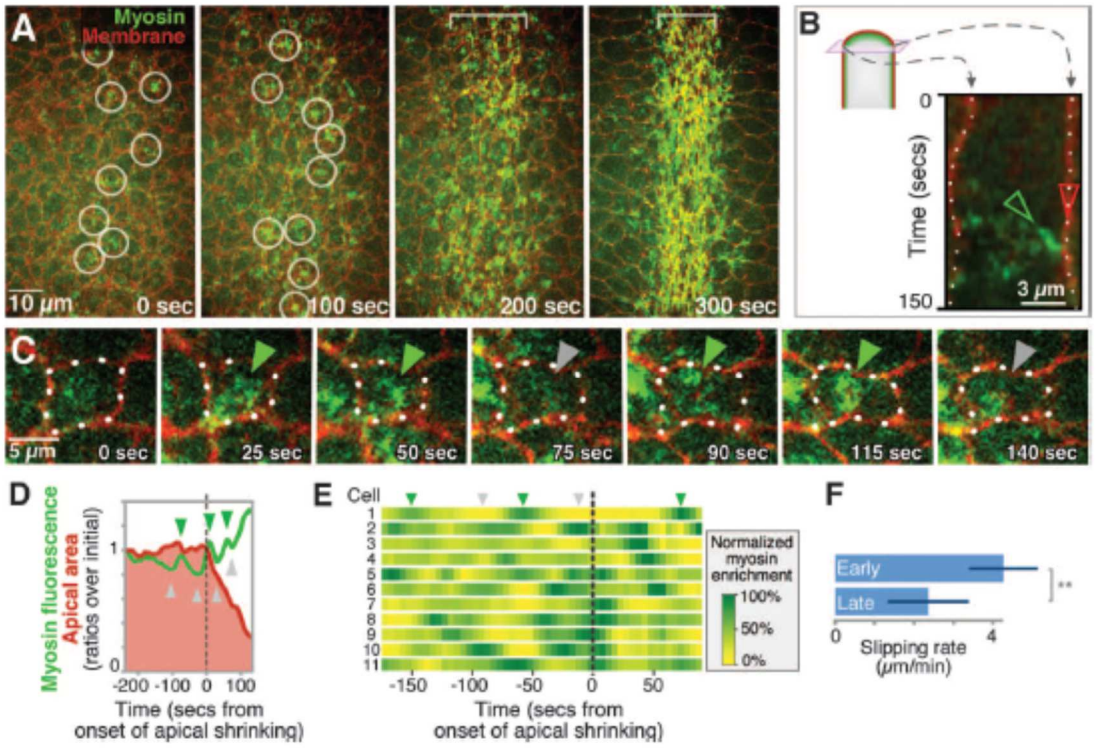

(A) Drosophila ventral furrow formation. Circles mark apical myosin enrichment seen before apical cell profiles began to shrink. (B) Kymograph of a cell (diagrammed) showing myosin (green) movement toward a stationary cell-cell boundary (red) before apical shrinking began. (C) Myosin coalesced (green arrowheads) and dissipated (gray arrowheads) before apical cell profiles began to shrink. This is shown quantitatively from one cell in (D) and from 11 cells chosen at random in (E). Heatmaps in (E) show local maxima of apical myosin levels (three-timepoint running averages of myosin level at each timepoint minus the average of 10 timepoints before and after, normalized to maximum and minimum). Green and gray arrowheads mark one case as in (C). Cell 3 is a rare example in which peaks were not seen before apical shrinking began. (F) Slipping rate, defined as in Fig. 1I, early

(before apical shrinking, n = 33 cells, 3 embryos) and late (during apical shrinking, n = 27 cells, 3 embryos), $P < 0.01$ (Student's t test).

Figure 3.3. Cortical tension associated with apical constricton is established early and changes little as apical shrinking accelerates in *C. elegans*

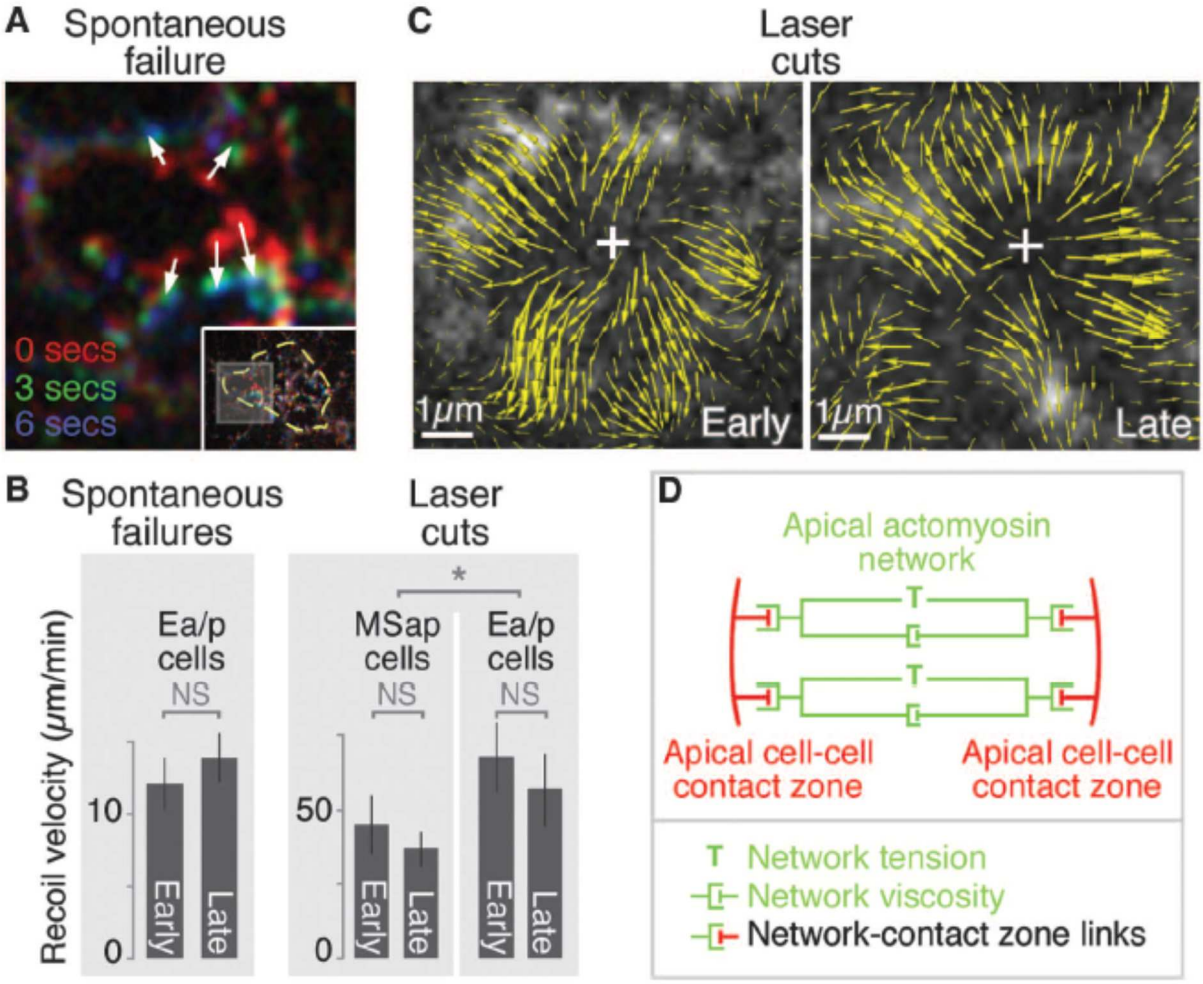

(A) A spontaneous failure, with three timepoints overlain in three colors. (Inset) Entire Ea/p cell apical cortex outlined with enlarged region indicated. Arrows mark individual myosin particles springing apart. (B) Similar data from Ea/p cortical laser cuts done in early or late stages by means of PIV as in Fig. 1H. (C) Initial recoil speeds of myosin particles after spontaneous failures at early (n = 13 myosin particles within 1 mm of center of recoil, six embryos) and late (20 particles, seven embryos) stages, or after laser cuts (48 particles within 4 mm of cut site, seven embryos per stage). Exponential decay T1/2 was 2.20 s in early stages, n = 12

particles; 2.38 s in late stages, n = 20 particles. (D) Working model of forces acting on contact zones (red) and within Ea/p apical actomyosin networks (green, with multiple, interconnected network elements represented as two elements here for simplicity). Results suggest that cortical tension (T) and network stiffness or viscous drag (green dashpots) within Ea/p change little from early to late stages.

Figure 3.4. Targeting classical cadherin and Rac signaling prevents coupled movements but not actomyosin contraction

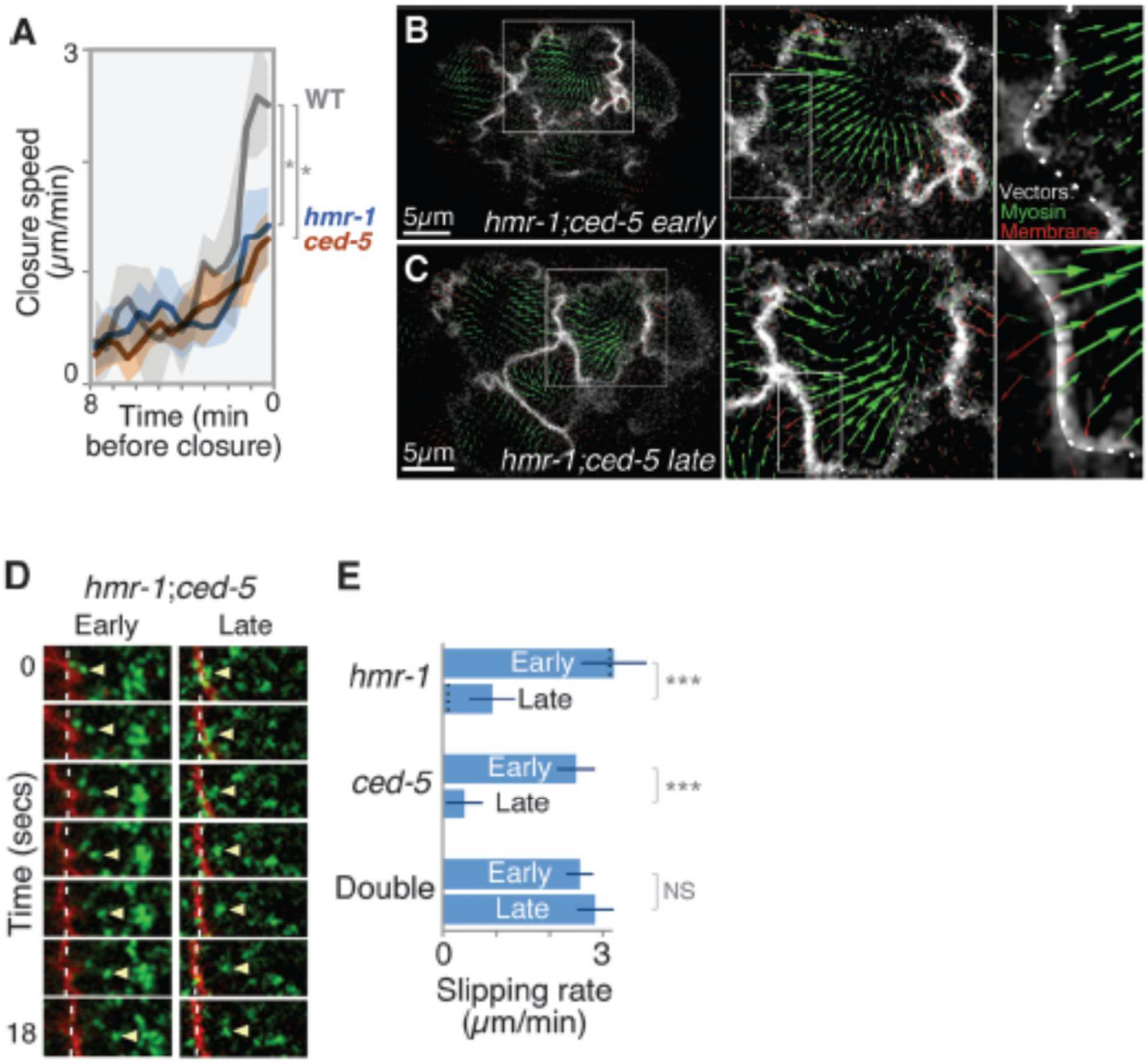

(A) Closure speed (micrometer-per-minute decrease in average diameter) of apical cell areas in *hmr-1(RNAi)* or *ced-5(n1812)* does not reach the speed found in wild-type embryos (*P < 0.05). (B and C) PIV in *hmr-1(RNAi); ced-5(n1812)* doubles. Myosin moves centripetally with little membrane movement in the same direction at either stage. This is shown for individual particles in (D), with quantification as in Fig.

1I in (E). Black dotted lines on *hmr-1* bars in (E) mark wild type for comparison. ***P < 0.001 (Student's t test).

Figure 3.5. Images of myosin and plasma membrane at four timepoints in gastrulation, collected by Bessel beam structured plane illumination (Planchon et al., 2011)

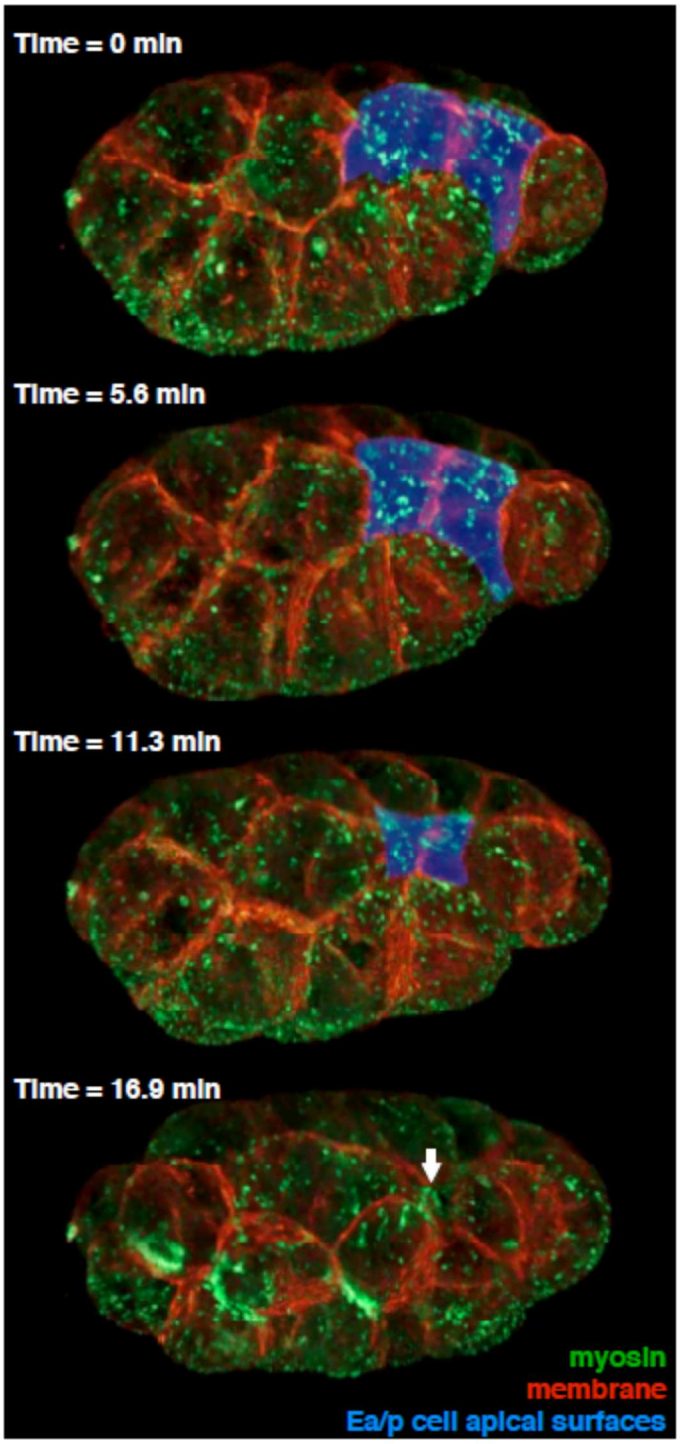

Each of the four timepoints was built from 1510 raw images: 151 200-nm z-planes, 5- phase structured illumination, in two color channels. Exposed surfaces of Ea/p cells are pseudocolored blue. Ea/p cells fully internalize between the third and fourth timepoint. Times are min after the first frame shown. The site of closure of neighboring cells is marked (arrow). Myosin rings can also be seen in some AB-derived cells undergoing cytokinesis in final frame. See Movie S1 for 3-dimensional views at each timepoint.

Figure 3.6. Movements of myosin and F-actin

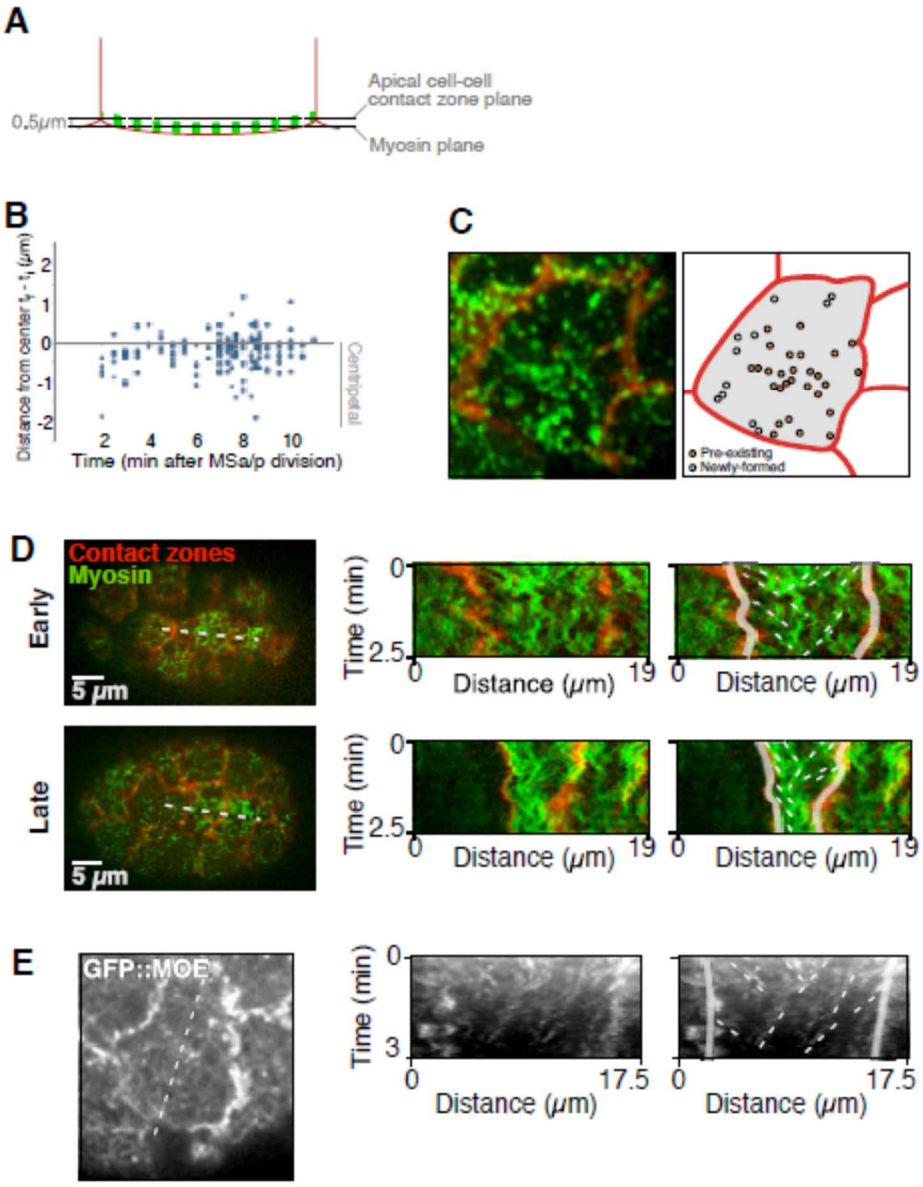

(A) Diagram of imaging strategy used to record apical cell-cell contact zone and apical myosin movements. Imaging planes used for myosin (NMY-2::GFP, green) and contact zones (mCherry::PH, red) were approximately 0.5μm apart. This diagram shows the cell's width relative to the distance between imaging planes as roughly matching the width of a typical cell's apical surface at the beginning of the

early stage (~12μm across). (B) Most myosin particles move centripetally. Graph shows distance of myosin particle from the center of the Ea/p apical surface at the end of a myosin track (t_f) subtracted from the distance at the beginning of a myosin track (t_i). (C) New myosin particles form near contact zones. Myosin particles were tracked for 30 secs, and particles were classified as pre-existing (present throughout the 30 secs) or newly-formed (appearing during the 30 secs) at the end of this period. (D) Myosin particle movements in kymographs. Left image: NMY-2::GFP marking myosin in the Ea/p apical cortex. Center and right: kymograph and diagram respectively of region under dotted line in image at left, with contact zones (solid line) and NMY-2::GFP tracks (dotted lines) traced in the diagrams. (E) GFP::MOE, showing F-actin movements at early stage in a kymograph as for myosin above.

Figure 3.7. The actomyosin network is contractile and dynamic

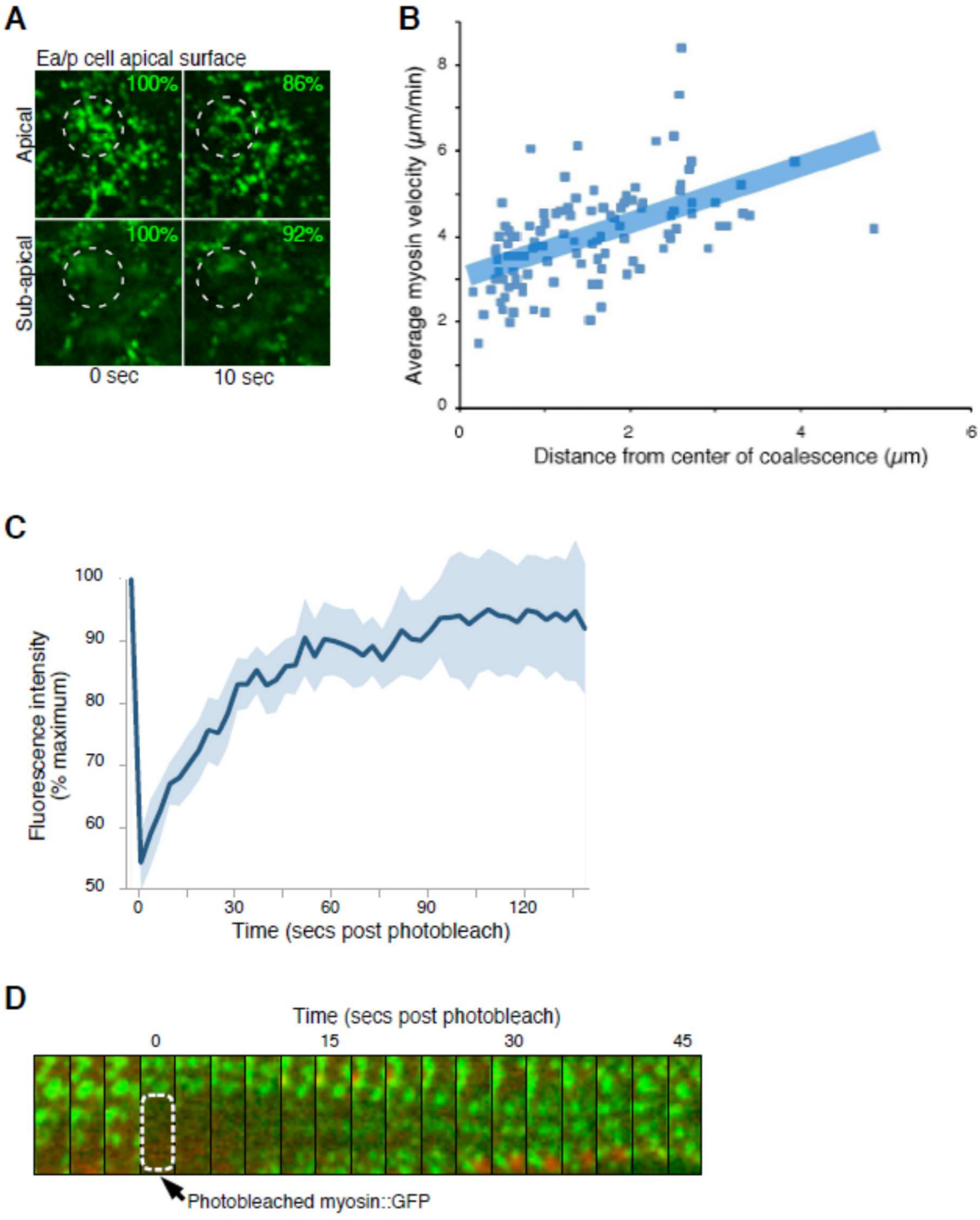

(A) As they moved centripetally, individual myosin particles periodically disappeared. This disappearance appears to represent disassembly of myosin particles rather

than movement out of view, as the particles did not move to a sub-apical plane. Apical plane and 0.5μm basal to the apical plane (sub-apical) are shown at two time points from an NMY-2::GFP labeled embryo. Shown is a cluster of myosin particles that began to coalesce in the apical plane (circled) and then disappeared. The cluster did not then appear in the sub-apical plane. Indicated in green is the average fluorescence intensity for the each circled area expressed as a percent of the initial fluorescence intensity. (B) Speed of myosin particle movement plotted against the distance of each myosin particle from the coalescence center. A linear trendline is indicated. An increase in speed with distance from a coalescence center has been interpreted similarly before, as consistent with contraction of a network in the one-cell embryo (Munro et al., 2004). Speeds near the center of each coalescence were non-zero, most likely a result of some movement of coalescence centers during tracking. (C) Fluorescence recovery after photobleaching (FRAP) of NMY-2::GFP in the apical cortex of Ea/p cells. Plotted is the fluorescence intensity of the bleached region as a ratio of an unbleached region, over time, as a percent of the pre-bleach ratio (n=9 embryos). 95% confidence intervals are indicated in light blue. T1/2 of recovery is 29.3 ± 12.6 s (mean ± 95% confidence). The degree of recovery, with 95% confidence intervals on either side of 100% recovery, indicates no detectable immobile myosin fraction. (D) Montage of photobleached region (outlined in white) recovering over time. Recovery appears to occur both by lateral movements of particles along the apical plane and by exchange of myosin on and off particles; examination of smaller regions where recovery occurred by progressive brightening

of existing particles confirmed that full recovery occurred independently of obvious particle movements (not shown).

Figure 3.8. Diagram of early and late stage movements

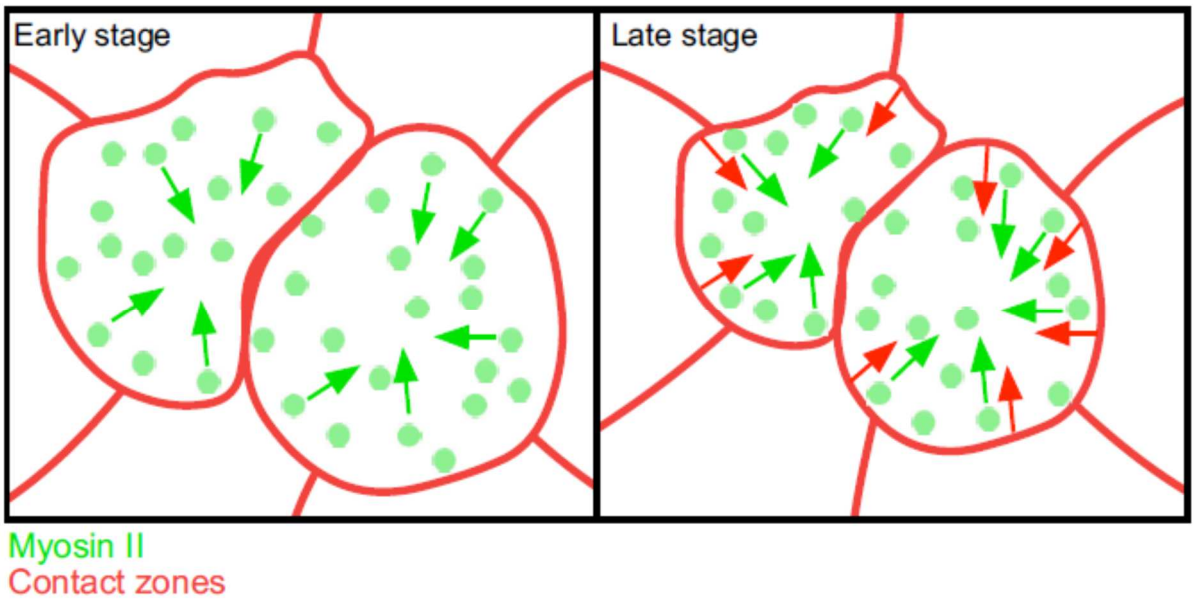

Diagram of a simplified view of myosin particles moving centripetally (green arrows) without much accompanying membrane movement in the early stage, and with membrane movement in concert (red arrows) in the late stage.

Figure 3.9. Estimating the efficiency of actomyosin network-contact zone connection by comparing data from a simulation to data from cells

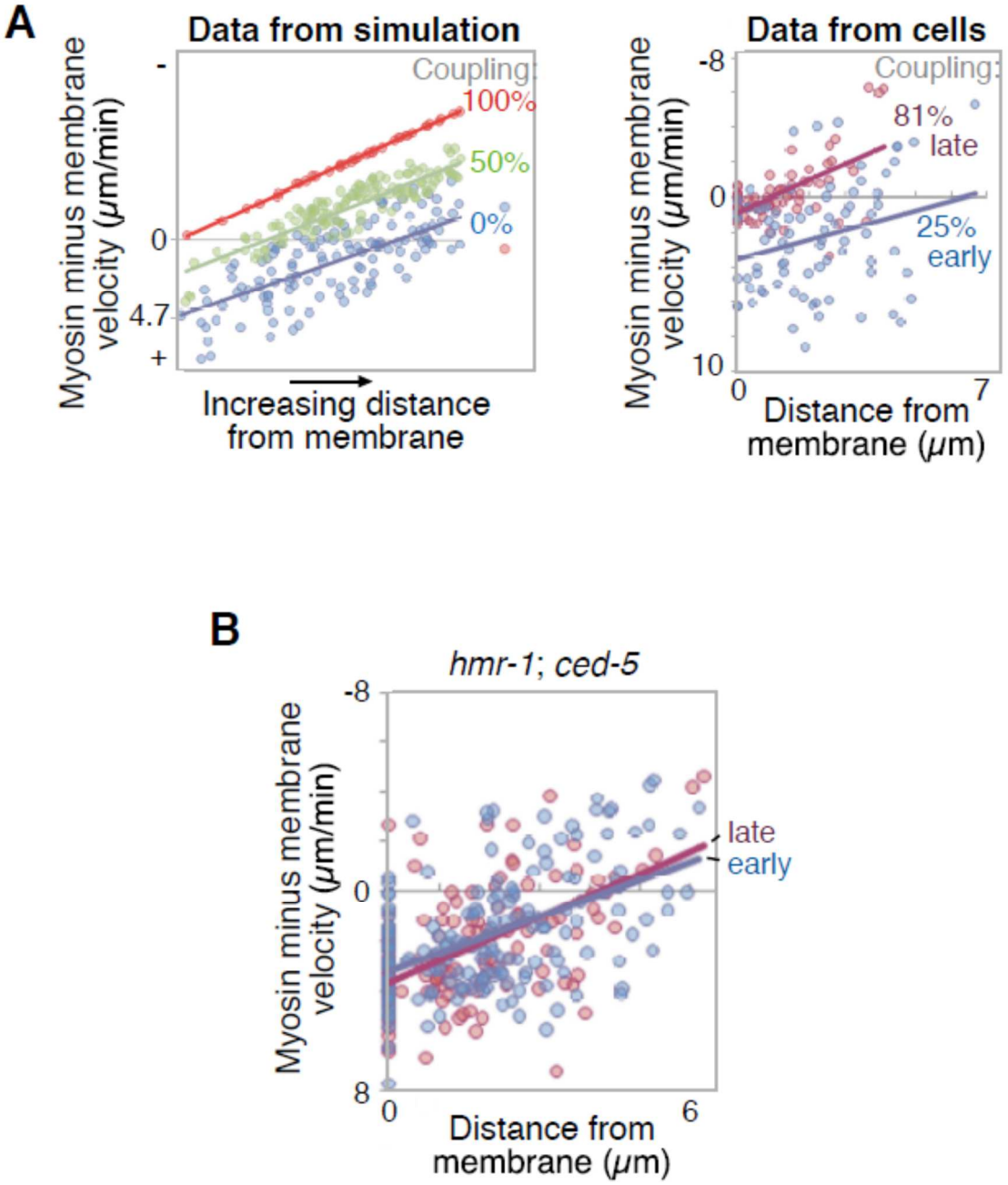

(A)Left: Data from a simulation (See Methods; Movie S6) with myosin particle movements connected to contact zone movements with 0% (blue), 50% (green) or

100% (red) efficiency. Right: Equivalent data from wild-type cells, and (B) from *hmr-1; ced-5* cells.

Figure 3.10. Overlying cell surfaces appear to move centripetally, as the myosin particles do, during the early stage

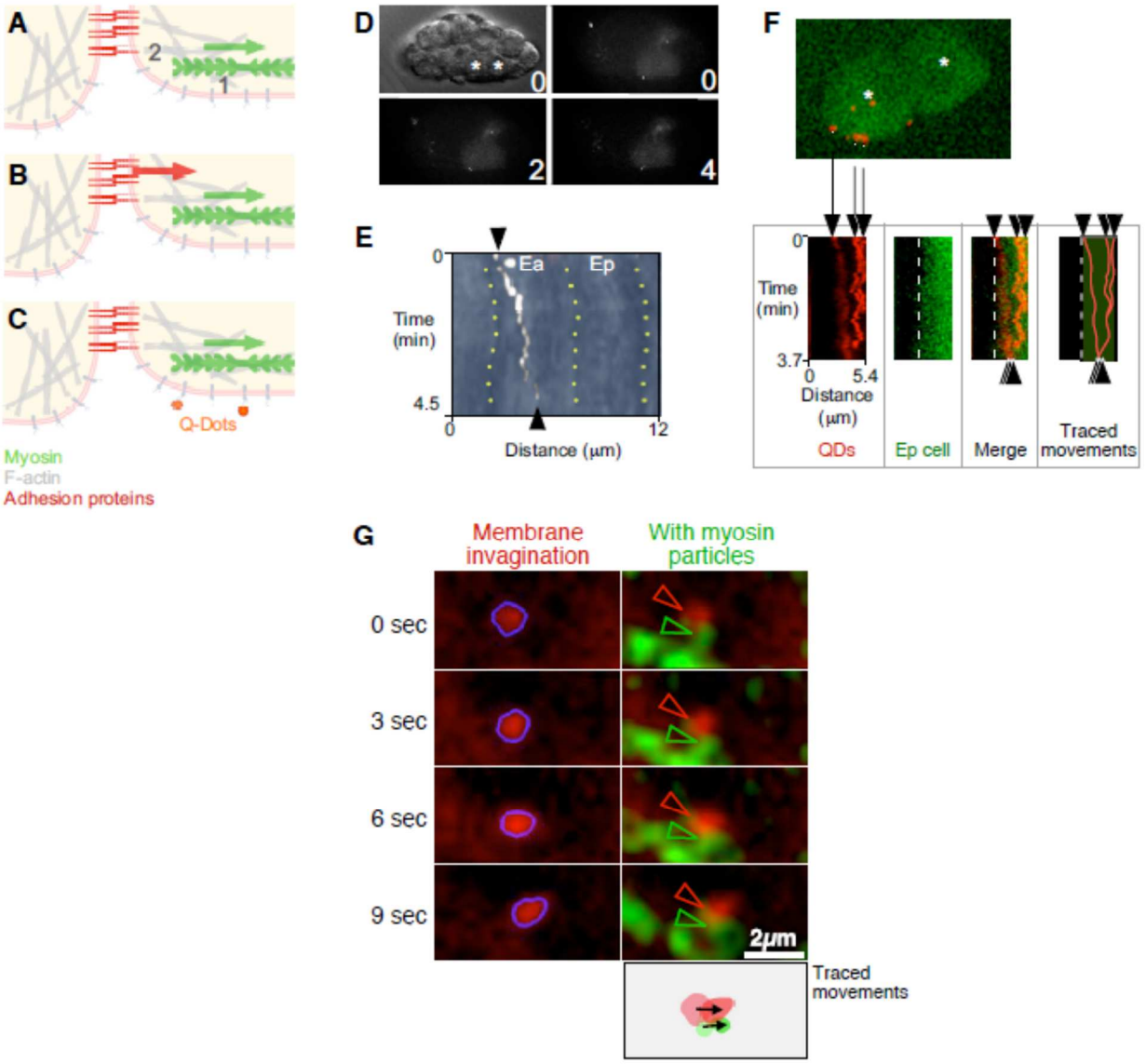

(A-C) Diagrams of myosin (green) and contact zone (red) movement. Our results suggest that apical constriction involves mechanically connecting apical cell contact zones to a dynamic actomyosin network that is already under tension, and actively contracting, before such connections are efficiently established. What is initially unconnected? We hypothesized that the cortical actomyosin network might be poorly connected to the cell surface (A, position 1), as in *Drosophila* cells where

actomyosin can flow in two opposing directions without accompanying movement of nearby membrane protrusions (Rauzi et al., 2010). Alternatively, the actomyosin network might be poorly connected specifically to the contact zones (A, position 2). (B) Diagram of coupled myosin and contact zone movements in the late stage. (C) To distinguish between these models, we used Quantum Dots (Jaiswal and Simon, 2004) as stably fluorescent fiduciary marks on cell surfaces. Quantum Dots applied to cell surfaces are presumed to associate nonspecifically with surface macromolecules of the extracellular matrix or glycocalyx. (D-F) Quantum Dots placed on the Ea/p cell surface moved towards the center of theapical surface (at 3.61 ± 0.88 μm/min) before narrowing of apical surfaces. (D) DIC image of a devitellinized embryo, and corresponding fluorescence images to reveal Quantum Dots. Time is indicated in minutes after the first frame. (E) A kymograph of the Quantum Dot above on the overlying cell surface, with cell boundaries indicated by yellow dots. Black arrowheads mark the initial and final positions of the Quantum Dot, which began near a contact zone, and moved to the center of the apical surface of Ea. (F) Another embryo expressing *end-1::*GFP, marking the Ea/p cells (green), that was devitellinized and coated with Quantum Dots (red), indicated by black arrows on kymographs. The kymograph shows coalescing Quantum Dots (red), with little accompanying centripetal movement of the edge of Ea (green, outlined by dotted white line). Black arrowheads indicate the initial (top) and final (bottom) Quantum Dot positions on the kymograph, and a diagram illustrates the traced movements. (G) We confirmed this result by a second method, examining GFP-labeled myosin particles and nearby spots of enriched mCherry-PH domain marker,

marking PIP2-enrichment, in the apical plasma membrane. mCherry::PH-enriched spots (one is shown, circled in blue), interpreted as membrane invaginations because they were seen in the apical plasma membrane and just below the plasma membrane, moved in concert with neighboring myosin particles. Lower right drawing shows tracings of first and last timepoints above.

Therefore, during the early stage, it appears that connections between the apical actomyosin network and the overlying cell surface are intact, and the apical actomyosin network contractions must fail to cause centripetally-directed plasma membrane movements specifically at the apical cell contact zones, rather than across the entire apical surface.

Figure 3.11. Embryos deficient in cadherin-catenin complex proteins and Rac signaling have gastrulation defects

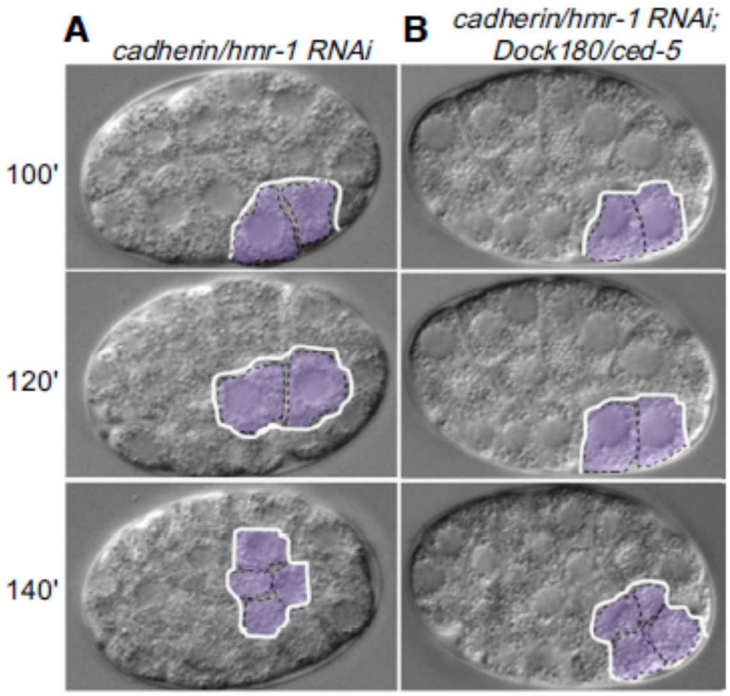

If contact zones become mechanically connected to preexisting actomyosin network contractions as we propose, then we predicted that it should be possible to genetically separate contractions from coupled movements, by identifying genes required for coupled movements and not contractions. We began by examining the sole classical cadherin in *C. elegans*, HMR-1. HMR-1 is localized to cell-cell contact zones in *C. elegans* epithelia, it is required for F-actin attachments to contact zones at later stages (Costa et al., 1998), and it is known to function redundantly in cell-cell adhesion and gastrulation (Grana et al., 2010). We targeted *cadherin/hmr-1* by RNAi and found that shrinking of Ea/p apical cell surfaces did not reach the speed measured in wild-type embryos (Fig. 4), although the Ea/p cells (pseudocolored purple) eventually internalized (A). Given this subtle closure speed defect, we

screened through a set of genes that might act redundantly. (B) Ea/p cells failed to internalize in some double *hmr-1(RNAi);ced-5(n1812)* embryos. See Table S1 for numbers and results from other cadherin-catenin complex proteins and Rac signaling pathway members. Time is minutes after 1st cell division.

Figure 3.12. *hmr-1(RNAi); ced-5(n1812)* embryos appear to have normal endomesodermal cell fates and normal F-actin and myosin localization

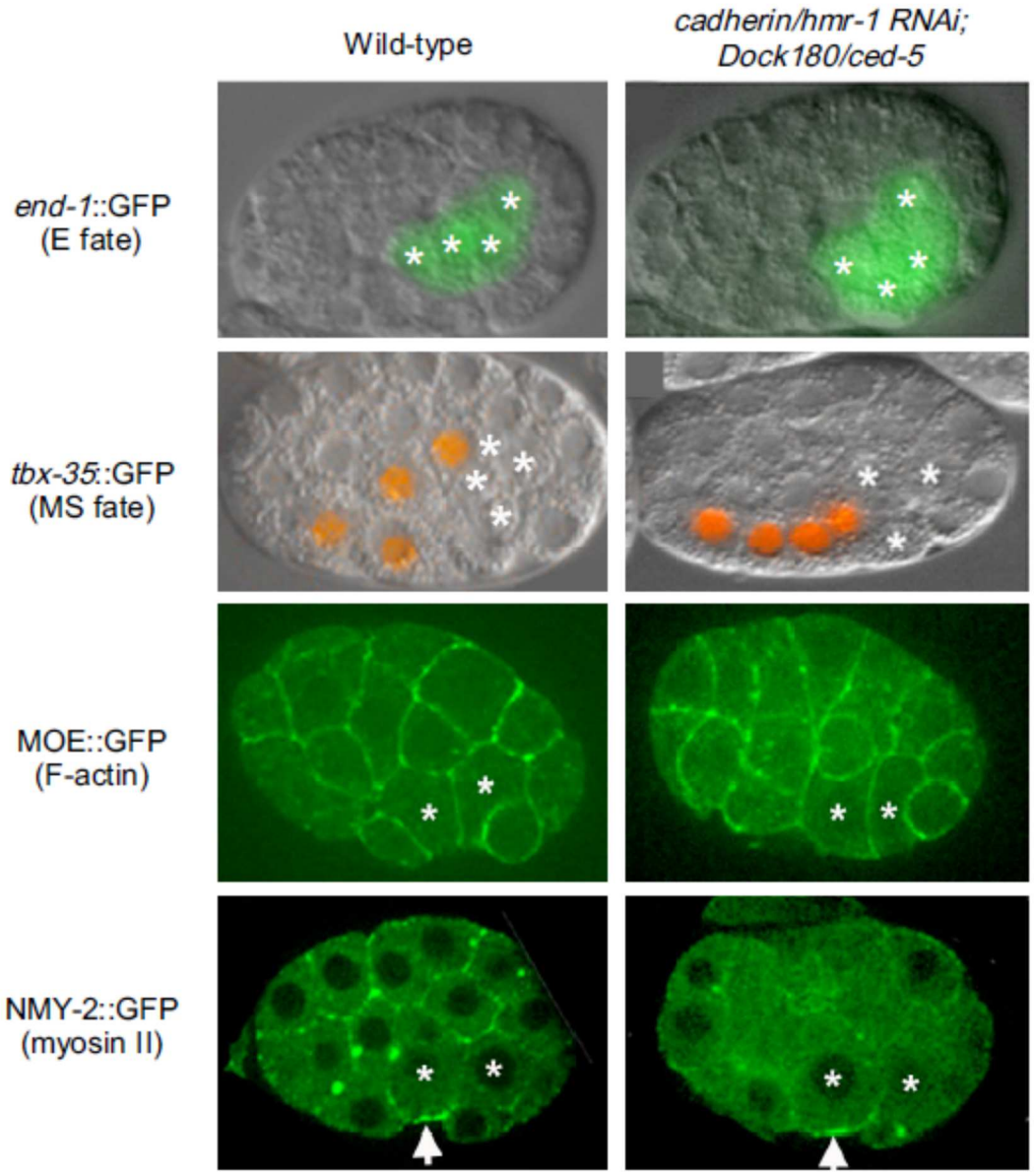

Analysis of wild-type embryos (left panels) and *hmr-1(RNAi); ced-5(n1812)* embryos (right panels). Ea/p cells are marked by asterisks. Only those embryos that exhibited Ea/p cell internalization defects in *hmr-1(RNAi); ced-5(n1812)* embryos were included here. Images show normal expression of an E cell fate marker, *end-1::GFP* (n=5/5 embryos), normal expression of an MS cell fate marker, *tbx-35::GFP*, in MS

granddaughter cells (n=3/3), and normal distribution of F-actin (n=13/13) and apically-accumulated NMY-2::GFP (white arrows) in lateral views of embryos (n=5/5).

Figure 3.13. *hmr-1(RNAi); ced-5(n1812)* embryos failed to establish coupled movements during late stages

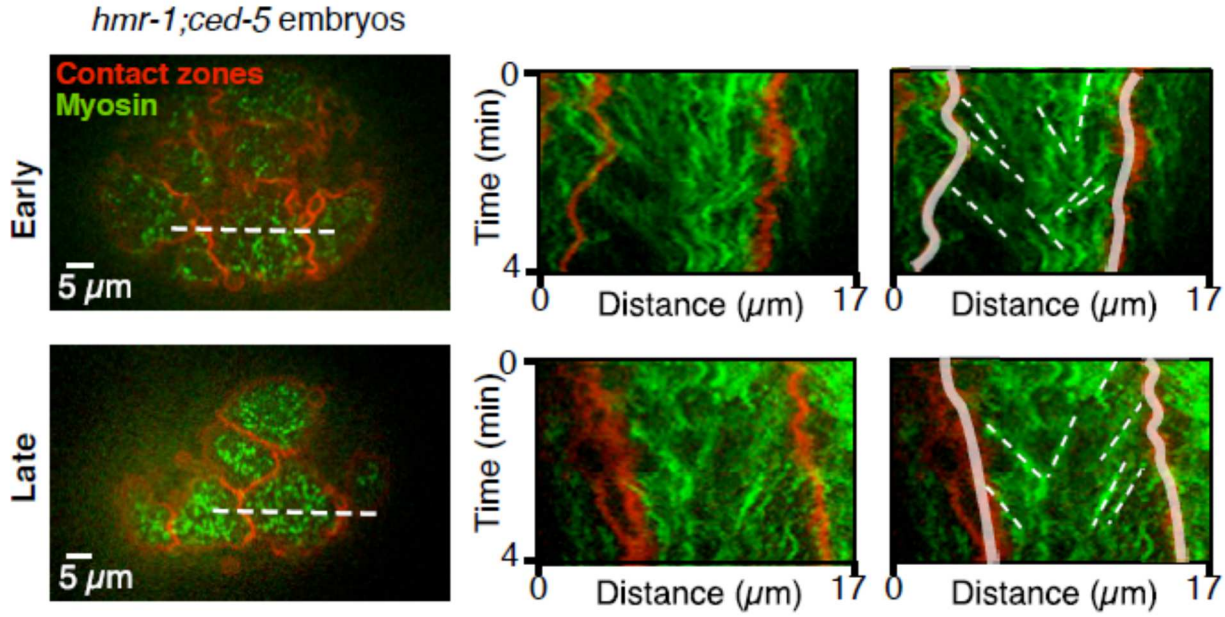

Kymographs (from regions under dotted lines) of myosin (green) and contact zones (red) in *hmr-1(RNAi); ced-5(n1812)* embryos during early and late stages reveal a defect in coupled movements in the late stage. Diagram at right highlights centripetal myosin movements (dotted lines) and contact zones (solid lines).

Figure 3.14. Centripetal myosin movements occurred in multiple cells

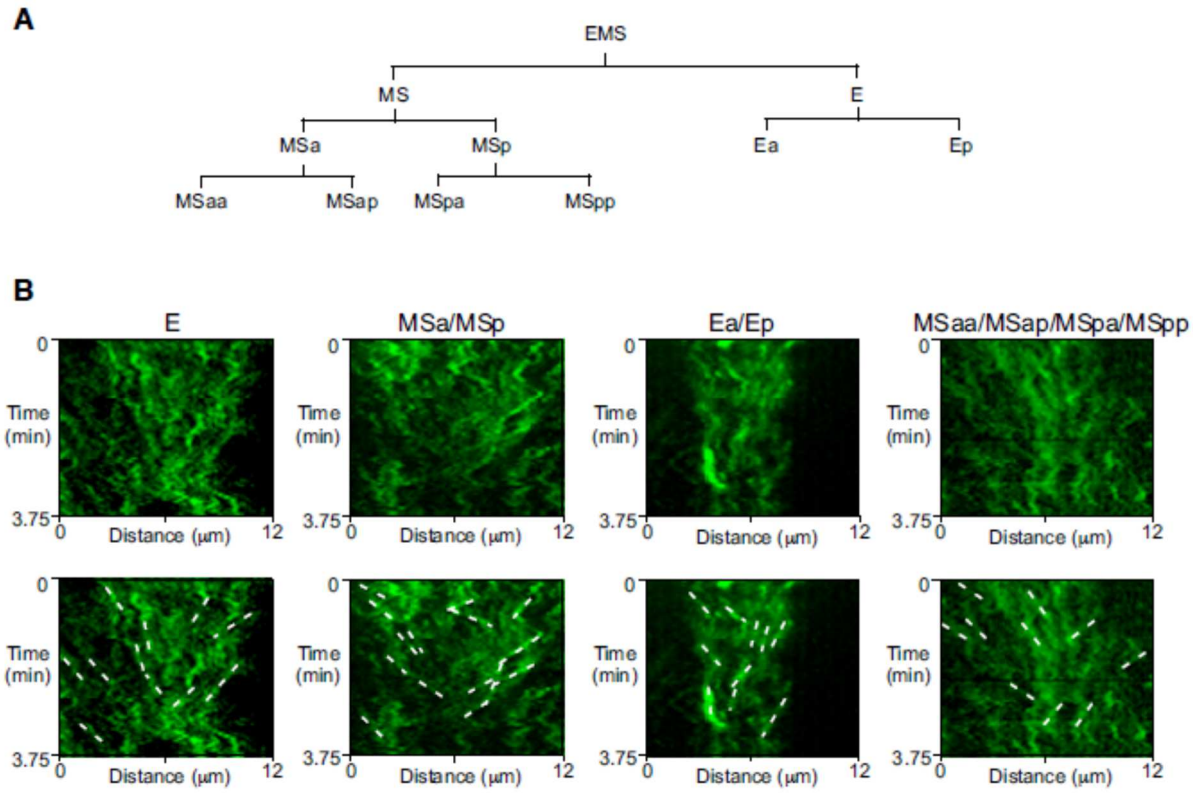

Why would actomyosin contractions begin so early in Ea/p? We speculate that the early actomyosin contractions in *C. elegans* might be a remnant of an actomyosin-based mechanism for capping apical proteins during apical-basal polarization at earlier stages. At the four- and eight-cell stages, actomyosin contractions have been implicated in redistributing apical

PAR proteins to a small apical cap on some somatic cells (Lee et al., 2006). Films of basolateral myosin particles from the 8-cell stage through endoderm internalization did not show apical-directed movement in lateral views of embryos, but we found that as in the Ea/p cells, the apical myosin particles moved centripetally in the E progenitor cell at the 8-cell stage, and in other non-internalizing cells after the 8-cell

stage (A) Cell lineage. (B) Kymographs of myosin-GFP in E, MSa/MSp, Ea/Ep, and MSaa/MSap/MSpa/MSpp cells (top panels), with outlined kymographs, showing some centripetal myosin movement in all of these cells (bottom panels). See Fig. 2.15 for PIV analysis. Consistent with the lower amount of activated myosin in non-Ea/p apical cortexes compared to Ea/p apical cortexes [8], these movements appeared slower in a non-internalizing cell than in Ea/p cells during gastrulation (2.34 ± 0.33 μm/min in MSap cells, 3.19 ± 0.14 μm/min in Ea/p cells, $p<0.0001$ by 2-tailed t-test; Fig. 2.15; note that the myosin rate in MSap does not change significantly over time, 2.20 ± 0.49, 2.61 ± 0.71, 2.24 ± 0.55 μm/min at 3 minutes before (n=26), 2 minutes after (n=23), and 8 minutes after MS daughters divide (n=27) respectively, $p>0.35$ for all pairwise 2-tailed t-tests). Our results suggest that the same actomyosin network movements that participate in apical-basal cell polarization starting at the four-cell stage may be co-opted and upregulated in specific cells later in development to drive the internalization of cells, and that the transition between these two events may be mediated in part by connecting the actomyosin network efficiently to the contact zones in only specific cells. Interestingly, while actomyosin flow may position PAR proteins [10], PAR proteins may also regulate myosin activity: Apical PAR proteins have been implicated in actomyosin-based contractions in *C. elegans* and *Drosophila* (Cheeks et al., 2004; David et al., 2010; Munro et al., 2004) and apical myosin localization (Nance et al., 2003) in *C. elegans*. If actomyosin contraction concentrates PAR proteins into apical caps in Ea/p, a feedback loop between PAR protein localization and actomyosin

activity might be responsible for biasing coalescences toward the center of the apical surface of each cell.

Figure 3.15. PIV of Ea and MSap cells at early and late stages

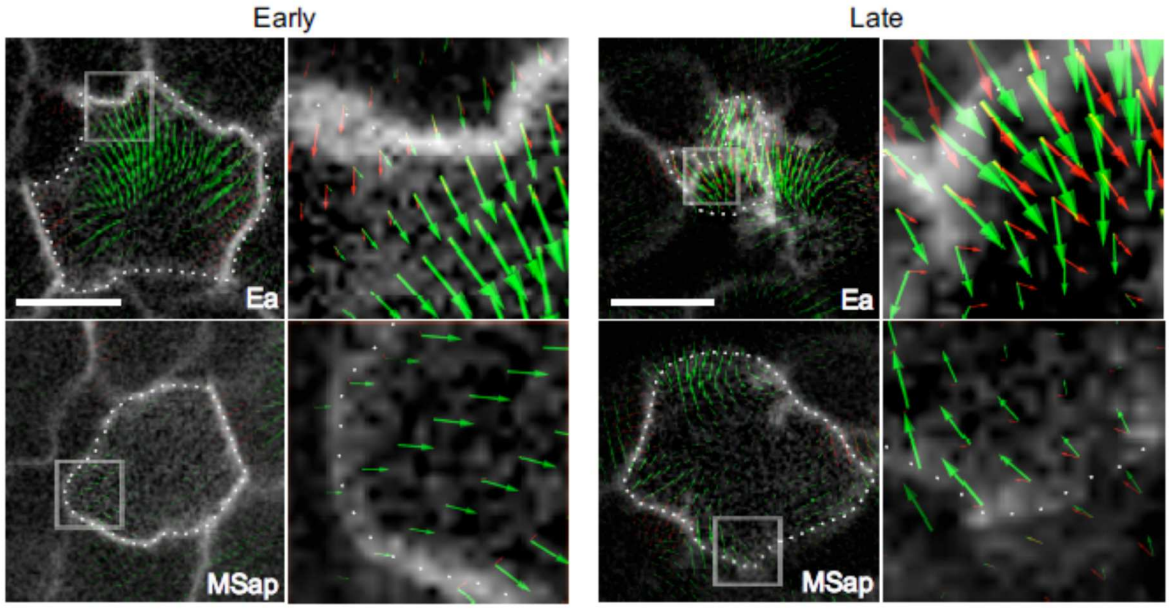

Individual cells are labeled are as in Fig. 3.1H. Scale bars are 5 μm.

REFERENCES

Brenner, S. (1974). The Genetics of Caenorhabditis Elegans. Genetics *77*, 71–94.

Cheeks, R.J., Canman, J.C., Gabriel, W.N., Meyer, N., Strome, S., and Goldstein, B. (2004). C. elegans PAR proteins function by mobilizing and stabilizing asymmetrically localized protein complexes. Curr. Biol. CB *14*, 851–862.

Copp, A.J. and Greene, N.D.E. (2010). Genetics and development of neural tube defects. J. Pathol. *220*, 217–230.

Costa, M., Raich, W., Agbunag, C., Leung, B., Hardin, J., and Priess, J.R. (1998). A Putative Catenin–Cadherin System Mediates Morphogenesis of the Caenorhabditis elegans Embryo. J. Cell Biol. *141*, 297–308.

David, D.J.V., Tishkina, A., and Harris, T.J.C. (2010). The PAR complex regulates pulsed actomyosin contractions during amnioserosa apical constriction in Drosophila. Dev. Camb. Engl. *137*, 1645–1655.

Dawes-Hoang, R.E., Parmar, K.M., Christiansen, A.E., Phelps, C.B., Brand, A.H., and Wieschaus, E.F. (2005). folded gastrulation, cell shape change and the control of myosin localization. Dev. Camb. Engl. *132*, 4165–4178.

Dudley, N.R., Labbé, J.-C., and Goldstein, B. (2002). Using RNA interference to identify genes required for RNA interference. Proc. Natl. Acad. Sci. U. S. A. *99*, 4191–4196.

Edgar, L.G. (1995). Blastomere culture and analysis. Methods Cell Biol. *48*, 303–321.

Fabry, B., Maksym, G.N., Butler, J.P., Glogauer, M., Navajas, D., and Fredberg, J.J. (2001). Scaling the microrheology of living cells. Phys. Rev. Lett. *87*, 148102.

Fernandez-Gonzalez, R., Simoes, S. de M., Röper, J.-C., Eaton, S., and Zallen, J.A. (2009). Myosin II Dynamics Are Regulated by Tension in Intercalating Cells. Dev. Cell *17*, 736–743.

Friedl, P. and Gilmour, D. (2009). Collective cell migration in morphogenesis, regeneration and cancer. Nat. Rev. Mol. Cell Biol. *10*, 445–457.

Grana, T.M., Cox, E.A., Lynch, A.M., and Hardin, J. (2010). SAX-7/L1CAM and HMR-1/cadherin function redundantly in blastomere compaction and non-muscle myosin accumulation during C. elegans gastrulation. Dev. Biol. *344*, 731–744.

Grill, S.W. (2011). Growing up is stressful: biophysical laws of morphogenesis. Curr. Opin. Genet. Dev. *21*, 647–652.
Grill, S.W., Gönczy, P., Stelzer, E.H., and Hyman, A.A. (2001). Polarity controls forces governing asymmetric spindle positioning in the Caenorhabditis elegans embryo. Nature *409*, 630–633.

He, L., Wang, X., Tang, H.L., and Montell, D.J. (2010). Tissue elongation requires oscillating contractions of a basal actomyosin network. Nat. Cell Biol. *12*, 1133–1142.

Hutson, M.S., Tokutake, Y., Chang, M.-S., Bloor, J.W., Venakides, S., Kiehart, D.P., and Edwards, G.S. (2003). Forces for morphogenesis investigated with laser microsurgery and quantitative modeling. Science *300*, 145–149.

Jaiswal, J.K. and Simon, S.M. (2004). Potentials and pitfalls of fluorescent quantum dots for biological imaging. Trends Cell Biol. *14*, 497–504.

Kachur, T.M., Audhya, A., and Pilgrim, D.B. (2008). UNC-45 is required for NMY-2 contractile function in early embryonic polarity establishment and germline cellularization in C. elegans. Dev. Biol. *314*, 287–299.

Kasza, K.E. and Zallen, J.A. (2011). Dynamics and regulation of contractile actin–myosin networks in morphogenesis. Curr. Opin. Cell Biol. *23*, 30–38.

Kiehart, D.P., Galbraith, C.G., Edwards, K.A., Rickoll, W.L., and Montague, R.A. (2000). Multiple Forces Contribute to Cell Sheet Morphogenesis for Dorsal Closure in Drosophila. J. Cell Biol. *149*, 471–490.

Lecuit, T., Lenne, P.-F., and Munro, E. (2011). Force generation, transmission, and integration during cell and tissue morphogenesis. Annu. Rev. Cell Dev. Biol. *27*, 157–184.

Lee, J.-Y. and Goldstein, B. (2003). Mechanisms of cell positioning during C. elegans gastrulation. Development *130*, 307–320.

Lee, J.-Y. and Harland, R.M. (2010). Endocytosis is Required for Efficient Apical Constriction During Xenopus Gastrulation. Curr. Biol. *20*, 253–258.

Lee, J.-Y., Marston, D.J., Walston, T., Hardin, J., Halberstadt, A., and Goldstein, B. (2006). Wnt/Frizzled Signaling Controls C. elegans Gastrulation by Activating Actomyosin Contractility. Curr. Biol. CB *16*, 1986–1997.

Martin, A.C. and Goldstein, B. (2014). Apical constriction: themes and variations on a cellular mechanism driving morphogenesis. Development *141*, 1987–1998.

Martin, A.C., Kaschube, M., and Wieschaus, E.F. (2009). Pulsed contractions of an actin–myosin network drive apical constriction. Nature *457*, 495–499.
Martin, A.C., Gelbart, M., Fernandez-Gonzalez, R., Kaschube, M., and Wieschaus, E.F. (2010). Integration of contractile forces during tissue invagination. J. Cell Biol. *188*, 735–749.

Mayer, M., Depken, M., Bois, J.S., Jülicher, F., and Grill, S.W. (2010). Anisotropies in cortical tension reveal the physical basis of polarizing cortical flows. Nature *467*, 617–621.

McCarthy Campbell, E.K., Werts, A.D., and Goldstein, B. (2009). A Cell Cycle Timer for Asymmetric Spindle Positioning. PLoS Biol *7*, e1000088.

Mitchison, T. and Kirschner, M. (1988). Cytoskeletal dynamics and nerve growth. Neuron *1*, 761–772.

Mooseker, M.S. and Cheney, R.E. (1995). Unconventional Myosins. Annu. Rev. Cell Dev. Biol. *11*, 633–675.

Munro, E., Nance, J., and Priess, J.R. (2004). Cortical flows powered by asymmetrical contraction transport PAR proteins to establish and maintain anterior-posterior polarity in the early C. elegans embryo. Dev. Cell *7*, 413–424.

Nance, J. and Priess, J.R. (2002). Cell polarity and gastrulation in C. elegans. Dev. Camb. Engl. *129*, 387–397.

Nance, J., Munro, E.M., and Priess, J.R. (2003). C. elegans PAR-3 and PAR-6 are required for apicobasal asymmetries associated with cell adhesion and gastrulation. Development *130*, 5339–5350.

Odell, G.M., Oster, G., Alberch, P., and Burnside, B. (1981). The mechanical basis of morphogenesis. I. Epithelial folding and invagination. Dev. Biol. *85*, 446–462.

Planchon, T.A., Gao, L., Milkie, D.E., Davidson, M.W., Galbraith, J.A., Galbraith, C.G., and Betzig, E. (2011). Rapid three-dimensional isotropic imaging of living cells using Bessel beam plane illumination. Nat. Methods *8*, 417–423.

Rauzi, M., Verant, P., Lecuit, T., and Lenne, P.-F. (2008). Nature and anisotropy of cortical forces orienting Drosophila tissue morphogenesis. Nat. Cell Biol. *10*, 1401–1410.

Rauzi, M., Lenne, P.-F., and Lecuit, T. (2010). Planar polarized actomyosin contractile flows control epithelial junction remodelling. Nature *468*, 1110–1114.

Roh-Johnson, M., Shemer, G., Higgins, C.D., McClellan, J.H., Werts, A.D., Tulu, U.S., Gao, L., Betzig, E., Kiehart, D.P., and Goldstein, B. (2012). Triggering a Cell Shape Change by Exploiting Pre-Existing Actomyosin Contractions. Science *335*, 1232–1235.

Sawyer, J.M., Harrell, J.R., Shemer, G., Sullivan-Brown, J., Roh-Johnson, M., and Goldstein, B. (2010). Apical constriction: A cell shape change that can drive morphogenesis. Dev. Biol. *341*, 5–19.

Solon, J., Kaya-Copur, A., Colombelli, J., and Brunner, D. (2009). Pulsed forces timed by a ratchet-like mechanism drive directed tissue movement during dorsal closure. Cell *137*, 1331–1342.

Toyama, Y., Peralta, X.G., Wells, A.R., Kiehart, D.P., and Edwards, G.S. (2008). Apoptotic Force and Tissue Dynamics During Drosophila Embryogenesis. Science *321*, 1683–1686.

Weijer, C.J. (2009). Collective cell migration in development. J. Cell Sci. *122*, 3215–3223.

Wottawah, F., Schinkinger, S., Lincoln, B., Ananthakrishnan, R., Romeyke, M., Guck, J., and Käs, J. (2005). Optical rheology of biological cells. Phys. Rev. Lett. *94*, 098103.

CHAPTER 4: MYOSIN ACTIVITY POLARIZES THE CADHERIN-CATENIN COMPLEX IN APICALLY CONSTRICTING CELLS

Introduction

Cell-cell adhesion is a hallmark of multicellular life. Animal embryos, in particular, depend on the precise regulation of cell-cell adhesion in order to accomplish morphogenesis (Wu and Yap, 2013). Several adhesion molecules have been identified that function in this context. Among the best-studied examples are the cadherins (Hynes and Zhao, 2000).

Cadherins are single pass transmembrane receptors that undergo homophillic association both in *trans* with cadherins on adjacent cells and in *cis* with cadherins within the same plasma membrane (Wu et al., 2010, 2011). Further, cadherins can associate with numerous intracellular binding partners that can control cadherin localization and function. β-catenin binds to the cytoplasmic tail of cadherin and is essential for linking cadherin to the actin cytoskeleton though α-catenin and potentially other adaptors (Abe and Takeichi, 2008; Knudsen et al., 1995; Yonemura et al., 2010), yet the precise relationship between the cadherin-catenin complex (CCC) and the actin cytoskeleton remains intensely-studied and controversial (Gates and Peifer, 2005). The combination of cadherin homophillic *trans* association and linking to the actin cytoskeleton mechanically couples adjacent cells in a tissue (Borghi et al., 2012). This mechanical coupling is essential to propagate myosin-generated contractile force across a tissue during morphogenesis.

The nature of the relationship between myosin activity and the distribution and function of the CCC *in vivo* remains unclear. Most studies have relied exclusively on cultured mammalian epithelial or endothelial cells such as MDCK cells adhered to glass or plastic dishes. Further, these studies have produced contradictory results: some suggesting a positive relationship between myosin activity and CCC recruitment to junctions (Shewan et al., 2005) and others suggesting that myosin activity inhibits junction formation (Daneshjou et al., 2015; Toret et al., 2014). While cultured mammalian cells are amenable to experimental manipulation and live imaging, the mechanical microenvrionment of life on a glass dish may not accurately recapitulate the *in vivo* context.

Some *in vivo* studies have shed light on the relationship between upstream regulators of cytoskeletal dynamics and CCC distribution in a developmental context. Myosin has been shown in the early *Drosophila* embryo to be required for the remodeling of cadherin at cell-cell contacts in a planar polarized fashion (Bertet et al., 2004). Also, the folded gastrulation (Fog) pathway, a signaling cascade upstream of Rho-GTP and myosin activation is required for apical concentration of Armadillo, the Drosophila β-catenin homolog. Further, ectopic expression of Fog pathway components recruits Armadillo ectopically to the apical junction (Kölsch et al., 2007). Later studies showed that the CCC enriched at apical cell-cell junctions concomitantly with activation of apical myosin activity (Martin et al., 2009). Finally, actin cytoskeletal architecture appears important for regulating cadherin distribution as disrupting the linear actin nucleator Diaphanous in early embryonic *Drosophila* cells results in a depolarization of cadherin. That is, cadherin is no longer excluded

from contact free plasma membrane (Mason et al., 2013). While myosin has been shown to control cadherin distribution in a planar polarized fashion (Bertet et al., 2004), it remains unclear if myosin activity *per se* can regulate the apicobasal distribution of the CCC or if a parallel pathway downstream of Fog or Rho-GTP signaling controls CCC distribution.

Here, we use the early *C. elegans* embryo, a highly experimentally tractable system, to directly address whether and how CCC distribution is affected by the activity of myosin. We study this during an important and conserved developmental cell shape change known as apical constriction. During apical constriction, cells constrict their contact-free or apical surface. Defects in apical constriction in vertebrates are known to result neural tube defects, a debilitating type of birth defect (Wallingford et al., 2013). In the 26-28 cell stage *Caenorhabditis elegans* embryo apical constriction drives the internalization of the endoderm precursor (E) cells. At this stage, the two E cells enrich non-muscle myosin II/NMY-2 at their apical surface (Nance et al., 2003). NMY-2 assembles into distinct punctae that move centripetally along with the apical actomyosin meshwork (Roh-Johnson et al., 2012). Tension generated within this meshwork (Roh-Johnson et al., 2012) is thought to be transmitted to the E cells' apical cell-cell contacts, driving apical E cell surface area shrinkage. Finally, the *C. elegans* gastrula provides an excellent system to address the question of how myosin regulates cadherin distribution because it contains cells that display both differing levels of myosin and cortical tension (Roh-Johnson et al., 2012) allowing us to explore how physiological ranges of myosin activity and tension affect cadherin localization.

During E cell internalization, the CCC acts in parallel with a second adhesion molecule, SAX-7/IgCAM, to facilitate cell-cell adhesion (Grana et al., 2010). Thus, both the CCC and SAX-7 provide possible routes through which stresses generated in actin cytoskeleton can do the work of morphogenesis: that is, pulling on the surrounding cells in the embryo. Here, we insert GFP into the endogenous genes encoding all three essential CCC components using CRISPR/Cas9-triggered homologous recombination. Live confocal imaging reveals that CCC components enrich specifically at apical junctions predicted to be under high tension. We show that disrupting myosin activity, either through perturbing its activating kinase, MRCK-1, or by upshifting mutant embryos expressing a temperature sensitive NMY-2 allele, leads to a failure of apical enrichment of the CCC. These results provide the first direct, *in vivo* evidence that myosin activity is directly required for apicobasal polarization of the CCC.

Materials and Methods

C. elegans culture

Worms were cultured and handled as described (Brenner, 1974).

Mounting for imaging

For lateral mounts, embryos were dissected from gravid adults and mounted at the 2-4 cell stage onto poly-L lysine coated no. 1.5 glass coverslips in egg buffer. Embryos were then mounted onto pads composed of 2.5% agarose dissolved in 1x egg buffer.

For ventral mounts, embryos were dissected as above and mounted with a mouth pipette at the 3-4 cell stage such that the EMS cell was facing the coverslip. We used clay feet as spacers to prevent any compression of the embryos between the slide and coverslip.

Spinning disk confocal imaging

All tagged CCC strains and fluorescent transgenes were imaged on a Nikon TiE stand equipped with 50mW diode-pumped solid state lasers of 491nm and 563nm wavelengths, a Yokogawa CSUXI spinning disk head, and a Hamamatsu ImagEM EMCCD camera. Standard conditions for CCC strains were 50% laser power for 400ms exposure with 5x camera gain in 690MHz standard mode.

Image analysis

For lateral mounts, images were first selected from a z stack based on the Ea/Ep nuclei appearing in focus. Images were then filtered through a 1.5 pixel radius Gaussian blur filter in order to prevent outlier pixels from dominating the analysis. Fluorescence intensity was measured by drawing a 5px thick linescan along the Ea/Ep interface starting at the apical junction. We set an arbitrary threshold for the apical domain as the first 5 pixels (~1 μm) measured and the basolateral domain as pixels 10-25 (i.e. 2-5 μm away from the apical domain). We then took the maximum pixel value from each domain for each time point. We measured off embryo background by drawing a small region within ~20 μm of the embryo of interest and measuring average intensity. We calculated this background for each embryo at each timepoint and subtracted it from all measurements.

For ventral mounts, we compiled maximum intensity projections from five one-micron thick Z positions spanning to the apical domain. We then manually drew three pixel thick linescans along the Ea/Ep border, the MSa/Ea border, and the Ep/P4 border and measured the average fluorescence intensity over background along each linescan.

CRISPR/Cas9 triggered homologous recombination

We injected one plasmid with a gene encoding a *C. elegans* codon optimized Cas9 coding sequence as well as a single guide RNA designed to induce a double stranded DNA break within 50 bp of the desired GFP insertion site (Dickinson et al., 2013). We also injected a plasmid encoding GFP and an *unc-119* selectable marker cassette flanked by LoxP sites. Flanking both the GFP and the *unc-119* gene were in-frame genomic homology arms of ~1.5 kb in length. We co-injected with three promoter-mCherry constructs and a plasmid containing a heat-shock inducible *peel-1* toxic gene to select against animals containing extrachromosomal arrays. To tag at or near the N-terminus we used a “broken GFP” strategy. That is, we engineered a repair template to contain a floxed unc-119 selectable marker cassette within a synthetic intron of the GFP gene. We knocked this construct into the N-terminus and isolated non-fluorescent heterozygous knock-ins (i.e. the unc-119 construct disrupted hmp-2 gene function and GFP function at this site). Next, we injected the unc-119 rescued heterozygous knock-ins with a germline promoter driven Cre recombinase. This excised the unc-119 cassette, yielding fluorescent Unc progeny. We were able to recover viable, fertile homozygotes bearing the N-terminal GFP::HMP-2 knock-in.

CCC RNA interference

RNAi by injection was performed according to a standard protocol (Dudley et al., 2002). Embryos were analyzed 18-28 hours later.

nmy-2(ts) experiment

We crossed the cadherin-GFP knockin strain to the *nmy-2(ne3409)* temperature sensitive strain to obtain animals homozygous for both alleles. We reared these animals at 15C, dissected four cell stage embryos from adults and mounted onto coverslips at 17°C alongside cadherin-GFP control embryos (less than 10 min), and returned the embryos to 15°C for 1.5 hours (i.e. the initiation of E cell internalization). Embryos were then upshifted to 26°C and imaged by spinning disk confocal microscopy.

Results

A novel system in which to study *in vivo* roles for the CCC

Previous attempts to study *in vivo* CCC dynamics in *C. elegans* have relied largely on transgene overexpression or knockout-rescue methods (Chihara and Nance, 2012; Maiden et al., 2013; Stetak and Hajnal, 2011). While these approaches have been fruitful for dissecting morphogenetic mechanisms, they have several shortcomings. Namely, transgene expression levels do not necessarily recapitulate normal levels; levels may be susceptible to change over generations due to epigenetic silencing; and the localization of tagged transgenes expressed at non-endogenous levels may not recapitulate that of the native protein (Conine et al., 2013; Seth et al., 2013). Also, protein null knockout alleles are not available for all

genes (Kwiatkowski et al., 2010), so transgene function can sometimes not be verified.

To circumvent these pitfalls and study the dynamics and localization of the CCC at endogenous levels, we used Cas9/CRISPR-mediated homologous recombination to tag the endogenous loci of all three essential *C. elegans* CCC homologs with fluorescent proteins (Fig. 4.7). This approach offers four distinct advantages: 1) since endogenous loci are tagged, all native transcriptional regulatory elements are preserved, 2) 100% of the protein of interest is fluorescently labeled (i.e. there is no unlabeled endogenous population), 3) since the genes tagged here are all essential, the viability of animals carrying the tagged genes reflects the functionality of the tagged proteins, and 4) fluorescence can be used to measure the level of endogenous protein knockdown by RNAi in embryos of specific stages.

We recovered viable homozygous strains with 0% and1% lethality for HMR-1/cadherin-GFP and HMP-1/α-catenin-GFP knock-ins, respectively. Tagging of HMP-2/β-catenin at the C-terminus and two internal loci failed to produce viable strains, suggesting that fusion proteins were non-functional (Fig. 4.7). However, tagging of HMP-2/β-catenin at the N terminus of the *a* isoform produced a strain with 0% lethality (Fig. 4.7). We, therefore, performed all subsequent experiments using the N-terminally tagged strain.

<u>Endogenous fluorescent tagging reveals spatiotemporally non-uniform localization of all cadherin-GFP to sites of cell-cell contact</u>

Examining the localization of fluorescently labelled cadherin-GFP, GFP-β-catenin, and α-catenin-GFP knock-ins by live embryo spinning disk confocal microscopy revealed that each of these components localized to sites of cell-cell contact in early *C. elegans* embryos (Fig. 4.1 A,C). Bright fluorescent punctae of CCC-GFP were particularly abundant in the cytoplasm of 2-4 cell stage embryos (Fig. 6.1A, arrowheads). These likely represent vesicles trafficking additional CCC to the plasma membrane. Furthermore, little signal was detectable at contact-free surfaces consistent with cadherins being constrained to sites of cell-cell contact through homoligation.

The abundance of cadherin-GFP appeared to vary across cell-cell contacts in the early embryo with some cell-cell interfaces containing more fluorescence signal than others (Fig. 4.1 A-D). Also, the intensity of Cadherin-GFP appeared to increase at sites of contact between cells undergoing mitotic rounding and their neighbors. Finally, the distribution of CCC components was non-uniform along individual cell-cell contacts; displaying bright punctae as well as dim regions (Fig. 4.1A-D).

<u>The CCC accumulates to varying degrees at different apical junctions</u>

While several interphase cell-cell contacts displayed some degree of apical CCC enrichment, this pattern was most striking at the contact between the apically constricting endoderm precursor cells, Ea and Ep (Fig. 4.1E, 6.2A). We observed apical enrichment of the CCC that was maintained throughout the late phase of the Ea/Ep cell cycles (Fig. 4.2A-B). We also observed CCC enrichment at borders between Ea and Ep and neighboring cells of various lineages as that was

maintained as the Ea and Ep cell cycles progressed (Fig. 4.3A-B). This enrichment was not uniform across all cell-cell contacts, being brightest and increasing the most at the apical junction between Ea and Ep (Fig. 4.1E, 4.3B).

We next sought to quantify in detail which junctions enriched cadherin over time. While the lateral mounts depicted above were effective for measuring cadherin distribution at some cell-cell interfaces, others were located deep within the tissue, and signal was poor due to the effects of spherical aberration that worsen when increasing depth. Further, in the lateral view, several cell-cell contacts of interest were oriented along the imaging (z) axis, the dimension of poorest resolution for a confocal microscope. To circumvent this problem we ventrally mounted embryos in order to obtain an *en face* (xy) view of cell-cell contacts, and we measured the levels of cadherin-GFP at the regions of the cell-cell contact between the two E cells and between the E cells and their neighbors. The apical intensity of cadherin-GFP displayed the largest fold increase at the contact between Ea and Ep, but also displayed a significant increase between Ea and MSap (Fig. 4.3A-B). However, the level of apical cadherin-GFP did not display a significant increase at the contact between Ep and P4, suggesting that this contact may possess alternative mechanical properties.

Since actomyosin-generated tension is predicted to be highest at the cell-cell contact between Ea and Ep as both cells are actively generating high tension (Roh-Johnson et al., 2012) and since Cadherin-GFP is brightest at this interface, we hypothesized that apically polarized actomyosin tension might be required to enrich the CCC specifically at the apical portion of cell-cell contacts.

To test this, we first examined whether the early, uncoupled actomyosin dynamics described in Roh Johnson, *et al*., might initially strip the CCC away from the membrane accounting for its lower levels early. We then tested the ability to link to the actin cytoskeleton was important for the CCC's apical localization. Finally, we directly tested whether myosin-activity *per se* governed CCC distribution.

Early centripetal myosin contractions do not deplete CCC components from the apical junctions

The early stage (2-8 minutes after the initiation of cytokinetic furrow formation in MSx daughter cells) of Ea and Ep cell internalization is characterized by a high degree of apical actomyosin contractility accompanied by little inward movement of the apical cell-cell contacts (Roh-Johnson et al., 2012). *C. elegans* HMP-1/α-catenin has been shown to possess a functional F-actin binding domain (Kwiatkowski et al., 2010). HMP-1/α-catenin can also bind HMP-2/β-catenin which can bind HMR-1/cadherin, a transmembrane protein. If the interaction between HMP-1/α-catenin and F-actin displayed higher avidity than the interaction between HMP-1/α-catenin and HMP-2/β-catenin or between HMP-2/β-catenin and HMR-1/cadherin, one would expect that HMP-1/α-catenin and/or HMP-2/β-catenin would cotransport with F-actin. Thus, we sought to test whether any CCC components cotransported with actin and myosin during stage at which actomyosin flows centripetally with little corresponding inward movement of cell-cell junctions. To do this, we generate strains co-expressing both-endogenously-tagged catenin-GFP and red fluorescent reporters of F-actin and myosin localization (mCherry-moesin actin binding domain and NMY-2/non-muscle myosin II heavy chain-mKate, respectively). We mounted these embryos ventrally to visualize *en face* centripetal actomyosin dynamics in the E

cells' apical cortices. During the uncoupled phase of apical constriction, we observed robust centripetal myosin and actin dynamics (Fig. 4.4A,C), but we did not observe accompanying movements in α-catenin-GFP. Furthermore, α-catenin-GFP colocalized precisely with a mCherry-PH domain fluorescent plasma membrane reporter. These results suggest that CCC components bind each other with higher affinity than HMP-1/α-catenin binds F-actin.

To test whether CCC components colocalize with each other, we generated a knock-in strain encoding a C-terminal fusion of HMR-1/Cadherin to the red fluorescent protein mKate2. We then crossed this strain to the HMP-1/α-catenin-GFP and GFP-HMP-2/β-catenin separately and imaged embryos by two-color spinning disk confocal microscopy. HMP-1/α-catenin-GFP and HMR-1/cadherin-mKate2 as well as GFP-HMP-2/β-catenin and HMR-1-cadherin-mKate2 colocalized at apical junctions throughout the process of apical constriction. Taken together, these results suggest that the interface between HMP-1/α-catenin and F-actin displays the weaker binding than binding among CCC components, and is the most likely missing link between the CCC and the F-actin cytoskeleton is between HMP-1/α-catenin and F-actin, not among CCC components.

Cadherin requires α and β catenin for apical junction enrichment

Cadherin binds to β-catenin which binds α-catenin which, in turn, binds actin, either directly or indirectly (Nagafuchi and Takeichi, 1989, Fig. 4.2G). We predicted, therefore, that if actomyosin tension was required to enrich cadherin apically, disrupting any link in the cadherin- β-catenin-α-catenin-actin chain would reduce apical enrichment of the CCC. To test this, we designed dsRNAs targeting α-catenin

and β-catenin cDNA sequence, injected them into cadherin-GFP expressing mothers, and assessed the effect on cadherin localization in their progeny embryos.

We first sought to test whether RNAi was effective at depleting the proteins of interest in early embryos. To test the degree of α-catenin and β-catenin knockdown in each individual embryo, we performed side by side by side imaging of uninjected cadherin-GFP knock-in embryos, dsRNA injected GFP knock-in embryos uninjected wild type embryos to provide a baseline for embryonic autofluorescence. All three embryos were positioned within the same field of view, permitting identical imaging conditions between treatments (Fig. 4.8). This analysis revealed that the levels of fluorescence in HMR-1/cadherin-GFP, HMP-1/α-catenin-GFP, and GFP-HMP-2/β-catenin protein knockdown were indistinguishable from the wild type autofluorescence control embryos (Fig. 4.8). That is, the level of knockdown was statistically indistinguishable from 100%.

In the absence of α-catenin or β-catenin, Cadherin-GFP became less apically enriched at the border between the two apically constricting E cells during apical constriction and apical enrichment was not maintained over time (Fig. 4.4 C, D). Unexpectedly, the intensity of cadherin-GFP signal was increased along the basolateral contact between Ea and Ep as well as between other cells in the HMP-1/α-catenin and HMP-2/β-catenin knockdown embryos suggesting that, in some contexts, linking cadherin to the actin cytoskeleton may promote cadherin removal from the membrane (Fig. 4.4). Neither *hmp-1/α-catenin(RNAi)* nor *hmp-2/β-catenin(RNAi)* prevented cadherin-GFP from localizing to the plasma membrane. However, cadherin-GFP became less apically enriched at the border between the

two apically constricting E cells during apical constriction when HMP-1/α-catenin or HMP-2/β-catenin were depleted (Fig. 4.5 A-D). Together these results indicate that in the Ea and Ep cells, the catenins are dispensable for cadherin membrane targeting, but are important for its proper apicobasal polarity.

We next tested whether HMP-2/β-catenin required HMP-1/α-catenin for its apical localization. Unlike HMR-1/cadherin-GFP, GFP-HMP-2/β-catenin remained apically enriched under *HMP-1/α-catenin(RNAi)* conditions (Fig. 4.5G,H). This suggests that HMP-2/β-catenin may associate with the apical junction independently of its link to the actin cytoskeleton. We also noticed that in *hmp-1/α-catenin(RNAi)* embryos, the nuclear exclusion of β catenin appeared reduced, showing near-uniform localization in the nucleus and cytoplasm during interphase and nuclear enrichment during mitosis (Fig. 4.5G).

Actomyosin contractility regulates CCC distribution in apically-constricting cells

To test directly whether myosin activity governed the localization of cadherin during apical constriction we knocked down the myosin activating kinase MRCK-1 using dsRNA injection. We first verified the effectiveness of MRCK-1 knockdown by assessing the gastrulation phenotype in knockdown embryos. 100% of knockdown embryos displayed severe gastrulation defects, with either or both E cells dividing before internalization consistent with effective knockdown of MRCK-1.

We then examined the localization of HMR-1/cadherin-GFP under MRCK-1 knockdown conditions. In MRCK-1 knockdown conditions, the apicobasal polarization of HMR-1/cadherin-GFP was severely disrupted. The accumulation of

HMR-1/cadherin-GFP at the apical junction between the Ea and Ep cells was abrogated, and instead cadherin-GFP accumulated at the basolateral contact between Ea and Ep (Fig. 4.6A,B). Thus, MRCK-1 activity is required for proper establishment of cadherin apicobasal polarity.

To test whether the MRCK-1 might be required for apical cadherin enrichment because of its role in activating myosin, we used a temperature-sensitive allele of the essential early embryonic *C. elegans* non-muscle myosin II homolog to disrupt the function of NMY-2 specifically during E cell internalization. Such an approach was necessary because developmental events preceding E cell internalization such as embryonic polarization at the one cell stage and subsequent cell divisions require NMY-2 function. Previous studies revealed that this allele results in myosin loss of function within 20 seconds of shifting from the permissive temperature (15°C) to the restrictive temperature (26 °C) (Davies et al., 2014). We raised mothers and dissected embryos at the permissive temperature (15°C). After mounting at the four-cell stage, we aged the embryos at the permissive temperature for 2 hours. At this point we shifted the temperature to the restrictive temperature (26°C) and began imaging. At the restrictive temperature, we observed strong disruption in the apicobasal localization of cadherin-GFP. Cadherin-GFP was no longer enriched at the apical junction between the Ea and Ep cells. Instead, we observed ectopic recruitment to the basolateral junction between Ea and Ep, phenocopying the pattern observed in *mrck-1(RNAi)* embryos. In one case, the shift was done after the establishment of the apical cadherin enrichment, and apical enrichment was rapidly lost suggesting that NMY-2 activity is required for both maintenance and

establishment of apical cadherin. This, together with data earlier shifts, suggests that myosin activity is required for both establishment and maintenance of cadherin polarization.

Discussion

In this study, we deployed genome editing technology to study the biology of the cadherin catenin complex during apical constriction, an important developmental cell shape change. Live embryo fluorescence imaging revealed that the cadherin-catenin complex enriches at apical junctions in early embryonic cells undergoing apical constriction. Further, this apical localization requires association both alpha and beta catenins as well as the activity of Myosin 2.

Previous studies using antibody staining and transgene overexpression described the localization of the cadherin catenin complex as largely uniform (*reviewed in* Armenti and Nance, 2012). Our analysis reveals that this is not the case; the CCC enriches differentially both between and within cell-cell junctions of early embryonic cells. Further, the CCC enriches at junctions that are predicted to be under high tension: between apically constricting cells and at the borders of cells undergoing mitotic rounding. Interestingly, different cell lineages displayed differing amounts of CCC at their borders, suggesting that different lineages may be differentially adhesive to others. It will be interesting to know if this lineage-specific enrichment has biological consequences in terms of cell-cell communication, adhesion, or cell positioning. Indeed, HMR-1 is known to have a redundant role in guiding the division plane of the ABar cell which sets up left right asymmetry in the early *C. elegans* embryo (Grana et al., 2010).

In general, we found that depleting proteins required for the CCC to bind the actin cytoskeleton (i.e. α-catenin or β-catenin) results in failure to concentrate cadherin into the apical junction in apically constricting cells. However, GFP-β-catenin still accumulated apically when α-catenin was depleted suggesting that, contrary to conventional models, β-catenin may associate with the actin cytoskeleton independently of α-catenin. We cannot exclude the possibility that α-catenin RNAi did not deplete 100% of the endogenous protein, even though an independent set of experiments confirmed that knocking down α-catenin-GFP reduces embryonic fluorescence to levels indistinguishable from autofluorescent background (Fig. 4.8).

Previous studies from epithelial cell culture have revealed myosin-dependent enrichment of the CCC at cell-cell junctions (Shewan et al., 2005), and *in vivo* studies from *Drosophila* have shown that signaling upstream of myosin activation (i.e. Fog pathway and rho pathway) is required for proper localization of CCC components during apical constriction in ventral furrow cells (Dawes-Hoang et al., 2005; Kölsch et al., 2007; Martin et al., 2009; Mason et al., 2013). However, it was not known whether the effects on CCC localization were due to myosin activity *per se*, or due to an independent downstream effector of the rho pathway. We show that directly perturbing myosin activity, either by depleting a kinase required for its activity (MRCK-1) or by a temperature sensitive mutation in the predominant myosin 2 gene, *nmy-2*, causes a dramatic rearrangement of cell-cell adhesion components. This suggests that the relationship between cadherin recruitment and tension may be complex: in some cases tension stabilizes cadherin and in others it destabilizes it. Indeed, data from cell culture systems paint a complex picture in this regard: some

studies show that myosin activity is important for stabilizing the CCC at cell-cell junctions (Shewan et al., 2005) and others showing that Rac signaling and Arp2/3 branched actin nucleation are important for cadherin stabilization while Rho pathway and myosin activity inhibit junction formation and increase CCC turnover (Daneshjou et al., 2015).

Recent findings indicate that α-catenin can directly link β-catenin (and, thus, cadherin) to the actin cytoskeleton through a direct catch bond with F-actin when α-catenin is under tension (Buckley et al., 2014). In light of this result, we speculate the following positive feedback loop model for apical constriction: Localization of MRCK-1 by cell fate machinery and cell polarity machinery establishes apical actomyosin activity. F-actin binds weakly to α-catenin, then myosin-derived pulling force on F-actin activates a catch bond and enhances α-catenin's actin binding affinity. This improved actin binding affinity reduces the lateral diffusion of the CCC and results in CCC accumulation at the apical junction. Greater levels of cadherin at the apical junction permit improved coupling to centripetal myosin contractions which reduces the circumference of the apical junction, concentrating the same amount of cadherin into a smaller area of membrane. This increased concentration permits yet more efficient coupling between the apical junctions and F-actin, and the apical junctions move inward until the E cells are internalized.

Such a model would help explain instances of apical actomyosin contractions that are not accompanied by corresponding movements of apical junctions (Roh-Johnson et al., 2012). Further, these results highlight the importance of studying

protein localization and dynamics at wild type levels, as biological systems are sometimes sensitive to the precise dose of protein.

It remains unknown mechanistically how myosin positions the CCC at apical junctions. Potentially, tension-dependent linking to the F-actin cytoskeleton reduces the lateral diffusivity of cadherin specifically at apical sites where tension is abundant and this results in cadherin accumulating there. Alternatively, myosin could alter the actin architecture in such a way (i.e. reduce branching or promote cross-linking) as to promote more efficient association between the CCC and F-actin. It will be interesting to dissect the mechanistic contribution of myosin to CCC localization.

Further, we still do not know how or whether SAX-7 associates with the F-actin cytoskeleton. Previous studies show that HMR-1/cadherin knockdown alone does not prevent the timely internalization of the Ea and Ep cells, although there is a subtle delay (Grana et al., 2010). Likely, SAX-7 is providing an independent tension bearing link between apical junctions and the actin cytoskeleton; it will be interesting to learn what this is.

Here, we deploy a novel approach for studying morphogenesis, tagging essential genes at their endogenous loci and measuring their localization and dynamics. We adapt this approach to quantify knockdown effectiveness in a new way: not from bulk protein derived from mixed stage tissue, but in individual embryos at the developmental stage of interest. In the future, this approach could be used to simultaneously quantify the effectiveness of partial RNAi at a site of interest and examine phenotypes. Such an approach would provide the researcher with a rheostat to tune protein levels to any level desired between 0 and 100% of

endogenous expression. We hope that these tools will permit more precise *in vivo* dissection of molecular mechanism.

Figures

Figure 4.1. HMR-1/cadherin-GFP enriches non-uniformly at cell-cell contacts in early *C. elegans* embryos

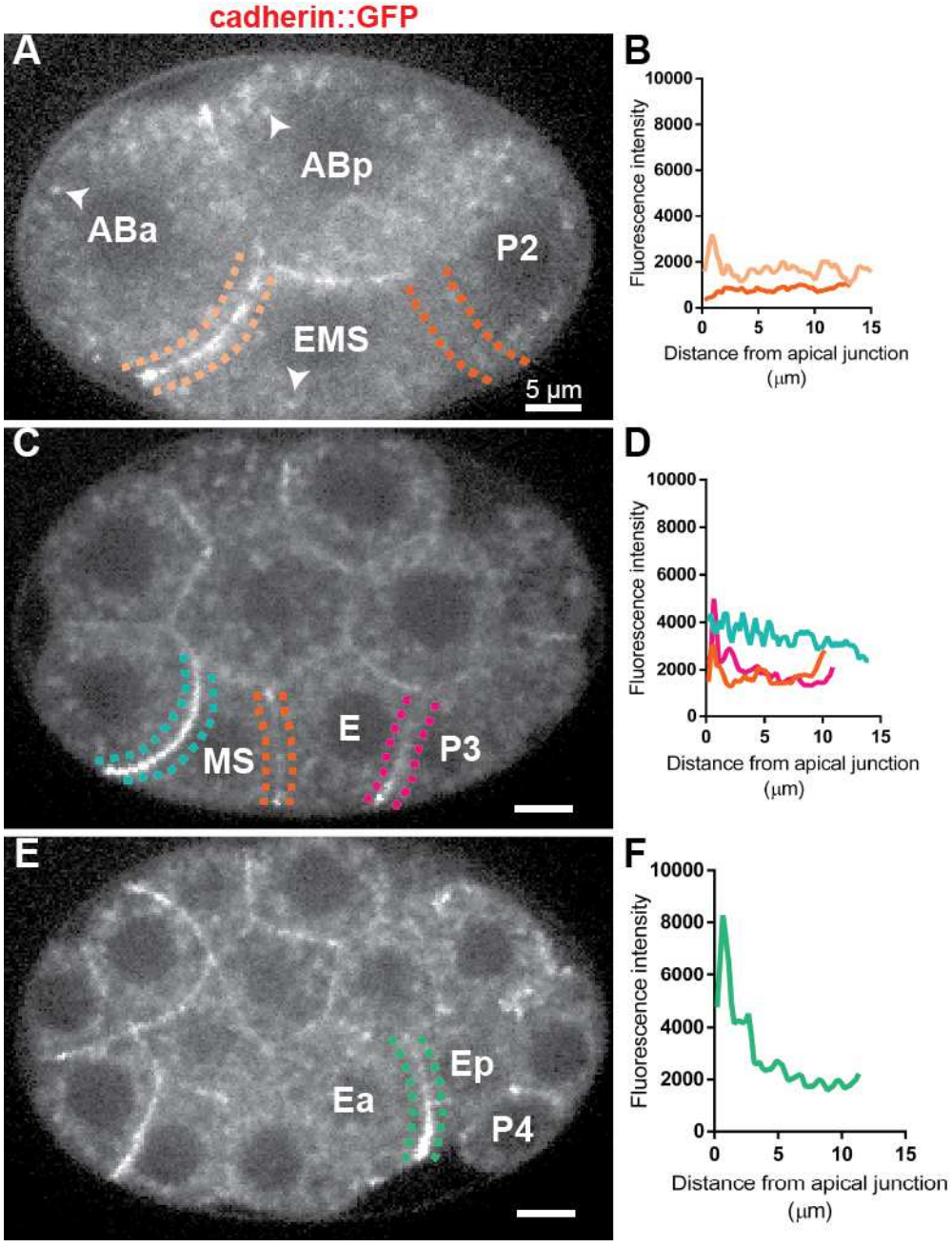

(A,C,E) Spinning disk confocal fluorescence images of HMR-1/cadherin-GFP in embryos at the 4-cell, 12-cell, and 28-cell stages, respectively. Arrowheads in (A)

depict cytoplasmic punctae of cadherin. (B,D,F) Fluorescence intensities along linescans at selected cell-cell contacts in the embryo. Color of linescans corresponds to the color of the outlines circumscribing the borders in (A,C, and E). Note the dramatic increase in intensity at the border between the apically constricting Ea and Ep cells (E,F).

Figure 4.2. Cadherin Catenin Complex (CCC) enriches apically in apically constricting cells

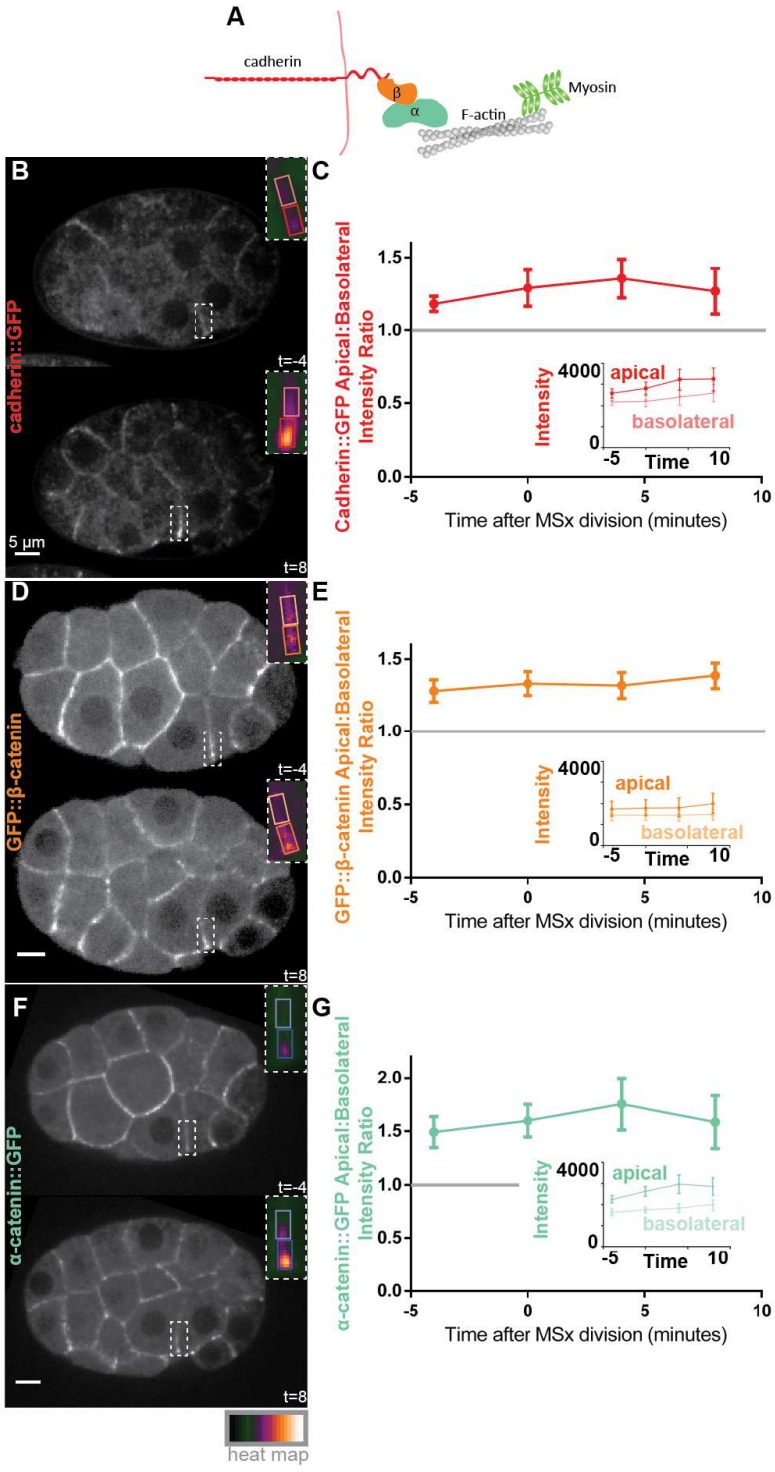

(A) Schematic of the CCC, plasma membrane, F-actin, and non-muscle myosin with colors used to reflect labeling in the figures. (B,D,F) Spinning disk confocal fluorescence images of CCC components tagged with GFP. The border between the apically constricting E cells is highlighted with a dotted white box which is enlarged and pseudocolored in the inset (top right). Areas used for quantification of apical and basolateral intensities in C, E, and G are circumscribed with colored boxes. (C,E,G) Plots depicting apical to basolateral intensity ratio of fluorescence of CCC components. (inset) Apical (dark colors) and basolateral (light colors) fluorescence intensity values over time for all CCC components. All error bars represent 95% confidence interval. * $p<.05$.

Figure 4.3. HMR-1/Cadherin-GFP enriches differentially over time at different cell borders associated with apically constricting cells

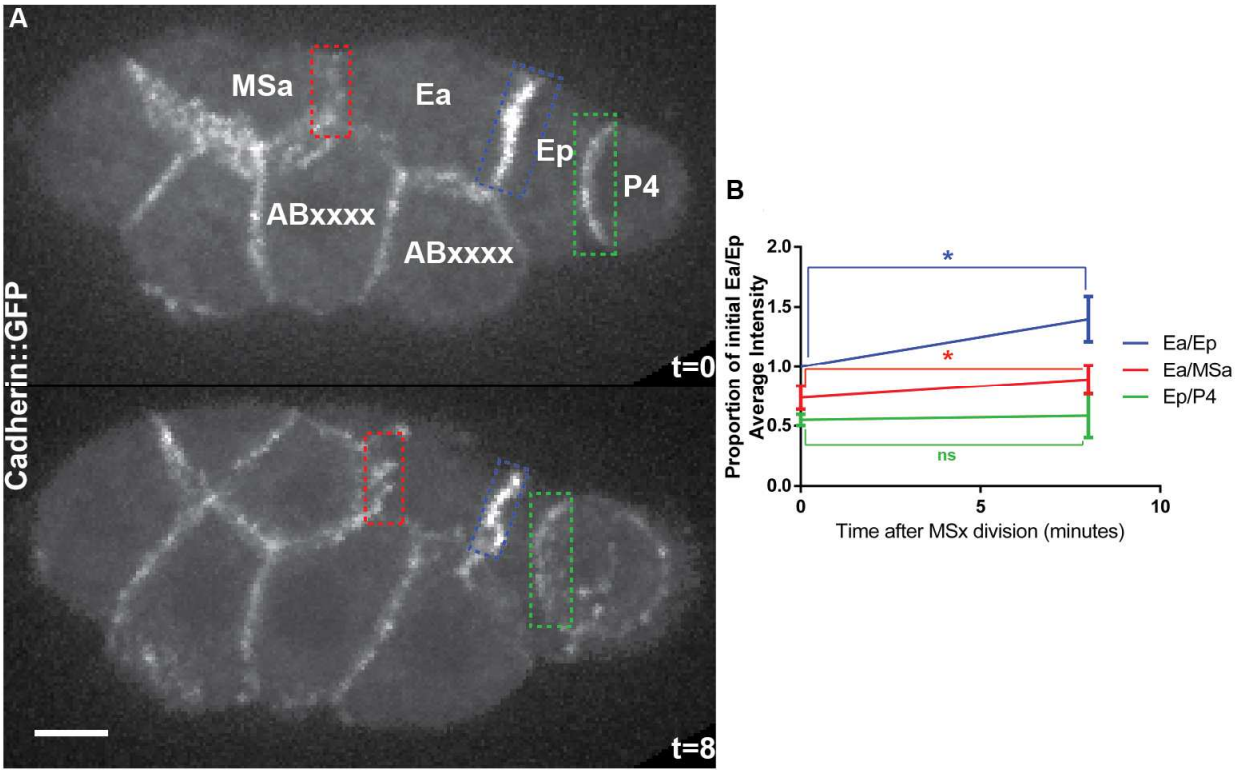

(A) Spinning disk confocal fluorescence images of HMR-1/cadherin-GFP expressing embryos at zero and eight minutes following MSa/p cell division initiation. Cell identities are labelled, and borders quantified in (B) are highlighted with colored dotted boxes corresponding to the symbols, lines, and error bars depicted in (B). (B) Fluorescence intensity normalized to the brightness of Ea/Ep at the time of MSa/p cell division initiation. Significant increases in HMR-1/cadherin accumulation are observed over time at Ea/Ep and Ea/MSa borders, but not at Ep/P_4. Error bars represent 95% confidence interval. * $p<.05$.

Figure 4.4. Cadherin Catenin Complex (CCC) components enrich at apical cell-cell junctions and do not display centripetal co-transport with actomyosin

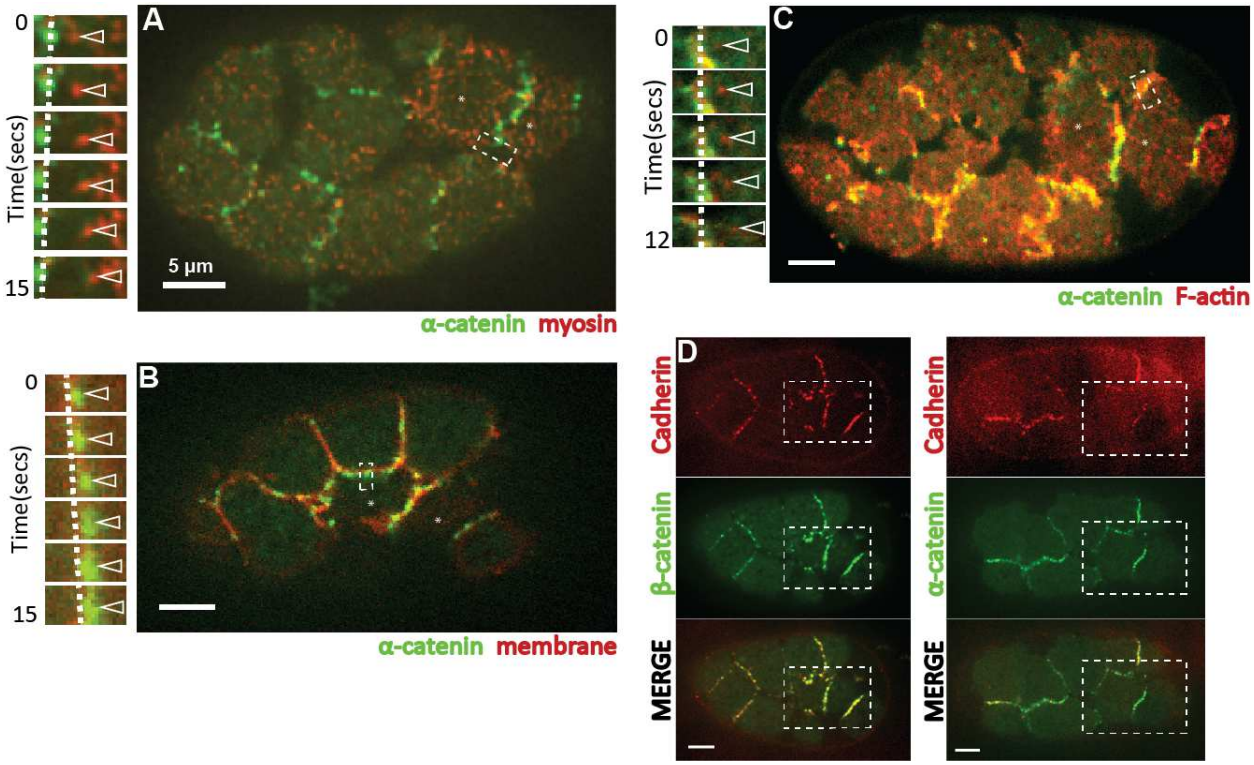

(A) Confocal fluorescence image of HMP-1/α-catenin-GFP and NMY-2/non-muscle myosin II-mKate2. Apically constricting cells are labeled with asterisks. Left panel: montage of multiple timepoints depicting centripetal dynamics of a myosin puncta (red) spatially separating from HMP-1/α-catenin-GFP at the apical junction. (B) Confocal fluorescence image of HMP-1/α-catenin-GFP and the plasma membrane marker mCherry-PH. Left panel: montage of multiple timepoints depicts colocalization of α-catenin-GFP and mCherry-PH in apically constricting cells (marked with asterisks). (C) Confocal fluorescence image of HMP-1/α-catenin-GFP and the fluorescent F-actin reporter mCherry-moesin actin binding domain (ABD). Left panel: montage depicts a puncta of mCherry-moesin ABD moving centripetally while HMP-1/α-catenin-GFP remains at the apical junction. Dotted boxes

circumscribe the regions used for montages. (D,E) Two color spinning disk confocal fluorescence images of GFP-HMP-2/β-catenin; HMR-1/cadherin-mKate2 and HMP-1/α-catenin-GFP; HMR-1/cadherin-mKate2, respectively. Apically constricting cells are circumscribed with a dotted box.

Figure 4.5. Some Cadherin Catenin Complex (CCC) components are interdependent for apical enrichment

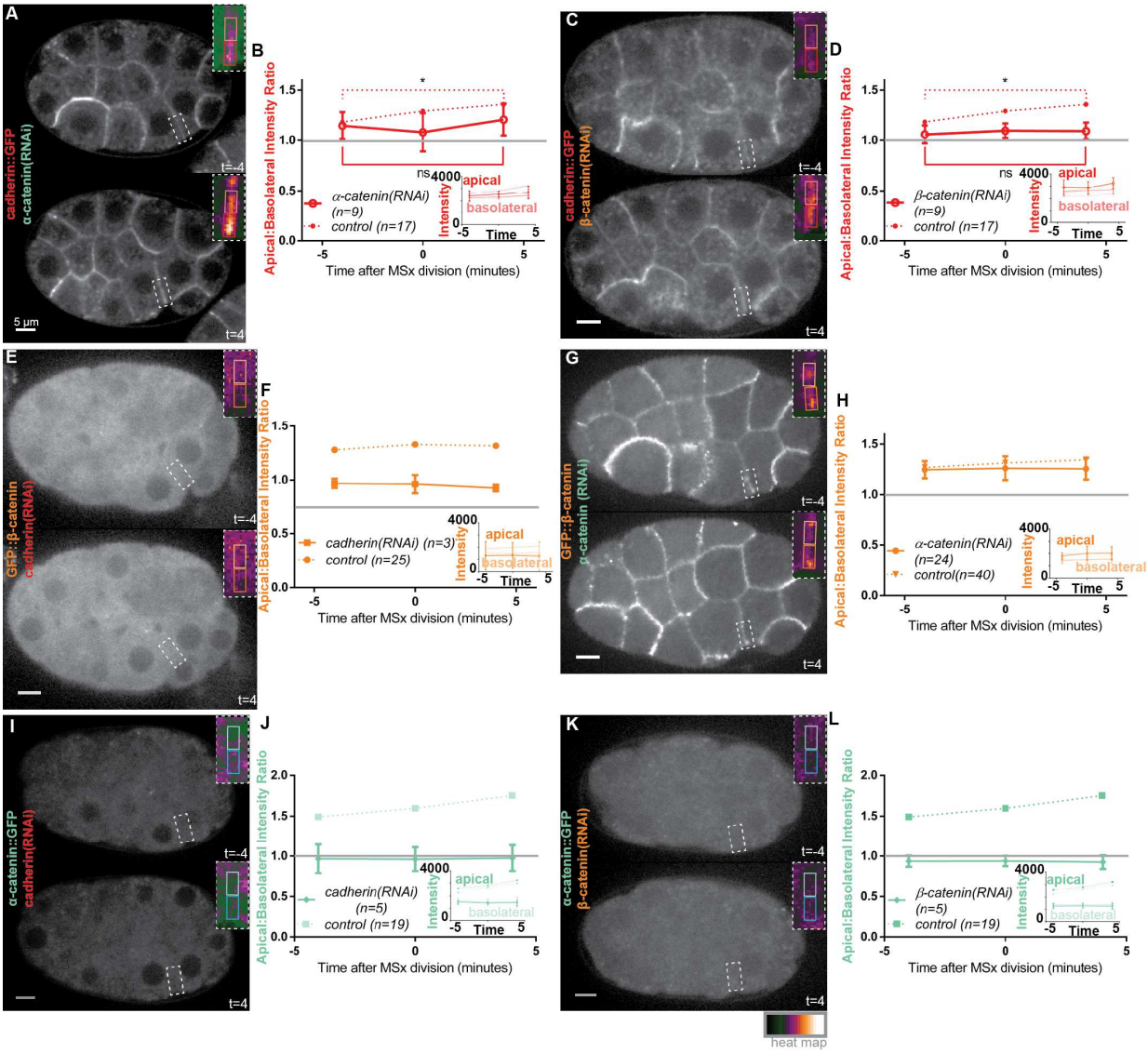

(A,C,E,G,I,K) Confocal fluorescence images of all combinations of CCC labeled components with other CCC components knocked down. HMP-1/α-catenin and HMP-2/β-catenin lose their membrane localization when membrane-proximal CCC components are disrupted while HMR-1/cadherin loses its apical localization when actin-proximal components are disrupted. The junction between the two apically constricting cells is highlighted by a dotted box which is magnified and

pseudocolored in the inset (top right). Images were acquired four minutes before and four minutes after cleavage furrow initiation in the MS daughter cells. (B,D,F,H,J,L) Quantification of apical to basolateral ratios of fluorescence intensity along the Ea/Ep border. Dotted lines correspond to uninjected control embryos, solid lines correspond to knockdown embryos. Inset: fluorescence intensity for control (dotted) and knockdown (solid) at both apical (dark colors) and basolateral (light colors) positions along the Ea/Ep contact. Error bars represent 95% confidence interval. * $p<.05$.

Figure 4.6. Myosin activity is required for apical enrichment of the Cadherin Catenin Complex (CCC) in apically constricting cells

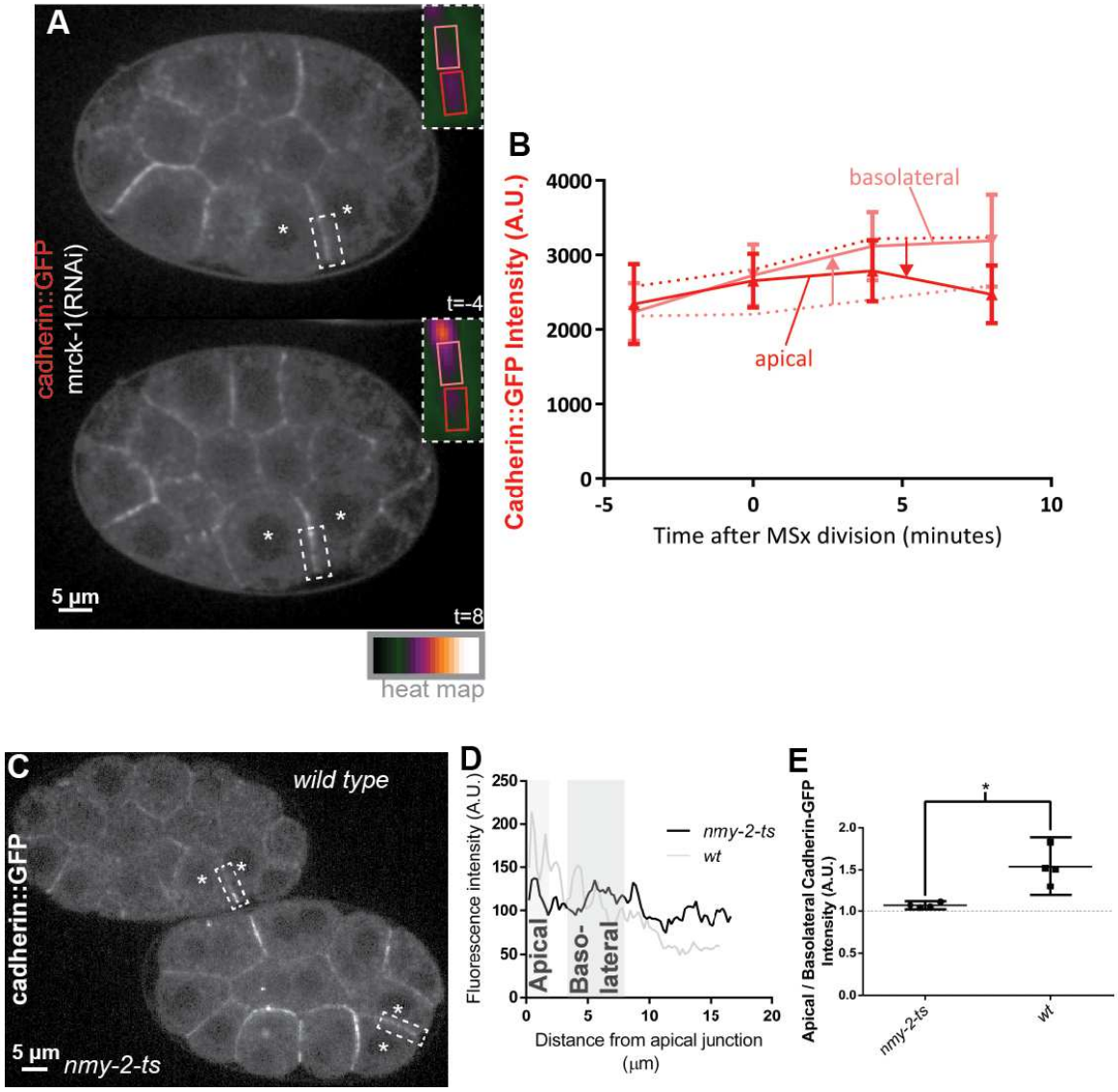

(A) Confocal fluorescence images of cadherin-GFP under *mrck-1* knockdown conditions. The border between Ea and Ep is circumscribed by a dotted box, which is pseudocolored and magnified in the inset (top right). Images were acquired four minutes before and eight minutes after MS daughter cell division. (B) Quantification of apical (dark colors) and basolateral (light colors) fluorescence intensities in

uninjected control (dotted lines) and *mrck-1* knockdown (solid lines) conditions. Apical intensity increases over time in the control, whereas basolateral intensity increases over time in the *mrck-1* knockdown embryos. (C) Side by side mounted *nmy-2(ts)* and wild type control embryos at the restrictive temperature (26°C) ~5 minutes after the temperature shift. Embryos are expressing HMR-1/cadherin-GFP. Apically constricting cells are noted by asterisks and the region used for the linescan in (D) is noted by the dotted boxes. (D) Fluorescence intensity values from a linescan performed along the Ea/Ep contact as noted by the dotted boxes in (C). (E) Apical to basolateral ratios of fluorescence intensities along the Ea/Ep cell contact in *nmy-2-ts* and wild type control embryos. Error bars represent 95% confidence interval. * $p<.05$.

Figure 4.7. Cas9/CRISPR triggered homologous recombination permits insertion of fluorescent protein (FP) genes at endogenous cadherin catenin complex (CCC) genes in the *C. elegans* genome

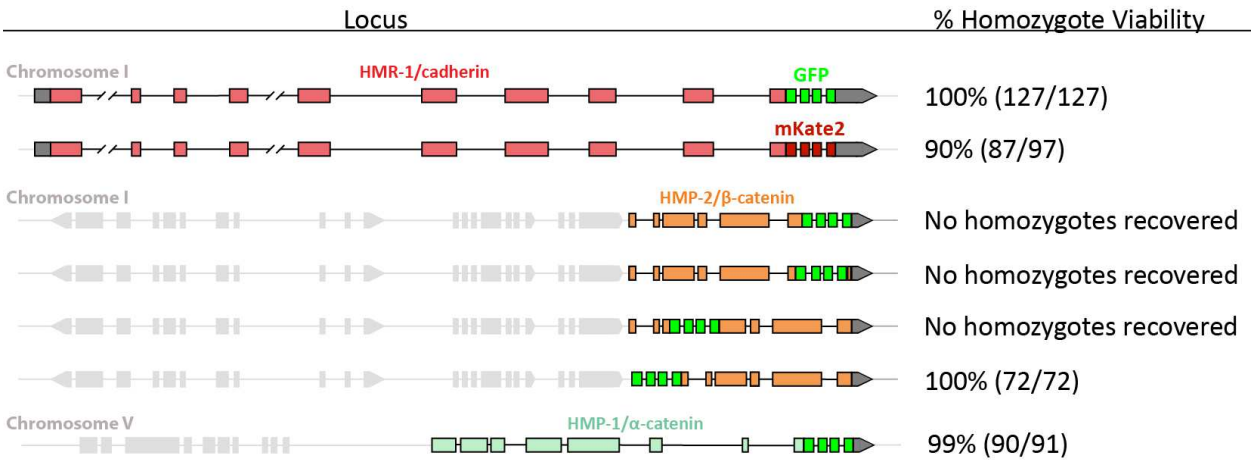

Gene models of all three essential *C. elegans* CCC genes with the sites of fluorescent protein insertion annotated. Exons are represented by colored boxes, introns by black lines, 5' and 3' untranslated regions by dark gray boxes, and intergenic or neighboring genes by light gray lines. Viable strains with low lethality were obtained for all three CCC genes.

Figure 4.8. Quantification of embryonic fluorescence in knock-in/knockdown embryos permits stage-specific verification of knockdown effectiveness

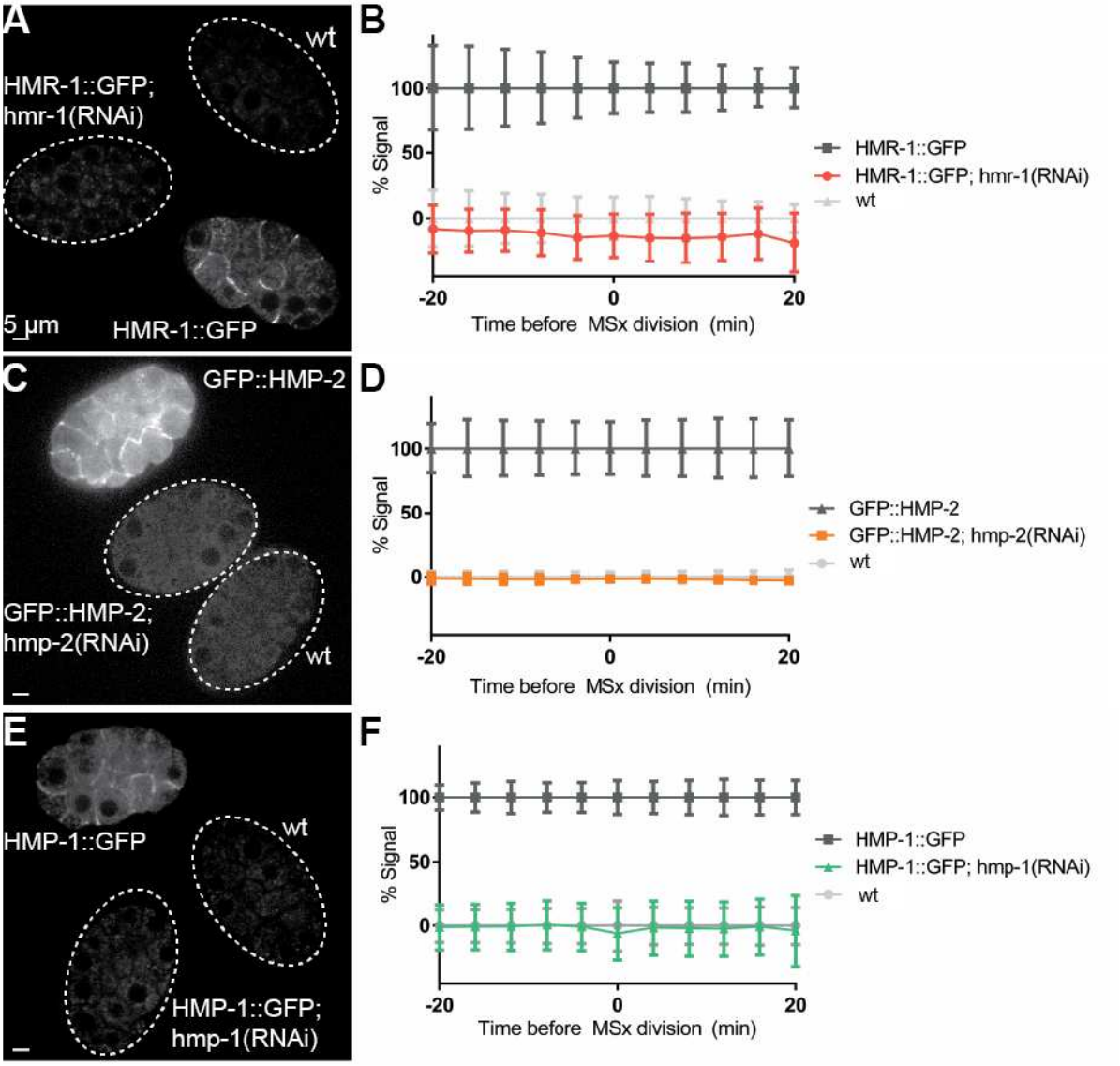

(A,C,E) Spinning disk confocal fluorescence images depicting triplet mounted, staged embryos of three genotypes in the same field of view. One embryo is a wild type autofluorescence control to provide a baseline for zero fluorescence signal, one is a control GFP knock-in embryo, and one is a knock-in embryo from a mother injected 24h prior with dsRNA targeting the knock-in gene. (B) Quantification of fluorescence reveals that the knock-in embryos' total fluorescence at times before

and after gastrulation stage is indistinguishable from wild type autofluorescence. Error bars represent 95% confidence interval. * $p<.05$.

REFERENCES

Abe, K. and Takeichi, M. (2008). EPLIN mediates linkage of the cadherin–catenin complex to F-actin and stabilizes the circumferential actin belt. Proc. Natl. Acad. Sci. U. S. A. *105*, 13–19.

Armenti, S.T. and Nance, J. (2012). Adherens Junctions in C. elegans Embryonic Morphogenesis. In Adherens Junctions: From Molecular Mechanisms to Tissue Development and Disease, T. Harris, ed. (Springer Netherlands), pp. 279–299.

Bertet, C., Sulak, L., and Lecuit, T. (2004). Myosin-dependent junction remodelling controls planar cell intercalation and axis elongation. Nature *429*, 667–671.

Borghi, N., Sorokina, M., Shcherbakova, O.G., Weis, W.I., Pruitt, B.L., Nelson, W.J., and Dunn, A.R. (2012). E-cadherin is under constitutive actomyosin-generated tension that is increased at cell-cell contacts upon externally applied stretch. Proc. Natl. Acad. Sci. U. S. A. *109*, 12568–12573.

Brenner, S. (1974). The Genetics of Caenorhabditis Elegans. Genetics *77*, 71–94.

Buckley, C.D., Tan, J., Anderson, K.L., Hanein, D., Volkmann, N., Weis, W.I., Nelson, W.J., and Dunn, A.R. (2014). Cell adhesion. The minimal cadherin-catenin complex binds to actin filaments under force. Science *346*, 1254211.

Chihara, D. and Nance, J. (2012). An E-cadherin-mediated hitchhiking mechanism for C. elegans germ cell internalization during gastrulation. Development *139*, 2547–2556.

Conine, C.C., Moresco, J.J., Gu, W., Shirayama, M., Conte, D., Yates, J.R., and Mello, C.C. (2013). Argonautes promote male fertility and provide a paternal memory of germline gene expression in C. elegans. Cell *155*, 1532–1544.

Daneshjou, N., Sieracki, N., Amerongen, G.P. van N., Schwartz, M.A., Komarova, Y.A., and Malik, A.B. (2015). Rac1 functions as a reversible tension modulator to stabilize VE-cadherin trans-interaction. J. Cell Biol. *208*, 23–32.

Davies, T., Jordan, S.N., Chand, V., Sees, J.A., Laband, K., Carvalho, A.X., Shirasu-Hiza, M., Kovar, D.R., Dumont, J., and Canman, J.C. (2014). High-resolution temporal analysis reveals a functional timeline for the molecular regulation of cytokinesis. Dev. Cell *30*, 209–223.

Dawes-Hoang, R.E., Parmar, K.M., Christiansen, A.E., Phelps, C.B., Brand, A.H., and Wieschaus, E.F. (2005). folded gastrulation, cell shape change and the control of myosin localization. Dev. Camb. Engl. *132*, 4165–4178.

Dickinson, D.J., Ward, J.D., Reiner, D.J., and Goldstein, B. (2013). Engineering the Caenorhabditis elegans genome using Cas9-triggered homologous recombination. Nat. Methods *10*, 1028–1034.

Gates, J. and Peifer, M. (2005). Can 1000 reviews be wrong? Actin, alpha-Catenin, and adherens junctions. Cell *123*, 769–772.

Grana, T.M., Cox, E.A., Lynch, A.M., and Hardin, J. (2010). SAX-7/L1CAM and HMR-1/cadherin function redundantly in blastomere compaction and non-muscle myosin accumulation during C. elegans gastrulation. Dev. Biol. *344*, 731–744.

Hynes, R.O. and Zhao, Q. (2000). The Evolution of Cell Adhesion. J. Cell Biol. *150*, 89–96.

Knudsen, K.A., Soler, A.P., Johnson, K.R., and Wheelock, M.J. (1995). Interaction of alpha-actinin with the cadherin/catenin cell-cell adhesion complex via alpha-catenin. J. Cell Biol. *130*, 67–77.

Kölsch, V., Seher, T., Fernandez-Ballester, G.J., Serrano, L., and Leptin, M. (2007). Control of Drosophila Gastrulation by Apical Localization of Adherens Junctions and RhoGEF2. Science *315*, 384–386.

Kwiatkowski, A.V., Maiden, S.L., Pokutta, S., Choi, H.-J., Benjamin, J.M., Lynch, A.M., Nelson, W.J., Weis, W.I., and Hardin, J. (2010). In vitro and in vivo reconstitution of the cadherin–catenin–actin complex from Caenorhabditis elegans. Proc. Natl. Acad. Sci. *107*, 14591–14596.

Maiden, S.L., Harrison, N., Keegan, J., Cain, B., Lynch, A.M., Pettitt, J., and Hardin, J. (2013). Specific conserved C-terminal amino acids of Caenorhabditis elegans HMP-1/α-catenin modulate F-actin binding independently of vinculin. J. Biol. Chem. *288*, 5694–5706.

Martin, A.C., Kaschube, M., and Wieschaus, E.F. (2009). Pulsed contractions of an actin–myosin network drive apical constriction. Nature *457*, 495–499.

Mason, F.M., Tworoger, M., and Martin, A.C. (2013). Apical domain polarization localizes actin-myosin activity to drive ratchet-like apical constriction. Nat. Cell Biol. *15*, 926–936.

Nagafuchi, A., and Takeichi, M. (1989). Transmembrane control of cadherin-mediated cell adhesion: a 94 kDa protein functionally associated with a specific region of the cytoplasmic domain of E-cadherin. Cell Regul. *1*, 37–44.

Nance, J., Munro, E.M., and Priess, J.R. (2003). C. elegans PAR-3 and PAR-6 are required for apicobasal asymmetries associated with cell adhesion and gastrulation. Development *130*, 5339–5350.

Roh-Johnson, M., Shemer, G., Higgins, C.D., McClellan, J.H., Werts, A.D., Tulu, U.S., Gao, L., Betzig, E., Kiehart, D.P., and Goldstein, B. (2012). Triggering a Cell Shape Change by Exploiting Pre-Existing Actomyosin Contractions. Science *335*, 1232–1235.

Seth, M., Shirayama, M., Gu, W., Ishidate, T., Conte, D., and Mello, C.C. (2013). The C. elegans CSR-1 argonaute pathway counteracts epigenetic silencing to promote germline gene expression. Dev. Cell *27*, 656–663.

Shewan, A.M., Maddugoda, M., Kraemer, A., Stehbens, S.J., Verma, S., Kovacs, E.M., and Yap, A.S. (2005). Myosin 2 Is a Key Rho Kinase Target Necessary for the Local Concentration of E-Cadherin at Cell–Cell Contacts. Mol. Biol. Cell *16*, 4531–4542.

Stetak, A. and Hajnal, A. (2011). The C. elegans MAGI-1 protein is a novel component of cell junctions that is required for junctional compartmentalization. Dev. Biol. *350*, 24–31.

Toret, C.P., Collins, C., and Nelson, W.J. (2014). An Elmo–Dock complex locally controls Rho GTPases and actin remodeling during cadherin-mediated adhesion. J. Cell Biol. *207*, 577–587.

Wallingford, J.B., Niswander, L.A., Shaw, G.M., and Finnell, R.H. (2013). The continuing challenge of understanding, preventing, and treating neural tube defects. Science *339*, 1222002.

Wu, S.K. and Yap, A.S. (2013). Patterns in Space: Coordinating Adhesion and Actomyosin Contractility at E-cadherin Junctions. Cell Commun. Adhes. *20*, 201–212.

Wu, Y., Jin, X., Harrison, O., Shapiro, L., Honig, B.H., and Ben-Shaul, A. (2010). Cooperativity between trans and cis interactions in cadherin-mediated junction formation. Proc. Natl. Acad. Sci. U. S. A. *107*, 17592–17597.

Wu, Y., Vendome, J., Shapiro, L., Ben-Shaul, A., and Honig, B. (2011). Transforming binding affinities from three dimensions to two with application to cadherin clustering. Nature *475*, 510–513.

Yonemura, S., Wada, Y., Watanabe, T., Nagafuchi, A., and Shibata, M. (2010). α-Catenin as a tension transducer that induces adherens junction development. Nat. Cell Biol. *12*, 533–542.

CHAPTER 5: FUTURE DIRECTIONS

Our study reveals new insight about the nature of cell-cell junctions during apical constriction, an important developmental cell shape change. Namely, the broadly-conserved cadherin catenin complex displays striking apicobasal polarization in apically constricting cells, and this polarization requires the activity of non-muscle myosin II.

Our study also represents a methodological advance for the study of cell biology in *C. elegans*. We use CRISPR/Cas9-triggered homologous recombination to insert genes encoding fluorescent proteins at the endogenous loci encoding our proteins of interest, allowing for the maintenance of all endogenous regulatory information. Further, we develop a new method to quantify the level of RNAi effectiveness with spatiotemporal resolution. We expect that this method will be generally applicable across all biological systems that permit RNAi, genome editing, and fluorescence imaging.

Our study also raises several important questions to address with future investigation. Namely, how do the levels of apical cadherin catenin complex affect the efficiency of apical constriction? What is the nature of the interaction between the F-actin cytoskeleton and the cadherin catenin complex (i.e. does HMP-1/α-catenin bind actin filaments directly, or is this binding mediated by a linker protein such as DEB-1/vinculin or AFD-1/afadin)? How does myosin activity contribute to the

localization of the cadherin catenin complex? That is, does myosin activity allow for stronger binding between α-catenin and actin filaments and thus restrict the diffusion of the cadherin-catenin complex at the apical junction? Alternatively, does interaction between the cadherin catenin complex and actomyosin block endocytosis of the cadherin catenin complex in a spatiotemporally-specific manner? Yet another possibility is that as-yet-undetected basal to apical actomyosin flow drags the cadherin-catenin complex apically. Also, why does the basolateral junction between Ea and Ep get brighter in the absence of myosin activity? Does myosin promote cadherin catenin complex stability in some cellular contexts, but promote turnover it in others?

Our study also raises questions about the molecular mechanism by which SAX-7/IgCAM, a redundant cell-cell adhesion protein, contributes to gastrulation. Namely, does SAX-7 provide a mechanical link between the cell-cell junction and the actomyosin cytoskeleton? If so, which SAX-7 binding partners provide a path allowing interaction with F-actin, and how are these binding interactions regulated over time? Does SAX-7 display the same apicobasal polarization as the cadherin-catenin complex in apically constricting cells, and if so, is this apicobasal polarization also dependent on myosin activity? Future work ought to fluorescently tag SAX-7 at its endogenous locus and examine whether it, too, displays myosin-dependent apical enrichment in apically-constricting cells.

One limitation of our study is that it relied purely on localization data from live cell microscopy and genetic methods to infer information about the interactions among proteins. While this approach was fruitful in identifying a new link between

myosin activity and apical polarization of cell-cell adhesion components, we do not know the biochemical nature of this link. In the future, it will be important to perform biochemical studies to identify the network of protein-protein interactions which underlies this link. For example, it would be interesting to pull down HMP-1/α-catenin-GFP and perform protein identification of binding partners by mass spectrometry. Interactions could then be validated by using CRISPR/Cas9-triggered homologous recombination to insert an affinity tag in candidate CCC binding partner proteins and testing whether they interact biochemically with α-catenin by crossing the HMP-1/α-catenin-GFP strain to the affinity tagged candidate strain and pulling down HMP-1/α-catenin-GFP and probing for the candidate's affinity tag by Western blot. The converse experiment could also be performed: pulling down the candidate by the affinity tag and blotting for GFP to test for HMP-1/α-catenin-GFP binding. Further, one could test for a direct protein-protein interaction by expressing each component in bacteria, purifying, and testing for direct binding *in vitro* by pull down.

The biochemical methods outlined above would provide information about the nature of protein-protein interactions, but they lack spatiotemporal resolution. In order to obtain this, one could test whether the interactions identified above actually occur in the E cells during gastrulation stage by performing single molecule pull down (SiMPull) using lysate from staged embryos or, potentially, from individual dissected cells at the appropriate developmental stage (Jain et al., 2012). Briefly, a coverslip would be coated with an antibody specific for an affinity tag on the protein of interest and passivated such that non-specific proteins do not associate with the coverslip. In our case, we would coat the coverslip with anti-GFP. The sample (in our

case, a gastrulation staged embryo or dissected E cells from a gastrulation staged embryo expressing HMP-1/α-catenin-GFP and candidate interactors tagged with mCherry) would then be lysed on top of the coverslip. We would use two color total internal reflection (TIRF) microscopy to visualize GFP-positive diffraction limited spots that are tightly associated with the coverslip and test whether mCherry-positive diffraction-limited spots colocalize with them. The dynamics of this colocalization would provide information about the affinity of binding between HMP-1/α-catenin-GFP and the interacting protein of interest. This approach, though difficult, would provide insight into the precise spatiotemporal regulation of binding interactions between the cadherin-catenin complex and the F-actin cytoskeleton. These interactions are worth understanding because they provide fundamental insight into the biology of epithelial cells across animal phyla.

While traditional biochemical methods are essential for dissecting the molecular mechanisms of cell biology, they do not always capture interactions that are transient, weak, or dependent on a precise mechanobiological context. For example, work from James Nelson and Bill Weis's groups initially failed to identify a binding interaction between the ternary cadherin catenin complex and actin filaments (Drees et al., 2005; Yamada et al., 2005). Later work from this group revealed that the ternary cadherin catenin complex *can* bind to actin filaments, but this occurs as a catch bond between α-catenin and the actin filament requiring the application of mechanical force (Buckley et al., 2014). In order to identify interactions that might be transient in nature, one could employ an enzymatic tagging approach. One such approach uses a bacterial biotin ligase enzyme (BirA) that has been modified to

promiscuously tag all exposed lysine residues within a small radius (Liu et al., 2013). One could use CRISPR/Cas9-triggered homologous recombination to insert the gene encoding BirA into the native HMP-1/α-catenin locus. This enzyme would biotinylate all proteins within a small radius HMP-1/α-catenin, and one could then use streptavidin-coated beads to pull down interactors. As before, one could use mass spectrometry protein identification to identify binding partners and test for function of candidate interactors with future experiments. The strength of this approach is that it casts a wide net, identifying even weak or transient interactors. However, it will likely also produce a large number of false positive interactors, so subsequent experiments will be essential to validate any targets.

Much of my work has focused on studying the molecular mechanisms of cell-cell junction formation during apical constriction. However, apical constriction may not be the sole mechanism contributing to the internalization of the E cells during *C. elegans* gastrulation. Previous studies have identified several behaviors in cells neighboring the E cells that could contribute to gastrulation movements and cell positioning. For example, F-actin-rich, Arp 2/3 dependent cellular extensions are known to form at the interface between the E cells and their MS descendant neighbors, though it is unclear whether these extensions drive E cell internalization (Roh-Johnson and Goldstein, 2009). Also, P_4, the germline precursor cell bordering Ep to the posterior, displays anteriorly directed blebbing as it advances anteriorly and the E cells internalize, but it is also unknown whether this behavior contributes to E cell internalization (Pohl et al., 2012; Roh-Johnson and Goldstein, 2009). Finally, there is weak evidence that neighboring cell divisions may contribute to

gastrulation movements, as ablation of the P_3 cell or certain neighboring AB lineage neighbors prevented internalization, indicating that some neighboring cells must be alive for the E cells to internalize (Pohl et al., 2012). Thus, apical constriction appears to be necessary, but perhaps not sufficient for E cell internalization.

The work described here has provided novel insight into a fundamental question in animal development. That is, how do embryonic cells produce force and transmit that force to the surrounding tissue? I have shown that the cadherin catenin complex, a key mediator of force transmission between cells, is polarized in response to the activity of myosin II, a key member of the force producing machinery. It is my hope that this insight will propel future studies into understanding how molecular machines operate within cells and tissues to produce the endless forms most beautiful apparent in nature.

REFERENCES

Buckley, C.D., Tan, J., Anderson, K.L., Hanein, D., Volkmann, N., Weis, W.I., Nelson, W.J., and Dunn, A.R. (2014). Cell adhesion. The minimal cadherin-catenin complex binds to actin filaments under force. Science *346*, 1254211.

Drees, F., Pokutta, S., Yamada, S., Nelson, W.J., and Weis, W.I. (2005). α-Catenin Is a Molecular Switch that Binds E-Cadherin-β-Catenin and Regulates Actin-Filament Assembly. Cell *123*, 903–915.

Jain, A., Liu, R., Xiang, Y.K., and Ha, T. (2012). Single-molecule pull-down for studying protein interactions. Nat. Protoc. *7*, 445–452.

Liu, D.S., Loh, K.H., Lam, S.S., White, K.A., and Ting, A.Y. (2013). Imaging Trans-Cellular Neurexin-Neuroligin Interactions by Enzymatic Probe Ligation. PLoS ONE *8*, e52823.

Pohl, C., Tiongson, M., Moore, J.L., Santella, A., and Bao, Z. (2012). Actomyosin-based Self-organization of cell internalization during C. elegans gastrulation. BMC Biol. *10*, 94.

Roh-Johnson, M., and Goldstein, B. (2009). In vivo roles for Arp2/3 in cortical actin organization during C. elegans gastrulation. J. Cell Sci. *122*, 3983–3993.

Yamada, S., Pokutta, S., Drees, F., Weis, W.I., and Nelson, W.J. (2005). Deconstructing the Cadherin-Catenin-Actin Complex. Cell *123*, 889–901.